Concurrent neurochemical and neurophysiological investigation of fMRI signals

Dissertation

der Mathematisch-Naturwissenschaftlichen Fakultät

der Eberhard Karls Universität Tübingen

zur Erlangung des Grades eines

Doktors der Naturwissenschaften

(Dr. rer. nat.)

vorgelegt von

Ekaterina Mitricheva

Aus Tajikistan/USSR

Tübingen

2021

Gedruckt mit Genehmigung der Mathematisch-Naturwissenschaftlichen Fakultät der Eberhard Karls Universität Tübingen.

Tag der mündlichen Qualifikation:	18.02.2021
Stellvertretender Dekan:	Prof. Dr. József Fortágh
1. Berichterstatter:	Prof. Dr. Nikos Logothetis
2. Berichterstatter:	Prof. Dr. Andreas Bartels

ACKNOWLEDGEMENTS

I am indebted to many people who supported and encouraged me to accomplish this Ph.D. thesis. It is with immense gratitude that I acknowledge the continuous support and help of Professor Dr. Nikos Logothetis without whom this work would not be possible. Indeed, this thesis in its entirety was motivated by his hypotheses and previous studies. The research could not have been realized without the infrastructure (hardware and MATLAB analysis toolboxes) that he kindly provided to me. It also gives me great pleasure to acknowledge Professor Dr. Andreas Bartels for his continuous support and helpful guidance. I would also like to thank Privat-Dozent Dr. Dr. Hamid R. Noori who constantly encouraged me to pursue this project and provided scientific support throughout the entire work. I would like to thank my colleague Dr. Rui Kimura for his support in the initial phases of the experiments. Last by not least, I would also like to express my sincere gratitude to Mr. Axel Oeltermann, Mr. Michael Beyerlein, Mr. Eduard Krampe and Mr. Luis Miguel Pascual for developing hardware components and the technical assistance during MRI experiments.

ABSTRACT

Functional magnetic resonance imaging (fMRI) is a frequently-used non-invasive technique to investigate the operational organization of the brain. In particular, blood-oxygen-level-dependent (BOLD) fMRI has become a mainstay of basic and clinical neuroscience. However, the colorful images that fMRI produces often mask the immense complexity of the underlying neurobiological processes generating them. While previous studies conducted in non-human primates suggest a notable correlation between BOLD and neocortical local field potentials (LFP). LFP itself is the result of neural microcircuits, the so-called excitation-inhibition networks (EIN), that integrate signals from glutamatergic and GABAergic neurons in a complex dynamical manner. Thus, to understand the neural basis of BOLD signals, it is inevitable to characterize its causal relationship with dynamical states of EIN. Methods for simultaneous electrophysiological, neurochemical and imaging experiments are therefore essential to unveil the mystery of the neuronal origin of fMRI and may lead to answers unlikely to be obtained by using either technique alone. In particular, it would allow us to decompose the BOLD response into its excitatory and inhibitory components, which is of outmost importance for identifying brain states in animals and humans. In this thesis, the development of a novel MRI-based microelectrode-based technology is introduced that allows simultaneous recording of glutamate, GABA, neural activity and BOLD in consistent time-scales in several brain regions. Measurements were conducted in two brain pathways, namely the somatosensory and visual systems. The results suggest that BOLD signal is related to a complex and often opposite interplay of glutamatergic and GABAergic neuronal populations. The overall findings not only improve our understanding of the neurobiological processes that underly functional imaging of the brain, but will ultimately support efforts for development of new therapeutic strategies for neuropsychiatric diseases.

Zusammenfassung

Die funktionelle Magnetresonanztomographie (fMRT) ist eine häufig verwendete nicht-invasive Technik zur Untersuchung der operativen Organisation des Gehirns. Dabei ist insbesondere die Blut-Sauerstoff-Level-abhängige (engl. BOLD) fMRT zu einer tragenden Säule der Grundlagen- und klinischen Neurowissenschaften geworden. Die farbenfrohen Bilder, die die fMRT erzeugt, verdecken jedoch oft die immense Komplexität der zugrunde liegenden neurobiologischen Prozesse, die diese Bilder erzeugen. Frühere Studien, die an nicht-humanen Primaten durchgeführt wurden, legen eine bemerkenswerte Korrelation zwischen BOLD und neokortikalen lokalen Feldpotentialen (LFP) nahe. LFP selbst ist das Ergebnis neuronaler Mikroschaltkreise, der so genannten Erregungs-Hemmungs-Netzwerke (EIN), die Signale von glutamatergen und GABAergen Neuronen auf komplexe, dynamische Weise integrieren. Um die neuronale Basis von BOLD-Signalen zu verstehen, ist es daher unumgänglich, ihren kausalen Zusammenhang mit dynamischen Zuständen von EIN zu charakterisieren. Die Entwicklung einer Technik für gleichzeitige elektrophysiologische, neurochemische und bildgebende Experimente ist aus diesem Grund unerlässlich, um das Geheimnis des neuronalen Ursprungs der fMRT zu lüften, und kann zu Antworten führen, die mit keiner der Techniken allein erreicht werden können. Insbesondere würde es uns erlauben, die BOLD-Reaktion in ihre exzitatorischen und inhibitorischen Komponenten zu zerlegen, was für die Identifikation von Hirnzuständen bei Tieren und Menschen von größter Bedeutung ist. In dieser Arbeit wird die Entwicklung einer neuen MRT-basierten Mikroelektroden-Technologie vorgestellt, die die gleichzeitige Aufzeichnung von Glutamat, GABA, neuronaler Aktivität und BOLD in konsistenten Zeitskalen in mehreren Hirnregionen ermöglicht. Die Messungen wurden in zwei Informationsverarbeitungswege im Rattenhirn, nämlich im somatosensorischen und im visuellen System, durchgeführt. Die Ergebnisse deuten darauf hin, dass das BOLD-Signal mit einem komplexen und oft gegensätzlichen Zusammenspiel glutamaterger und GABAerger Neuronenpopulationen zusammenhängt. Die Gesamtergebnisse verbessern nicht nur unser Verständnis der neurobiologischen Prozesse, die der funktionellen Bildgebung des Gehirns zugrunde liegen, sondern werden letztlich die Bemühungen um die Entwicklung neuer therapeutischer Strategien für neuropsychiatrischen Erkrankungen unterstützen.

Table of Contents

1 Introduction

1.1 Brief history of non-invasive medical technologies before MRI.

The curiosity to understand how human body works has always been a part of human nature. Under the assumption that structure is a direct indicator of function, the early approaches, until the 19th century, were based on cataloging body parts either post-mortem or by means of surgical operations. The first structural, *in vivo,* non-invasive method was discovered by Wilhelm Conrad Röntgen in Würzburg, Germany on November 8, 1895. By using a Ruhmkorff induction coil, a mercury interrupter, and a Hittorf Crookes vacuum tube, he discovered a fluorescence in a screen of barium platino-cyanide. He doubted that this was a result of cathode rays because at that time, it was thought that their nature was understood. To test this hypothesis, he started experiments with various bodies at different distances, which interrupt the cathode rays and although they were supposed to be quite opaque, he still could see the fluorescence on the screen. At that moment, he realized that he is dealing with an unknown radiation, the penetrating power of which varied approximately with the density of the interrupting body. Subsequently, he decided to use his own and his wife's hand as an object for test and he saw a shadow of the bones. Next what he did was to change the screen by a photographic plate and repeat the procedure. Already one and a half months later, Röntgen submitted the first known article on X-rays with the title "Über eine neue Art von Strahlen" where he talks about absorption properties of different materials: paper, wood and also metal. This was the beginning of the new era of non-invasive diagnostics (Underwood, 1945). X-ray remains since its discovery one of the most important techniques in medical diagnostics. However, despite the fact that the discovery of X-rays was among the most significant breakthroughs in medicine and science, this method does not represent a universal key to all questions about human body organization or function. While x-rays illuminate human skeleton, the thickness of the skull provides a natural barrier for observation of brain structure. Moreover, the spatiotemporal resolution of x-rays limits their ability to enhance our knowledge of bodily, and particularly brain function.

Another important structural, non-invasive diagnostic method that is worth including in this synopsis is so-called ultrasound technology. Yet, before going through the

history of ultrasound, it's worth briefly describing one significant finding, without which this method would not have been possible. When moving relatively to the source of a wave, then an observe would measure an alteration in wave frequency. The phenomenon discovered in 1842 by Christian Doppler, named in his honor Doppler effect or Doppler-Shift, has now been studied in detail and we know that the frequency shift is proportional to the speed of movement of structures and depends on the direction of their movement: if the movement is directed towards the sensor, the frequency increases, if from the sensor the frequency decreases. Ultrasound uses longitudinal waves for visualization of internal parts of the human body and has a frequency of more than 20 KHz. This is more than the frequency of vibrations perceived by the human ear. Our perceived frequencies known as sounds, are within the range of 16-20 Hz to 20 KHz. Ultrasonic waves, which look like a series of thickenings and discharges of a medium, on the other hand, are beyond our auditory capacity, yet a useful tool in medicine: Namely, they were initially used as a method of treating arthritis, stomach ulcers, asthma, etc., and as of the 40-50s of the 20th Century as a critically important diagnostic method,. The founder of diagnostic ultrasound is considered to be an Austrian neurologist, psychiatrist Karl Theodore Dussik (Shampo and Kyle, 1995), who first used ultrasound for diagnostic purposes. He determined the location of brain tumors by measuring the intensity of the passage of an ultrasonic wave through the skull, similar to a metal flaw detector. Interestingly, it was later discovered that the images obtained by Dussik were only artifacts of the reflection of sound waves from the bones of the skull. In 1955, Ian Donald from UK conducted the first studies of tumors, solid and cystic. With the support of Ian Donald, engineer Tom Brown created the "*Mark 4*" device, the first prototype of an ultrasound system based on an instrument used to detect industrial defects in ships. And few years later, in June 1958, he and his two co-authors (J. Macvicar and T.G. Brown) published in the journal *The Lancet* the first image of the fetus in second trimester of pregnancy (Donald et al., 1958). To date, ultrasound is among the most commonly used non-invasive imaging techniques for soft body tissue. Moreover, using Doppler effect, ultra sound measures the direction and vascular velocity of blood cells, as the properties of reflected sound waves change due to the motion of blood cells. However, the use of ultrasound in neuroscience remains restricted to the study of external blood flow as the waves that it induces cannot penetrate the skull and thus cannot provide any additional insights on intracerebral hemodynamics.

In addition to the x-ray and ultrasound, other non-invasive methods began to emerge in the beginning of 20th century. Electroencephalography (EEG) - an electrophysiological method for the recording of electrical activity occurring from the brain (Britton et al., 2016) – is among the earliest and most prominent ones that contrasts the previous methods by having a functional (instead of structural imaging) focus. The presence of electrical processes in the brain of animals was already mentioned as early as 1849 in the studies of Du Bois-Reymond (Du Bois-Reymond, 1848). However, the development of EEG as an independent section of electrophysiology began in 1875-1876 after the works of Danilevsky (Danilevsky, 1891) and Caton (Caton, 1891), which described the vibrational nature of electrical potentials of the brain.

In 1924, psychiatrist Hans Berger from Germany pioneered the EEG in humans. He was actually the first to describe the different wave-frequencies or rhythms that are present in normal and abnormal brains, such those known today as delta, alpha, beta, gamma, etc. We now know that this kind of band-limited fluctuations reflect to a different extent brain states, and their transitions. The diagrams (registering fluctuations in the electrical potentials of the brain through the cranial integument) obtained, were called electroencephalograms. The work of Berger, as well as the EEG method itself, became widely recognized only after May 1934. Adrian and Matthews were the first to convincingly demonstrate Berger's rhythm at a meeting of the Physiological Society in Cambridge (Adrian and Matthews, 1934). Few years later, in 1936, the English neurophysiologist G. Walter discovered abnormal δ-activity in brain tumors (Walter, 1936). This suggested that electroencephalography can be used to clarify the location of tumors. W. Grey Walter's discovery of δ - and β-activity and their connection with pathological disorders in the brain marked the beginning of clinical EEG. EEG became a method for the evaluation of dynamic cerebral functioning and could be mainly useful for assessing patients with organic brain lesions, suspected seizures, epilepsy, or inflammatory diseases and allowed us to identify various patterns of electroencephalography that are characteristic of various forms of brain damage, various functional states - active wakefulness, sleep, coma, etc. While this method gives access to cortical processes, its major shortcoming is that it does not provide true knowledge of the function of deep brain structures.

1.2 Cerebral hemodynamics as a surrogate for brain function.

The aforementioned methodologies have been of great importance for medicine as well as for brain research, and their use is likely to continue for decades, if not centuries, albeit potentially as an auxiliary strategy. Revolutionary in medicine and research, however has been the discover of so-called magnetic resonance imaging (MRI). MRI is essential for the structural and functional investigation of the brain, and it also happens to have a fascinating history, reflecting bright minds and their curiosity-driven research.

A key moment in the path, which led to the current MRI, was the discovery of spatial localization and function-specific changes of the cerebral blood flow (CBF). An Italian physiologist named Angelo Mosso decided to examine the brain of a peasant named Michele Bertino (Mosso, 1880), who had survived a horrific accident that cracked open his skull and left sections of his brain exposed. Mosso put together a simple apparatus and used it to measure brain pulsations, while Bertino was performing various tasks. At the same time, he measured systemic pulses in the forearm of Bertino. He noticed the following things: 1) Under 'neutral' quiet conditions the forearm and brain pulses remained unchanged; 2) Yet, each time the church-bells rang in town, blood surged through Bettino's lobes. and 3) When Mosso asked him whether the bells reminded him of a prayer, his response, namely that he actually thought of Ave Maria, induced a blood increase in his exposed veins. Soon Mosso noticed that blood actually pulsed each time Bertino was thinking in general, e.g. when he did multiplication. None of these events were related to his systemic pulses. Mosso inferred that CBF increases locally during neuronal activity. This fascinating study was also one of the first investigations against the notion of "*watering the entire garden for the sake of one thirsty flower*".

A second critical step happened less than a decade later by observations of Roy and Sherrington (Roy and Sherrington, 1890) in 1890. In their animal experiments, they measured both cerebral volume (CBV) and blood pressure changes, using a novel monitoring device. Changes in volume and pressure were monitored with an oncograph and kymograph, respectively. In their study, they demonstrated that weak electrical stimulation of the sciatic nerve causes short-term changes in both CBV and

blood pressure. They also showed a striking dissociation induced by pharmacological intervention. Injections of morphine, for instance, strongly reduced blood pressure, while increasing volume. Based on many such cases of dissociation, Roy and Sherrington concluded that "*the brain possesses an intrinsic mechanism by which its vascular supply can be varied locally in correspondence with local variations of functional activity*".

These discoveries serve nowadays as basis for functional neuroimaging, as CBF and CBV changes can be measured quantitatively using noninvasive methods, such as the fMRI.

The ultimate link between cerebral hemodynamics and magnetic resonance imaging was established by another significant finding, namely that the magnetic properties of hemoglobin (Hb) depend on the concentration of deoxyhemoglobin (dHb). These magnetic properties of the blood were discovered by Linus Pauling and Charles Coryell in 1936 (Pauling and Coryell, 1936a, b). They took cattle blood, put it into a tube, which they suspended with a wire from one arm of this balance, and hung between the poles of an electromagnet. They adjusted the balance and then they passed current through the electromagnet. The tube was attracted to the magnetic field, and the extent of displacement was directly correlated with the concentration of deoxyhemoglobin in the blood. Linus Pauling had long provided evidence that the ferrous part of the heme makes deoxyhemoglobin paramagnetic, otherwise it's diamagnetic. Hb and dHb have different relaxation times and this could be in principle exploited to extract information about the oxygenation (activation) state of a tissue, such as the brain.

1.3 Magnetic resonance imaging.

The emergence of MRI as an exceptional imaging tool in medicine is considered to be 1973. Exactly then, the Professor of chemistry and radiology of the State University of New York, Paul Lauterbur, published an article in the scientific journal *Nature* with the title "*Image formation by induced local interactions. Examples employing nuclear magnetic resonance*" (Lauterbur, 1989), albeit the underlying technology, namely the nuclear magnetic resonance (NMR) evolved several decades earlier. In specific, in 1946, two physicists Felix Bloch (Bloch et al., 1946) and Edward Purcell (Purcell et al., 1946) identified a physical process that is based on the magnetic properties of the atomic nuclei of certain elements of the periodic system. They found that the nuclei located in the magnetic field absorb energy in the radiofrequency range and subsequently re-emit it when switching to their original energy state. This phenomenon was called NMR.

In 1952, both scientists received the physics Nobel prize for "*their development of new methods for nuclear magnetic precision measurements and discoveries in connection therewith*". MRI technique capitalizes on the interaction between a strong magnetic field (approximately 5 orders of magnitude higher than Earth's magnetic field), commonly generated by a superconducting electromagnet, radiowaves, and specific nuclei (hydrogen, carbon 13, fluorine, sodium, and phosphorus) that possess spin, i.e. quantized angular momentum. The term *magnetic resonance* refers to this induction of transitions between energy states, and it occurs when the frequency of the excitation pulse is at the so-called Larmor (or resonance) frequency.

In some detail, the human body consists of about 4/5 of water, about 90% of the substance is hydrogen - 1H. The hydrogen atom is the simplest chemical structure. In its center there is a positively charged particle, the proton, and on the periphery, a much smaller mass: the electron. While the electron constantly rotates around the proton, the proton itself shows an autorotation behavior. It rotates approximately around its own axis, and at the same time its axis of rotation describes a circle, so that a precession cone is obtained. The frequency of precession rotation of the proton is very high - about 40 MHz, i.e. 40 million revolutions in 1 s. It is common knowledge that the rotation frequency is directly proportional to the magnetic field strength and is called the Larmor frequency, $\omega=\gamma B_0/2\pi$ (γ: gyromagnetic ratio; B_0:

strength of the magnetic field). The motion of a charged particle forms a local magnetic field, whose vector coincides with the direction of the cone of rotation. Thus, each proton can be represented as a small magnet (spin), which has its own magnetic field and poles - North and South (Brown, 2014). Protons have the highest magnetic moment and, as noted above, the highest concentration in the body. Obviously, outside of a strong magnetic field, such small spins are randomly oriented. However, when exposed to a strong magnetic field, which forms the basis of a magnetic resonance imaging scanner, they naturally line up along the main magnetic vector B_0. The resulting longitudinal magnetization of spins is then at maximum. If then a powerful radio-frequency pulse of a certain (resonance) frequency is applied, i.e. close to the Larmor frequency, all protons are forced to rearrange perpendicularly (90°) to the main magnetic vector B_0 and perform synchronous rotation, causing the actual nuclear resonance.

Longitudinal magnetization becomes zero, but transverse magnetization arises, since all spins are directed perpendicular to the main magnetic vector B_0. Under the influence of B_0, the spins gradually converge back to their initial state; a process that is referred to as relaxation. Depending on time constants, different relaxation processes can be classified such as the T_1, T_2 or T_2*. The inverse of each is called relaxation rate and denoted by R_i (Logothetis, 2008). Lateral magnetization decreases and longitudinal magnetization increases. Chemical bonds or the existence of crystal lattices influence the speed of these processes. the possibility of free energy release with the transition of an electron from a higher to a lower energy level (for water, these are macromolecules in the environment) inhomogeneity of the magnetic field.

The theory of NMR was continuously developed and the effect of nuclear magnetic resonance was used in physics and chemistry for molecular analysis and ultimately by Lauterbur for the first time in medical context, His seminal work became the basis for extensive further research. In 1975, Richard Ernst proposed magnetic resonance imaging using phase and frequency coding, a method which is currently used in MRI (Kumar et al., 1975). A few years later Peter Mansfield (Mansfield, 1977) advanced Lauterbur's method with the introduction of echo-planar imaging (EPI), establishing how to analyze the signals that the human body sends in a magnetic field. He further

improved mathematical algorithms for image acquisition. For these achievements Peter Mansfield together with Nikos Logothetis (for their achievements in understanding the field of functional Magnetic Resonance Imaging) were elected as foreign associates of the National Academy of Sciences, USA, in 2009 (www.nasonline.org). His work made it possible to obtain complete two-dimensional images in an extremely short time, for which, together with Lauterbur, he was awarded the Nobel prize in medicine and physiology for "*discoveries concerning magnetic resonance imaging*" in 2003 (Mansfield, 2004). A great contribution to the promotion and accessibility of the method was also made by the scientist Raymond Vahan Damadian, who is one of the first researchers of the principle of tomography, the creator of the first commercial scanner and the holder of a patent for the method of magnetic resonance imaging. In the early 80's, William A. Edelstein and his collaborators used this method to demonstrate the representation of the human body. It took approximately 5 minutes to get a single image. Less than a decade later (1986), one could obtain the images with 5s time-resolution without any significant loss of quality. After the successful introduction of MRI in medical practice, this method gained wide popularity and became one of the main tools for the study of pathological conditions in humans, actively used in differential diagnosis, monitoring and treatment of patients and biomedical research.

Indeed, due to the absence of harmful ionizing radiation, as well as the possibility of a non-invasive method for diagnosing various parts of the body (neuromuscular system, musculoskeletal system, structure of cartilage tissue, parenchymal organs of the abdominal cavity, etc.) in 2-D or 3- D planes, MRI is considered the gold standard for diagnosis patients of all age groups. Despite the fact that MRI gives an idea of the organizational structure it lacks any information about physico-chemical state of the tissue. Therefore, perhaps the most significant development in MRI was the discovery of the blood oxygenation level-dependent (BOLD) contrast and the subsequent development of functional magnetic resonance imaging (fMRI) (Ogawa et al., 1990). The dHb is restricted in the intracellular space of red blood cells, which in turn are restricted in blood vessels, and these facts allow us to reach a good visualization by using MRI. Previous investigations (Duong et al., 2002)[paraphrased] have shown that "*gradients of magnetic fields can be induced by* differences in *susceptibility between sections that contain deoxyhemoglobin and their*

encompassing volume". Such inhomogeneities have a strong effect on another relaxation process called T_2*, which permits imaging of blood vessels. Ogawa noticed that pulse sequences that are sensitive to inhomogeneity differences, generate signal-dropouts whenever the concentration of dHb increases. In his study, he manipulated the O_2 content of the air breathed by rats and demonstrated the strong effects of oxygenation on T_2* contrast.

In practice, the usual signal enhancements are present because that neural activation elicits hemodynamic responses that increase regional oxygen slightly more than needed as Raichle and Fox showed with their studies (Fox et al., 1988). Notably, during neural activation the BOLD signal is actually increasing rather than decreasing. the activation within a brain region causes an increase in blood flow and the use of glucose, but not a commensurate increase in the oxygen consumption rate. Thus, increased blood flow results in a smaller fraction of dHb, less signal loss and BOLD signal can be easily recognized. Although this contrast is widely used, many basic questions regarding the neural, glial and vascular events underlying the hemodynamic responses still remain.

1.4 Functional MRI and neural activity.

BOLD contrast has been a real splash in basic research, in particular in neural and cognitive sciences. Functional MRI relies on the tight relationship between brain activity, metabolism and blood flow. Changes in regional activity increase energy metabolism, and therefore, for the functioning of neural networks, it is necessary to provide a high flow of oxygenated blood to the active area in order to satisfy the need for more oxygen (hemodynamic response). This process is initiated by the expansion of nearby microvessels (the microvasodilator effect). Changes in blood oxygenation as well as tissue perfusion have different effects on relaxation time and can be used to create image contrast (Logothetis and Pfeuffer, 2004).

As mentioned above, BOLD is directly related to the level of blood oxygen saturation, which allows to perform functional neuroimaging. BOLD-fMRI has a significant number of advantages, the most important of which are high spatiotemporal resolution, and the ability to visualize the entire network of brain regions in parallel with the simultaneous performance of certain tasks by the subject of the study,

although functional activations can also be detected through direct measurements of perfusion, blood volume or water diffusion Moreover, BOLD is often used to generate functional connectivity maps. In order to create such networks, BOLD is recorded in all brain voxels and then a cross-correlation analysis is performed to find out which structures have correlated activity at the same time-points. These correlation scores are then put into correlation matrices among brain regions and by using threshold, a network can be generated of correlated regions. The same principle is applied for brain responses to stimuli and for brain at rest. All this makes the fMRI, one of the leading tools for studying cognition. The method appears therefore to have, in principle, the potential to address critical questions, including those about cortical organization and functioning, dynamic neuronal changes during learning and recovery from injury, and about the relation of perception, cognition, emotion and consciousness to brain activity. Today, MRI scanners can be found on site at virtually every institution, it is therefore not surprising than a growing number of investigators see this technique as an essential tool that complements their behavioral studies. However, fMRI is not a universal key to many questions. For example, using fMRI alone, it is impossible to understand the structure of a local microcircuit, what is the cellular basis of the BOLD signal or what neuronal and neurochemical processes are associated with functional connectivity networks. Other questions are what is the underlying neurobiology of a resting state or which transmitter systems relate to those changes in network connectivity in disease that are different from healthy state?

The neurometabolic coupling depends on various processes in addition to neural activity patterns such as dynamics of neurotransmitters and neuromodulators, vascular constraints, astrocyte activity, pericytes and capillary control mechanisms and signaling processes, as well as volume transmission, i.e. the release of neurotransmitters and modulators from axonal vesicles in the pericellular space, in parallel and often independent of synaptic transmission. We already have some good ideas about how BOLD signal relates to neural activity. In 2001, Nikos Logothetis presented a study, in which he used intracortical recordings of neuronal signals at the same time with a fMRI response from a visual cortex in macaque monkeys (Logothetis et al., 2001b). In order to reveal the neural origin of the BOLD signal, Logothetis and his colleagues analyzed how BOLD signal correlates with different

classes of neural activity, particularly the local field potentials (LFP) as well as single- and to multi-element activity (MUA). By simultaneously recording intracortical electrophysiology and neuroimaging, he demonstrated that increase in BOLD signal obtained from visual cortex of monkeys well-correlated with LFP signal. Logothetis and his colleagues have further demonstrated an anatomical specificity expressed as a gradient from cortex towards subcortical brain regions (Logothetis et al., 2012a). These differences could have been generated via complex interactions at network level between different brain regions. Since cortical and subcortical regions have different cytoarchitecture and microcircuits, the locally observed correlations are more likely caused by excitatory, inhibitory and modulatory feed-forward and feed-back loops in different brain areas and even different cortical layer networks.

All in all, as Logothetis stated in his seminal review in Nature (Logothetis, 2008)[pages 876-877]: "*it is a sheer fact that fMRI signal cannot differentiate between function-specific processing and neuromodulation, between bottom-up and top-down signals, and it may occasionally confuse excitation and inhibition, as the latter can be directly on projection neurons or on interneurons, the activity of which is metabolically expensive, and can primarily drive the BOLD signal. In addition, the magnitude of the fMRI signal cannot be quantified to accurately reflect differences between brain regions, or between tasks within the same region. The origin of the latter problem is not our current inability to accurately estimate CMRO2 from the BOLD signal, but the fact that hemodynamic responses are sensitive to the size of the activated population, which may change as the sparsity of neural representations varies spatially and temporally*".

The aforementioned interpretation-ambiguity is not unique and specific to the MRI signals. For that matter, the interpretation of neural and neuroglial signals at all scales, as well as their combination can be characterized as an 'ill-posed' problem, a definition introduced by the French mathematician Jacques Hadamard. He correctly suggested that not all mathematical models of physical phenomena have a unique solution, that changes predictably and continuously, depending on initial conditions. Some are not well-posed and can be described by more than one solution, yielding multiple interpretations under the same conditions. What follows offers a brief description of signals and scales.

1.5 Signals, circuits, scales and strategies aiming at ambiguity reduction

As mentioned above, fathoming into the actual mechanisms of self-organization of a complex dynamic system (CDS), like the brain, strongly depends on learning to interpret neural activities recorded concurrently at different spatial and temporal scales. Dominant structural brain-attributes, that have been observed and scrutinized by very many scientists over many years are the ***modularity*** and ***nestedness*** that yielded the concept of so-called multiscale connectivity.

The former, stemming from Gall's speculative phrenology, followed by Brodmann's outstanding anatomical work, which yielded distinct function-specific regions or areas (e.g. sensory, motor, associational, etc.) has long been crucial for neuroscience, albeit at a rather large scale. Yet, following the groundbreaking studies of Camillo Golgi and Santiago Ramon y Cajal in the late nineteenth century, the studies of Vernon Mountcastle, David Hubel and Torsten Wiesel introduced the notion of cortical modules, subsequently experimentally and computationally described by Ron Douglas and Kevan Martin as ***canonical microcircuits*** consisting of nested positive and negative feedback loops, dubbed as "*recurrent circuits*". The detailed structure of such circuits is of fundamental importance for the understanding of local functional specialization, as well as the global interareal and interstructure communication. Networks with high modularity have dense connections between the nodes within modules but sparse connections between nodes in different modules.

Nestedness, on the other hand, initially introduced in ecology in an effort to describe the patterns of distribution of species in isolated habitats, refers to the structural constellation of multiscale subregions of complex networks. Studies in many of the aforementioned fields, including ecological organizations, genetics, neuroanatomy and neurophysiology, demonstrated a tendency for network-nodes to interact with subsets of all potential interaction partners of better-connected nodes. An exquisite example of nestedness is the aforesaid cortical recurrent circuits. The modularity of such microcircuits goes beyond scales and leads to nested hierarchical structures.

In general, multi-scale modules permit fast and optimized the allocation of information between brain areas. Thereby, similar tasks and feedbacks to stimuli are

processed within the modular structure. Last but not least, the structural recurrence of canonical microcircuits is likely related also to so-called functional nested oscillations, best known phase-amplitude coupling, whereby the amplitude of a faster rhythm is coupled to the phase of a slower one.

Connectivity, in other words the level and type of connectedness within a brain-like system, is currently considered to be a critically important transformative concept in understanding and describing complexity at a level that permits fathoming into the system's self-organization, and the state-dependent emergent behavior. The comprehensive map of neural connections, often seen as a dynamic wiring diagram, is designated as connectome. All three concepts, namely modularity, nestedness and connectivity (or connectome) share one pronounced characteristic: ***multiscale and multidisciplinary nature***. ***Microscopic, Mesoscopic & Macroscopic levels***, as well as their combinations in multiscale and multidisciplinary studies, are currently the dominating paths for a detailed and promising study of brain connectivity in all animals.

The ***Microscopic***, often even Nanoscale-level, connectome is confined to the investigation of small local circuits, describing connections between individual neurons at the synaptic level, and has successfully yielded electron microscopy-based whole brain connectomes in C. elegans and zebrafish larvae.

The ***Mesoscopic*** level, on the other hand move one spatial-step ahead and offers certain type of information from microcircuits and their interactions. As previously expressed (Logothetis, 2003)[paraphrased], if "*a sufficiently small sensor is at close proximity of the surface of a neuron or its soma, then we are capable of directly record spikes and interneuronal communication over time. Yet, if the distance between the sensor/microelectrode and the neurons increases, one is not anymore measuring signals from a single cell but the weighted average of electrical activity of a population of neurons, which is called the "mean Extracellular Field Potential (mEFP)". The averaging paradigm as well as the superposition principle, which in turn depends on orientation-dependent conductivity, make it very difficult to properly understand and interpret the mEFPs."* Yet, despite all these structure-, site- and size-dependent complications, the mEFP is remains a highly important neural signal in

basic, translational and applied research, yielding some insights (however ambiguous they may be), into multi-unit activity (MUA) and local field potentials (LFP) that are indicators of modularity, nestedness and interstructure-relationships.

Correct interpretation of the aforementioned micro- and mesoscopic signals can be significantly enhanced by simultaneous monitoring of the ***Macroscopic*** signals and macro-connectome, which provide us with information related to interarea and interstructure interactions. Examples of macroscopic signals are those measured by means of Electroencephalography (EEG), Magnetoencephalography (MEG), Positron emission tomography (PET) and the aforementioned fMRI that is most appropriate and promising, given its precise spatial localization, signal-quality, and its potential combination with MR spectroscopy and diffusion imaging.

The combination of micro-, meso- and macro-scale recordings may reduce but does not eliminate the ill-posed nature of collective neural signals. Concurrent measurements of neurotransmitter and neuromodulator concentration-changes, in contrast, may offer true insights into signal-interpretation, by permitting – for example – to some extent the dissociation of excitatory and inhibitory neural activity, the discrimination of signals propagating from sensory thalamus to cortex versus those originating in modulatory thalamic nuclei, such as the reticular thalamic nucleus (RTN), known for inducing the up-down states during slow-wave sleep, characterized by correlated modulation of Excitation and Inhibition, and by uncoupling synaptic from volume transmission, whereby the latter refers to the extrasynaptic release of neurotransmitters from the varicosities of axons containing granules filled with various neuro-substances. Successful implementation of rapid real-time methods that can record chemical signals with almost the same pace used in neurophysiological recordings, and combine them with MRI is likely to initiate in-depth studies of functional brain-organization. The first part of this multidisciplinary-multimodal project, presented in the thesis, addresses primarily but not exclusively the following questions:

[1] What is the Time-Frequency Profile (TFP) of each neurochemical signal following visual stimulation?

[2] What is the TFP of each neurochemical signal around strong spontaneous signal deflections, as of now dubbed as Chemical-Event-Triggered Trials, i.e. CET-Trials.
[3] Can we successfully detrend the Chemical Signals from the Induction of the corresponding electrophysiological signal?
[4] Does the degree of cross-correlation of CET-Trials depend on brain-state?
[5] What are the **CET**-**BOLD** and **CET-LFP** profiles
[6] What is the Glu and GABA TFP in CET-Trials triggered by well-known events, such as thalamic/cortical Spindles, Sharp Wave Ripples, or Gamma-Frequency- or Gamma-Amplitude Increases, along the lines of research with fMRS-fMRI
[7] What is the relationship of Glu/GABA to the positive & negative BOLD (PBR, NBR)
[8] What is the multistructure activity pattern in the case of CET-fMRI

1.6 Main approach in this thesis

The preceding thoughts elucidate the rationale of the Neuro-Chemistry project, that is of the effort to optimize concurrently engaged electrophysiological, neurochemical and MRI methodologies, in order to open up the road to a better understanding of the dynamic connectivity and neurophysiological activity underlying the behavior of animals trained to perform a variety of cognitive tasks. While the coupling of neurotransmission and neuromodulation to signals reflecting micro- and mesoscopic activities is critically important, in the first phase of this project, we chose to begin our investigations by concentrating on the synergistic electrical and chemical interactions underlying the dynamics of the BOLD-fMRI signal. Among others, understanding the relationship of BOLD-changes with the temporal profile of neurotransmitters may prove to be more effective due to the slower dynamics of the vascular responses.

Surely, the effects of various neurotransmitters and neuromodulators on the BOLD signal, can be also studied by utilizing pharmacological fMRI (phMRI), namely by assessing vascular responses to sensory stimulation, task-related activity or resting-state modulation, following relevant drug administration. For this purpose, different functional MRI methods including CBF-, CBV- or BOLD-fMRI can be applied to measure changes in cerebral perfusion, and gain insights into the effects of various pharmacological compounds on brain activity. On the one hand, changes in hemodynamics can be measured in response to the acute administration of

neuropsychiatric drugs (‘challenge phMRI’). On the other hand, the techniques also allow us to explore neurochemical mechanisms that relate to other process such as cognitive tasks.

Neuropsychiatric drugs, for instance, can be administered intracerebrally or systematically and changes in BOLD responses can then be assessed. Yet, such approaches are limited in scope and are highly variable (Mervin et al., 2020). Drug administration at the wrong time or in the wrong position will lead to unpredictable and non-representative results as changes in network dynamics depend strongly on where and when they were induced. Furthermore, the drugs themselves may change signal properties or interfere with the whole recording process. Drugs can also be harmful or even toxic, which further limits the range of application of pharmacological approaches. Most importantly, even in the best case of an optimal experimental design, the drug administration will not help in the understanding of activities of neural microcircuits and is unlikely to contribute into the resolution of the ambiguities underlying electrophysiological responses.

We therefore chose to characterize the multilayer basis of micro- and macrocircuits of functional connectivity networks and understand the neurochemical basis of hemodynamic response by recording all three categories of signals (i.e. neurochemical, neurophysiological and BOLD) at the same time, with comparable time resolution, and in the same space dimensions. Since the technology for concurrent neurophysiological and functional neuroimaging recordings has already been established, the key question, which formed the technical basis of this thesis, was how to add and integrate scale-consistent measurements of neurotransmitter concentrations into the existing methodology. There are currently a few techniques available that allow us to measure neurochemical changes *in vivo* and can help to determine spontaneous and stimulus-induced temporal changes of transmitter concentrations associated with neural activity within a region of interest (ROI).

***In vivo* microdialysis sampling** is probably the most prominent of such techniques. This method was introduced in the late 1950s and can be used to deliver exogenous compounds to the specified area, as well as adsorption and filtration unbound concentration of compounds from the brain or tissue (Kho et al., 2017). The general

principle is that a probe (of 280-300 µm diameter) with a semi-permeable membrane at its tip is inserted into a region of interest. The ROIs needs to have a length of at least 1 mm in one spatial direction, so that the measurement is specific. A fluid, similar to the cerebrospinal fluid (CSF) is then perfused into the probe, which helps collecting the osmotically diffused transmitters etc (into the probe) in dialysate solutions. Unfortunately, this method has a significant number of limitations. Indeed, the most critical problem with this technique is the time-resolution of the measurements. Although it is possible to assume the neural origin of the measured transmitters, the concentration of the obtained dialysate cannot be accurately associated with neural activity. This is largely due to the difference in measurement time scales since dialysate are often collected in intervals of tens of minute, while neural activity is recorded in millisecond scale. Although recent progress in microdialysis (Kennedy, 2013) indicates that in vitro the technique can potentially be used for sub-second observations, most in vivo microdialysis experiments are conducted with sampling rates ranging between 5 and 30 minutes (Noori et al., 2018). This is not sufficient to explore and investigate dynamical relationships between neurochemistry, and neurophysiology or BOLD, which both are processes occurring in far more refined time-scales. In addition, the size of the microdialysis probe presents a further limitation. Given the size of the brain of laboratory rodents, microdialysis measurement is restricted to relatively large brain regions and numerous functionally critical brain areas such as the habenula or thalamic subregions cannot be targeted accurately. Moreover, the implantation of a probe of this size has a great traumatic effect (Noori et al., 2018), which limits its use to often only one brain region per experiment.

Another strategy that can be pursued is to use magnetic resonance spectroscopy (MRS) to estimate glutamate and GABA levels in the brain. The 1H-MRS is a technique that allows us to observe absolute neurochemical levels in a non-invasive manner (Oz et al., 2014). In a recent study (Ip et al., 2017), combined fMRI and MRS was performed to correlate absolute glutamate levels with BOLD dynamics in response to visual stimuli. Such non-invasive acquisitions of neurochemistry and hemodynamics are very appealing. This methodology however, is not sufficiently sensitive to monitor basal excitation-inhibition (glutamate-GABA) network dynamics, suffers from the general limitation of 1H-MRS and thus cannot distinguish intra- and

extracellular levels. In this thesis, we intended to characterize how the different activity of glutamate and GABA neuron populations generate BOLD patterns at rest or stimulus-induced states. As the authors argued, their method could only find glutamate changes when visual stimulus was present. Therefore, this technique, at least at this stage, is not appropriate to answer the question of this thesis. In addition, it is unclear whether the method can reliably measure glutamate and GABA changes at the same time with the same accuracy.

An alternative to the above-mentioned methods for detecting neurotransmitters would be the electrochemical biosensors, in particular voltammetry (when neurotransmitter reacts to an enzyme-based layer, which leads to a change in the electrical potential), or amperometry (when the neurotransmitter reacts to an enzyme-based layer and induces an electrical current that can be measured). Electrochemical sensors follow the so-called Cottrell equation (see methods section) and therefore, in principle can be of arbitrary size, temporal resolution and highly selective to specific neurotransmitters.

Probably the most common type of ***amperometric sensors*** is the peroxidase-based one. On the surface of such sensors, through the interaction of 1 transmitter molecule with the enzyme layer, peroxidase in produced, which in turn by applying an appropriate electrical potential on the electrode contact (for example 600 mV for platinum) transforms into 2 electrons and water. It should be noted that the size of such probes is usually smaller than 300 micrometers in diameter and the time-scale is in seconds. These facts made the amperometry/voltammetry method, a of promising approach for simultaneous investigation of neurotransmitter changes and neural activity on the same electrode. In recent years, there have been a few studies which successfully combined recordings of the electrophysiological activity with the measurement of neurotransmitter. The main focus of these studies was largely the concurrent measurement of dopamine (Johnson et al., 2008; Zhang et al., 2018) or glutamate alterations and neural activity (Lopez-Valenzuela et al., 2015; Wei et al., 2015). In general, the chemical signals obtained from amperometric studies are generally weak and depend on the size of the electrode (Cottrell equation gives a linear relationship, i.e. the bigger electrode the more signal). Therefore, the above-mentioned studies used comparably large contacts, which in turn would not allow

these technologies to be used for smaller brain regions such as thalamic sub-nuclei. In addition, no study on simultaneous recording of neurochemistry and neurophysiology reported GABA measurements or compatibility with MRI systems, both of which representing critical factors for the study of cellular basis of hemodynamic response.

Therefore, despite the successful use of biosensors in these studies, some factors are still unresolved: can we measure different transmitters at the same time? How can we measure GABA? Is the sensitivity of the sensor sufficient? Can we record in the MRI setting and whether the probe size can be reduced to allow NET-fMRI, i.e. multiple implantations?

Developing an experimental setup for scale-consistent, concurrent neurophysiological, neurochemical and functional imaging measurement have therefore the very real potential to unveil the mystery of the neuronal origin of fMRI. In addition, it can indeed provide insights into the underlying neurobiological processes associated with neurovascular coupling and global brain information processing that are unlikely to be obtained by using each technique alone. In particular, it would allow us to decompose the BOLD response into its excitatory and inhibitory components, which is of outmost importance for affecting brain states in animals (Noori et al., 2018) and humans (Kurcyus et al., 2018).

This thesis presents the first such simultaneous recordings using a novel combined electrophysiological-electrochemical measurement technique as well as active interference compensation methods for noise that is generated by field gradients applied during an fMRI measurement. The appropriateness of the technique for addressing the above-mentioned question was examined on somatosensory pathway comprised by primary somatosensory cortex (S1) and dorsal striatum or caudate putamen (CPu), and the primary visual system comprised by the relay-thalamus Lateral Geniculate Nucleus (LGN), the primary visual cortex (V1), and the pyramidal cell layer of hippocampus (PL). The main technical challenge of the current thesis was to construct a microscopic electrochemical multi-sensor such that each sensor is sufficiently small to fit in any brain region, and can selectively measure either glutamate or GABA, together with neural activity, remaining unaffected by the strong

interference induced by the alternating MRI gradients. Such a sensor would be theoretically possible, yet had not been realized ever before. Here, the focus was on amperometric sensors, since the MRI signal amplification systems were set to process electrical current. A solution was to modify a custom-made 16 channel MR compatible NeuroNexus electrode with a diameter of 35 micrometer such that in each brain region neural activity, glutamate and GABA could be recorded, while global brain scans were conducted (Figure1).

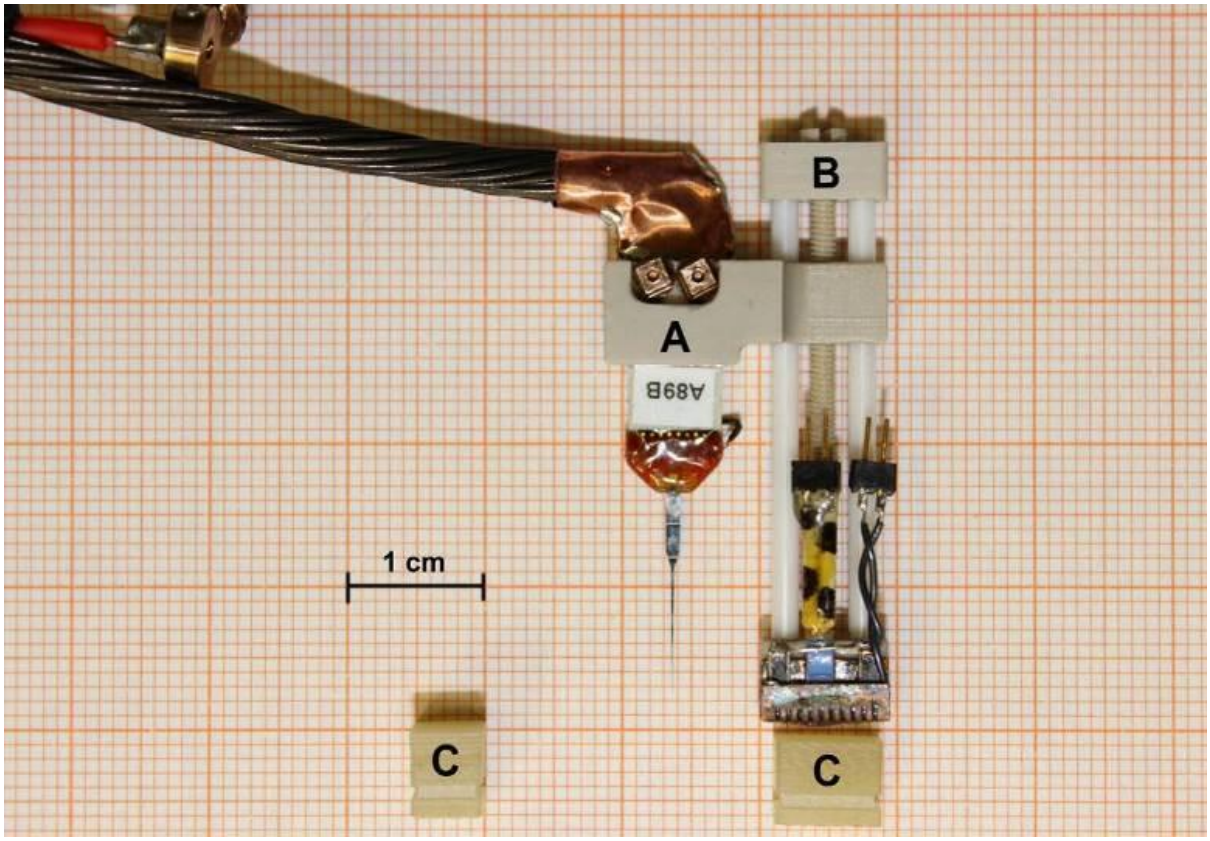

Figure 1. Photograph of the electrode (A) connected to the custom-made electrode holder (B) and a plastic platform for connecting the drive to skull (C).

The electrochemical measurement was based on peroxidase-based detection. We coated the electrode channel with glutamate and GABA sensitive enzymatic layers in an alternate manner. It means that within a voxel (1mm length) one channel was designated for glutamate, one channel was designated for GABA, one channel was designated neural activity and a channel acted as reference. The reference channel was critical, as it could show potential systemic noise or interference for instance induced by the interaction of other chemicals with the electrode (Qin et al., 2008).

First, we conducted in vitro sensitivity tests on the electrode to demonstrate the general feasibility and power of the system. Modification of amplifiers and the setups for dual recording of neurophysiology and neurochemistry from multiple channels were successful. We also optimized enzyme and electrode coating which gave us a seven-fold increase in sensitivity to glutamate on a ~10 times smaller contact surface (35 µm vs 343 µm) in comparison to a recent study for on glutamate amperometry (Zhang et al., 2018).

The same was also done with the GABA electrodes, which showed excellent sensitivity to GABA, but negligible Glutamate-sensitivity. We have also optimized the experimental procedure with respect to the anesthesia regime. Some anesthetic agents, such as the isoflurane have a strikingly negative affect on the neurovascular coupling and therefore, reduce the signal to noise ratio for BOLD measurements. We also selected the type of sensory stimulation, with the strongest measurable effect on both chemical signal and Multi-Unit-Activity (MUA). Moreover, we demonstrated that our signals of interest arevery stable in the challenging MRI environment. Generally, the gradients may induce large enough electrical potentials on the contacts, thereby changing the sensitivity of our detection method. However, we can demonstrate that fluctuations larger than 50 mV are necessary to alter the results, which does not happen in our case. In summary, our method allows us to simultaneously record electrophysiological activity, glutamate, GABA, neuronal activity and reference within one voxel and suggests different scenarios of how changes in glutamate and GABA concentrations relate to BOLD and neural activity.

Subsequent to this introduction, we offer a detailed description of the technical developments, and the ultimately applied methods. We then describe the results of the experiments in a functional order, from *in vitro* analysis of electrode sensitivity to *in vivo* tests outside the MRI scanner, over to the final measurements of all signals simultaneously. The last chapter is dedicated to discussing the method in light of previous investigations and providing an outlook for applications of this methodology.

2 Methods

Parts of this section have been previously reported in our preprint (Fathizadeh et al., 2019).

2.1 Animals. Sixty-two (n=62) adult (≥250 g, 2-5 months), male Wistar rats were used for the reported experiments. Wistar rats were selected for the experiments due to their wider skull. Moreover, Wistar rats are among the most commonly used laboratory animals world-wide (Noori et al., 2018) and this enhances the applicability and reach of this study. Animals were ordered from Charles River Laboratories (Sulzfeld, Germany) as specific pathogen free rats. In order to reduce the stress of the animals following transfer from the CR laboratories, the siblings were grouped together (groups of 3) upon arrival in individually ventilated cages. We kept a reverse light-dark cycle (8-to-8), so that we could conduct all measurements during the active period of the animals. Neurotransmitter concentrations are known to follow circadian rhythms (Magnone et al., 2003). Therefore, it is critical that the neurochemical measurements are performed consistently, when the animals are in a particular circadian state. Acclimatization period was at least 1 week. Room temperature and humidity were continuously monitored by three sensors and kept steady at (22.97±0.04°C) and (47.8±0.1%), respectively. The rats had ad libitum access to standard laboratory rat food and tap water. All animal experiments were approved by the local authorities (Regierungspräsidium Tübingen) and conducted in full accordance with the guidelines of the state of Baden-Württemberg and the European Commission. To minimize stress, all animals were weighted and transported in special non-transparent boxes with enrichment and food from the housing to the laboratory shortly before the experiment.

2.2 Reagents. In this study, a microelectrode array (see next section) was modified such that specific electrode contacts would act as amperometric sensors that contain glutamate oxidase (GluOx) as a key component. This enzyme is highly specific to glutamate (*kcat* = 75 s−1 (turnover rate) and *Km* = 0.23 mM) and with a high thermal stability of ~80 °C (Arima et al., 2009), is appropriate for *in vivo* measurements in mammals. The extracellular environment provides the necessary oxygen and water such that glutamate can be converted by GluOx into the products α-ketoglutarate, hydrogen peroxide, and ammonia (Kusakabe et al., 1983). Once an electrical

potential (often approximately 0.6 mV on platinum contacts) is applied, the side-product of hydrogen peroxide decomposes again into water and electrons that can easily be detected by amperometry. The main problem with this approach is however the high sensor fabrication costs and the rarity of commercially available glutamate oxidase and this project, as well, suffered from temporary unavailability of this enzyme, particularly due to production decline associated with Covid-19 crisis.

X-ray diffraction techniques (Arima et al., 2019) suggest that glutamate oxidase has a hexametric α2β2γ2 protein structure (figure 2A) with two funnel-shaped entrances that permit the interaction of glutamate with the deeply buried active binding site. In general, the preparation of glutamate biosensors requires certain enzyme immobilization steps, such as cross-linking, adsorption, entrapment and coating that were accurately conducted. Thereby, it is critical that GluOx is tightly bound to the electrode, while the structural and functional integrity are conserved. To this end, it is common to utilize bovine serum albumin as a stabilizing reagent and glutaraldehyde as crosslinker. Glutaraldehyde (C5H8O2) reacts with amino groups of LYS-residues on the enzyme surface and thus, crosslinks and immobilizes GluOx and bovine serum albumin on the nafion membrane. The cross-linking, in general, may lead to alterations in the confirmation of the GluOx and consequently, reduce sensitivity of the sensor and thus, it has to be conducted with special care. In addition, glutaraldehyde may lead to skin, nose, and eye irritations. This step was therefore conducted with outmost care and following high safety standards. The chemicals that were used in this study (see below) are to construct so-called first-generation sensors which have been previously (Tseng et al., 2004) shown to have fast response times and high sensitivity.

L-glutamate oxidase from *Streptomyces sp.* Expressed in *E. coli* (GluOx), GABASE from Pseudomonas fluorescens (GABA-transaminase and succinic semialdehyde dehydrogenase), ascorbate oxidase from *cucurbita sp.* (AscOx), Pyridoxal phosphate-6-azo (benzene-2,4-disulfonic acid) tetrasodium salt hydrate (PPADS), bovine serum albumin (BSA), nafion (5 wt% solution), glutaraldehyde (25% aqueous solution), cellulose acetate, L-glutamic acid (≥99%), and γ-aminobutyric acid (≥99%) were purchased from Sigma-Aldrich. Gibco Phosphate buffered saline (PBS, 0.05M;

7.4 pH) was obtained from ThermoFisher Scientific. The crystal or chemical structures of the major compounds are presented in Figure 2.

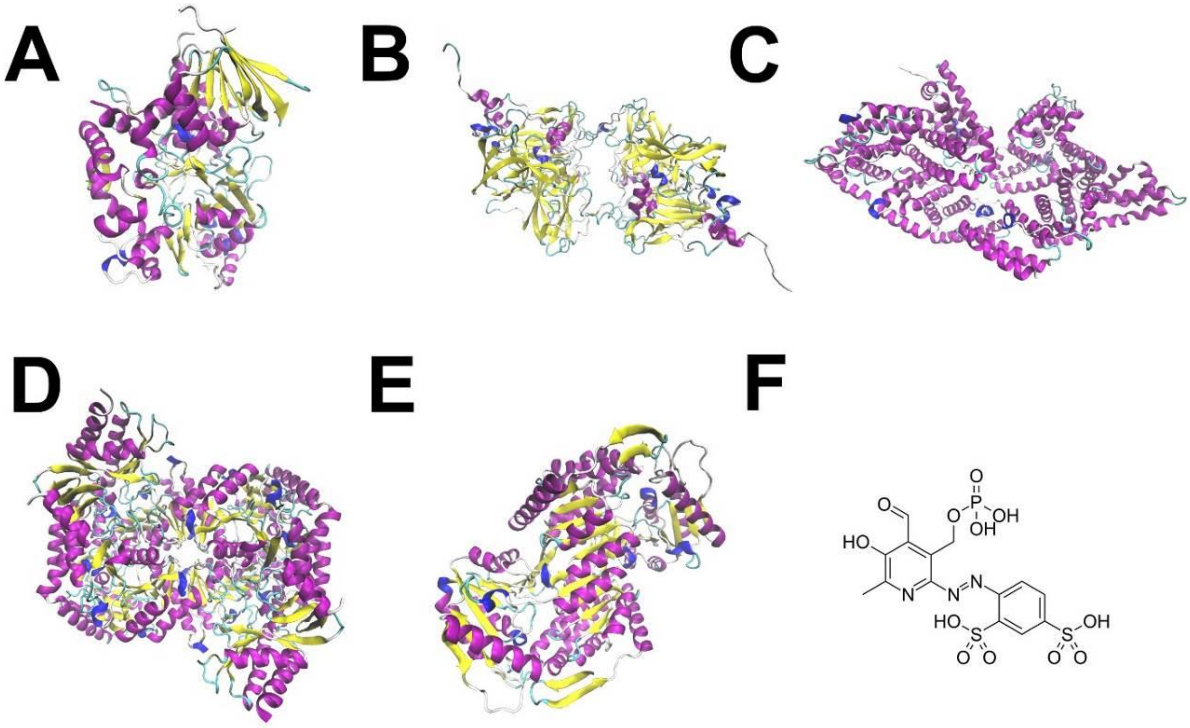

Figure 2. X-ray diffraction images (secondary structure designs) and the chemical structure of the main compounds used in this study. (A) Glutamate oxidase (2E1M) identified in 2009 by Arima and colleagues (Arima et al., 2009); (B) Ascorbate oxidase (1AOZ) identified in 1992 by Messerschmidt and colleagues (Messerschmidt et al., 1992); (C) Bovine serum albumin (4F5S) identified by Bujacz in 2012 (Bujacz, 2012); (D) and (E) refer to GABA-aminotransferase (1SZK) and succinic semialdehyde dehydrogenase (4OHT) that are used in preparation of GABAse (Liu et al., 2005) (Jang et al., 2014). (F) The chemical structure of PPADS. The codes refer to protein database (PDB) identifiers as provided by www.rcsb.org. All figures were made using the visual molecular dynamics software (https://www.ks.uiuc.edu/Research/***vmd***).

2.3 Electrodes. For simultaneous recording of neural activity and changes in neurotransmitter concentrations, custom-made silicon-based implantable ultrafine microelectrode arrays (MEA) composed of 16 iridium-stabilized contacts were used (Figure 3).

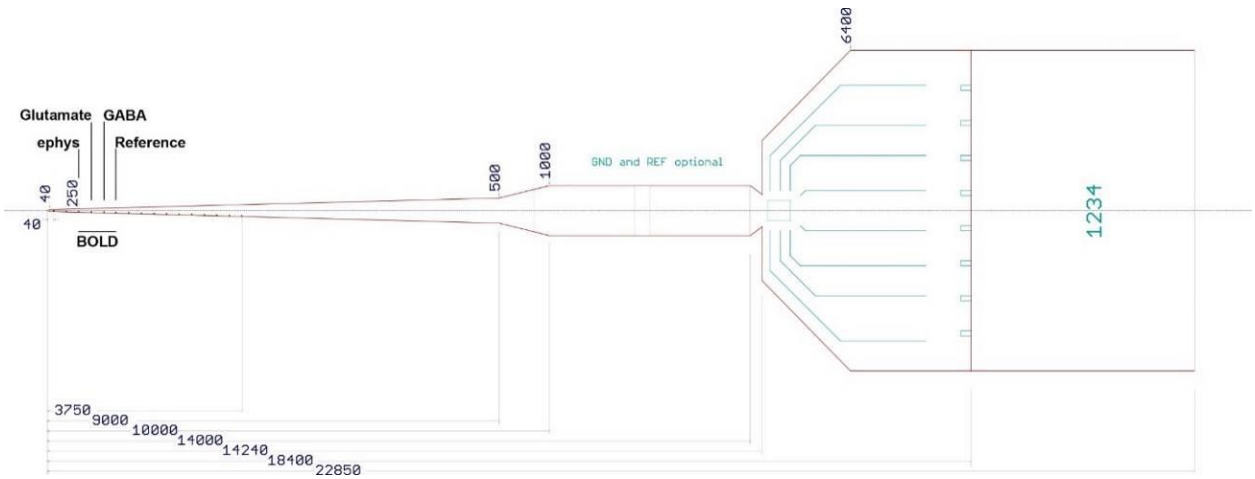

Figure 3. Layout of the custom-made silicon-based electrode (https://neuronexus.com/). The distance between each electrode channel is 250 µm. In average, the electrode contacts have an impedance of 0.5 MΩ at 1 kHz. Each channel has a diameter of ~35 µm. The ground and reference contacts at electrode top are critical for interference compensation induced by the gradients during echo-planar imaging. The designation of channels to electrophysiology (ephys), glutamate, GABA and reference is presented as an example and is predefined for each experiment, depending on the location and size of the targeted brain area with the investigated pathway. 'Reference' designates a control-channel for amperometry, which is coated identically with the other electrochemical channels with the exception that the coating mixture lacks the selective enzymes for glutamate or GABA. Therefore, it allows to detect interference by other 'unwanted' chemicals or field inductions.

The MEA has a thickness of 50 µm. Contacts on the electrode are 250 µm and have a diameter of 35 µm. Following previous investigations (Burmeister et al., 2020; Hu et al., 1994; Qin et al., 2008; Tseng et al., 2014), the MEA was modified such that specific channels operated as peroxidase-based amperometric glutamate- and GABA-responsive sensors. Electrochemical detection of glutamate is crucial for both types and occurs in the following manner. Oxidation of glutamate by GluOx produces α-ketoglutarate and hydrogen peroxide H_2O_2:

$$\text{Glutamic acid} + H_2O + O_2 \rightarrow \alpha\text{-ketoglutarate} + NH_3^+ + H_2O_2$$

The application of a potential on the iridium channel surface (Bianchi et al., 1962) (E=+0.9 V, E^0=+0.93V) versus Ag/AgCl reference, leads to gaining electrons from H_2O_2

$$H_2O_2 \rightarrow 2H^+ + O_2 + 2e^-$$

and thus, a measurable concentration-dependent electrical current (Hu et al., 1994; Qin et al., 2008). To monitor the GABA levels (Niwa et al., 1998), a dual enzyme-reaction scheme was used. First, the interaction of one GABA molecule and extracellular α-ketoglutarate with GABASE leads to succinic semialdehyde and one glutamate molecule:

$$\text{GABA} + \alpha\text{-ketoglutarate} \rightarrow \text{succinic semialdehyde} + \text{glutamic acid}$$

Second, the produced glutamate oxidized as described above by GluOx, which in turn produces α-ketoglutarate and hydrogen peroxide H_2O_2:

$$\text{Glutamic acid} + H_2O + O_2 \rightarrow \alpha\text{-ketoglutarate} + NH_3^+ + H_2O_2 \,.$$

A three-dimensional, manual, microdrop coating system was developed and used to selectively apply membrane and enzyme solution layers on specific contacts (Figure 4). This system allows us to accurately place drops of nafion and enzyme solutions selectively on each channel.

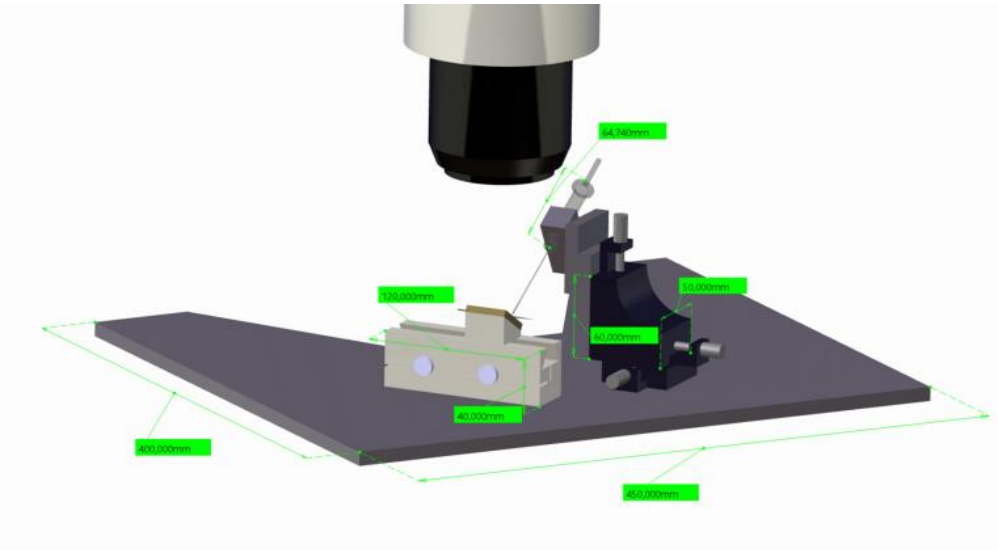

Figure 4. Schematic illustration of the 3-dimensional manipulator for targeted drop-coating of electrode channels. Nafion and the freshly prepared enzyme solutions are pulled into 0.5 µl Hamilton syringes. The very fragile electrode is fixed on a movable panel and brought to the focus area of the stereomicroscope. The manipulator allows to mechanically move the needle head right on top of the channel to be coated.

The neurophysiology channels were not modified. Channels designated as neurochemical probes were first covered by a layer of nafion (Gerhardt et al., 1984) and dried in the air for at least 10 minutes. The nafion membrane has a complex polymer structure that allows only small molecules to permeate it and due to its positive charge acts as an excellent barrier for interferences induced by ascorbate acid (Figure 5).

Figure 5. Photo of the electrode with coated channels number 14 and 15 after application and drying of in the air the coating components.

In order to monitor glutamate release (Hu et al., 1994; Qin et al., 2008), a freshly prepared enzyme solution (containing 2% GluOx, 0.3% AscOx for reduction of interference induced by ascorbic acid, 2% BSA as the enzyme stabilizer and 0.12% glutaraldehyde as the cross linker) was subsequently immobilized on the channel and air-dried for approximately 20 minutes. GluOx is a highly selective enzyme such that interference from unwanted reactions are very unlikely (Bohmer et al., 1989). To ensure the absence of non-specific neurochemical interference, we used background

sensors (i.e. sensors prepared identical to glutamate sensors but without GluOx) in close proximity (250 µm distance) of the glutamate sensors in vivo. Several mixture ratios were tested to obtain the optimal enzyme solution to measure GABA concentrations. In this study, we report findings based on a 5:1000 mixture for GluOx enzyme solution (as above) and GABASE. Following enzyme immobilization on all channels, the sensors were air-dried and immersed in PBS (pH 7.4) overnight.

2.4 In vitro Characterization. The above-mentioned electrochemical reactions result into a steady-state anodic current *I* that according to the Cottrell equation depends linearly on the neurotransmitter concentration *C,* the electrode area *A* and is inversely proportional to the electrolysis time *t*:

$$I = \frac{nFAD^{1/2}C}{\pi t},$$

with *n* denoting the number of electrons involved in the electrode reaction, *F* the Faraday constant and *D* representing the diffusion coefficient of the neurotransmitter. Therefore, a key aspect of the in vitro characterization of the sensors is to determine the sensitivity and linearity of the glutamate and GABA responses. To this end, the electrodes were placed in phosphate buffer solutions containing 1, 5, 10, 15, and 20 µM of glutamate or GABA arranged in a custom-made rotating multi-compartment carousel and a constant potential of +0.9V vs Ag/AgCl was applied. Since GABA sensors contain glutamate oxidase as well, extracellular glutamate may cause measurable interference. Thus, the neurotransmitter-induced currents on GABA sensors were compared for GABA and glutamate solutions of different concentrations to assess the sensitivity and selectivity of GABA sensors. In addition, response time were calculated as the time that the current needed to reach 95% of the steady-state (Tseng et al., 2014) and was estimated as <0.5 s. Linear regression analysis was used on the average of steady-state currents to obtain a functional relationship between induced currents and neurotransmitter concentrations as well as detection limits for the sensors.

2.5 Storage-stability of the electrodes. All our *in vivo* experiments were conducted in the day following enzyme immobilization. Many factors (e.g. issues with MRI

hardware or amplifiers electronics) may however lead to unavoidable shifts in experimental timing by up to a few weeks. Therefore, it is critical to investigate the storage stability of the modified microelectrodes. To this end, we evaluated the sensitivity of 10 sensor (kept dry at 4°C) by measuring the amperometric response current to 1, 5, 10, 20 µM of glutamate after 1, 3, 7, 14 and 21 days. Each time-point generates thereby a dose-response curve. Analysis of variance (one-way ANOVA, α=0.05) was used to statistically compare mean response values for each dose and the slope of the dose-response curves.

2.6 Concurrent recordings of spontaneous and stimulus-evoked neurochemical and neurophysiological in vivo. In the context of multimodal functional magnetic resonance imaging, gradient coils induce substantial noise on neurophysiological signals (Goense and Logothetis, 2008a; Logothetis et al., 2001a; Oeltermann et al., 2007). Moreover, the temporal changes in magnetic fields may affect the neurochemical dynamics and lead to biased observations of glutamatergic and GABAergic signal patterns. Thus, we conducted a series of 'reference' experiments in absence of external electromagnetic forces to determine the signal quality of the MEA for simultaneous measurement of glutamate and GABA concentrations and neural activity. To this end, spontaneous and stimulus-evoked activity were assessed in cortical and subcortical brain areas of 12 rats.

Before each experiment, the working area and instruments have been disinfected. All the instruments were cleaned in the ultrasonic bath (BRANSONICK CPX2800-E) with the special soap (RBS 35) and air dried before surgery. Stereotaxic system as well as working table were cleaned with disinfectant (DESCOSEPT AF). Heating pad was pre-warmed. The anesthesiologic and surgical protocols were carried out during the entire period of the experiments and all manipulations were performed according to the same principle.

Animal was placed in to the induction chamber and isoflurane gas was given in concentration of 5% with a 2:1 mixture of NO_2 and O_2 with a gradual decrease to 2%. During the whole experiment concertation of isoflurane was in the range of 1,5 - 2.5%. After the rat was under deep anesthesia (tail pinch and pedal withdrawal

reflexes were negative) head of the animal was shaved with an electric razor avoiding area around the eyes.

Whereupon the rat was placed on the heating pad with a rectal thermometer and placed/head-fixed in a stereotaxic system. The body temperature was monitored continuously and maintained at an equilibrium of 37°C. Both corneas were covered with ophthalmic ointment (in the case of CPu) to avoid retina dehydration or with a strip of cloth soaked in 0,9% NaCl solution. The fabric was moisturized regularly with 0,9% NaCl solution to prevent drying out. Before any invasive manipulation, to ensure that the rat was adequately anesthetized, tail pinch and pedal withdrawal reflexes were checked again. Operating field was treated with 7,5% Sol. Braunol (B. Braun Melsungen AG) three times from center to periphery. After that 1% Sol. Xilocain (AstraZenica GmbH) was injected subcutaneously along the skull. Bu using a sterile scalpel an anterior-posterior incision was made (about 2cm) in the middle of the scalp. Surrounding tissue has been removed to allow full access to lambda and bregma without muscle damage. Conjunctive tissue was removed with a spatula or/and cotton swab. To stop bleeding from the wound edges, a high temperature cautery kit (F.S.T. 18010-00) was used. The scalp surface was cleaned using 0.9% Sol. NaCl. For a more accurate determination of the coordinates, the positions of the Lambda and Bregma were brought to the same points from the surface of the skull. An error of no more than 0.3 mm was allowed (Paxinos et al., 1985). We used the rat stereotaxic atlas (Paxinos and Watson, 2013) to estimate the appropriate coordinates for craniotomy based on the skull size and dimensions. Then the necessary coordinates were marked on the surface of the skull. Spontaneous activities were investigated within the corticostriatal and thalamocortical pathways. Therefore, the MEA was placed in a manner that allowed the concurrent measurement of neurotransmitter concentrations and neurophysiology in both somatosensory cortex (S1) and caudate putamen (CPu) or lateral geniculate nucleus (LGN) and primary visual cortex (V1 or VCX) of the same animal. Coordinates – AP 0; LM -3,4 for corticostriatal recordings and AP -7; LN -3,7; VD 5,2 with an angle of 29 for thalamocortical recordings.

For fMRI-free experiments, visual stimulation of the retina with flickering monochromatic light was utilized. Blue (λ = 453 nm) and red (λ = 641 nm) SemiLEDs

Metal Vertical Photon Light Emitting Diodes were used to induce visual stimulation. The LED was attached to a custom-made holder and centrally placed frontal to the contralateral eye. Experiments were conducted in a dark room with lights off. A continuous stimulus was delivered at a rate of 1 for 700 ms duration and 300 ms rest, and 20 Hz for 35 ms duration and 15 ms rest. As previously discussed (Zitnik et al., 2014), the ultimate position of the microelectrode was adjusted by neurophysiological verification (ie. Characteristic neuronal firing induced by light stimuli). In both scenarios, an Ag/AgCl wire (halfcell EP08 (0.8mm dia. x 20mm), purchased from WPI-Europe) inserted into the neck muscle was used as a reference for the electrodes. Specific low-noise cables were constructed by Mr. Axel Oeltermann and the workshop of the Max Planck Institute to connect the electrodes with pre-amplification systems. For amplification and filtering of analog signals, an AlphaOmega multichannel processor (Alpha-Omega, Model: MPC Plus) was used. This setup is commonly used for neurophysiological recordings in our department. The use of a similar system was previously reported by our colleague Dr. Totah (Totah et al., 2018). The data acquisition device CED (Model: Power1401mkII) was used for signal digitalization (1 kHz: neurochemical signals; 25 kHz: electrophysiological signals) and the software Spike2 was used to monitor and store the recording sessions.

2.7 Impact of astrocytic glutamate release on measured signals. Neuroglia or glia (Greek: neuron-nerve + glia-glue) — one of the components of the nervous tissue in the brain and spinal cord, including cells of various origins, closely related to nerve cells and their processes and performing support, trophic, protective and a number of other functions, as well as playing a role in the processes of origin, transmission and conduction of nerve impulses.

Astrocytes are the most common type of glia cells, accounting for more than a half of the brain's gray matter volume. They are small stellate or spindle-shaped cells with a body diameter of 8-15 microns. Astrocytes develop during embryogenesis from neural tube epithelial cells that form spongioblasts, which turn into neuroblasts, and then into astrocytes. There are 2 types of astrocytes: *Protoplasmic* and fibrous astrocytes. *Protoplasmic* astrocytes have more processes than fibrous ones, and they branch more often; fibrous astrocytes have longer and less branched processes.

Astrocytes are involved in many regulatory processes including the modulation of concentration of extracellular neurotransmitters (Perea et al., 2009). In particular, it is known that in addition to neurons, astrocytes actively release glutamate. In our study we intend to simultaneously record neurochemical and physiological as well as BOLD signals, in particular to elucidate the cellular basis of the BOLD signal. However, the measured changes in glutamate concentrations can be of glial origin in addition to neuronal. Therefore, the measured concentrations by amperometry represent the entity of glial and neuronal glutamate. Since our major goal is to relate neural activity with neurochemistry and BOLD, it is critical to estimate the contribution of astrocytes on the dynamics of glutamatergic signals. One of the main mechanisms of glutamate release by astrocytes is through ionotropic purinergic receptors (Malarkey and Parpura, 2008). In order to determine clearly and accurately the contribution of astrocytes to the signals measured in our experiment, we reduce the glutamate release of astrocytes to a minimum. For this purpose, we first measured basal neurochemical and neurophysiological signals in anesthetized rats. Then, we intracerebrally administrated pyridoxalphosphate-6-azophenyl-2',4'-disulfonic acid (PPADS). PPADS is a selective P2X antagonist that has been shown to significantly reduce ATP-induced glutamate release from astrocytes (Domercq et al., 2006). Thus, in order to quantify the astrocytic part of glutamatergic signals, we administered 100 µM PPADS to somatosensory cortex (S1) in the close proximity (~500 µm) of the microelectrode and compared frequency and amplitude of glutamate signals as well as correlation of neural firing frequencies and the glutamate signal prior and following the intracerebral drug injection. To this end, PPADS was dissolved (protected from light) in deionized water. Identical with surgical procedures outside the MRI systems (see above).

Rats (n=8) were anesthetized with isoflurane (induction at 5%, maintenance at 1.5-2.5% combined with a 2:1 mixture of NO_2 and O_2) and then positioned in a stereotaxic apparatus. The craniotomy hole at 0 AP and -3.4 ML was sufficiently wide to permit simultaneous insertion of the MEA and an inclined. Following concurrent recording of baseline neural activity and glutamate concentration for 20 minutes, 2 µl of PPADS was injected with a flow rate of 0.05 µl/min using a Harvard apparatus pump. Signals were recorded throughout the entire experiment including the injection

period. After a break of five minutes, signals were measured to assess the post-infusion drug effects. All procedures are performed in animals under anesthesia without reawakening.

2.8 Concurrent measurements of spontaneous and stimulus-evoked neurochemical, neurophysiological and fMRI in vivo. The full potential of the present technology is to provide an in-depth understanding of the neurobiological basis of functional activation of neurocircuitries as observed by resting state and stimulus-evoked fMRI experiments. To this end, two fundamental pathways for processing sensory information in the brain, namely the corticostraiatal and the thalamo-cortical were investigated. While the corticostriatal pathway as an integral subnetwork of the basal ganglia (Noori et al., 2017) plays a key role in learning and execution of habits (Hidalgo-Balbuena et al., 2019; Smith and Graybiel, 2013, 2014), it is generally accepted that thalamic function is beyond a relay station and that the corticothalamic pathway is critical for processing sensory information(Briggs and Usrey, 2008). Due to the robustness of the signals obtained in fMRI-free conditions, these pathways were also investigated in the concurrent recordings of the neurochemical, neurophysiological and BOLD signals. If (due to technical reasons) signals could not be obtained from both regions simultaneously, data was collected from one brain area and analyzed.

For the MRI experiments, the surgical preparation of the animal was significantly different and challenging. Because of the complicated surgical preparation, with the further change of the anesthetic aid from isoflurane to fentanyl as well as the use of MRI, it was decided to use an MR compatible electrode holder. This allowed the implantation of the electrode shortly before placing the rat in the MRI while already being fixed in the animal bed. The holder is a custom-made plastic device 4 cm high with the ability to maneuver in to the Ventral – Dorsal direction (see figure 1B). The device is fixed on a plastic platform (see figure 1C) using the dental wax before electrode implantation. In turn, the plastic platform is attached directly to the skull with dental cement before craniotomy. To achieve the required angle of inclination, the edge of the platform can be trimmed, after which the platform is attached at a given angle to the skull.

Using dental cement, a funnel-shaped depression was made in the area of the proposed craniotomy to fill it up later with agar-agar during the experiment. This is necessary to prevent drying out of the brain surface while MRI scanning. Craniotomy was done by using a mini hand drill in the projection of region of interest (CPu or LGN). After the craniotomy the area was covered with a moistened in 0,9% NaCl solution sterile sponge and fixed with medical surgical tape. Animal was detached from the stereotaxis systems, the nose cannula for supplying isoflurane gas was replaced with a mobile custom made one, which allows the rat to be turned on its back. To perform catheterization of the femoral artery (for monitoring arterial blood gas levels and blood pressure) and vein (for injection of remifentanil), the animal is placed with the 'belly up' position. Area along the natural angle of the leg hind shaved and treated with iodine solution 3 times. With the help of surgical scissors, an incision of the skin about 1 - 1.5 cm long was made. If necessary a surgical retractor can be used to keep the wound. Using blunt forceps, the surrounding tissue were pushed to the side in such way, that there was a good view of the vein and artery. With an angled surgical probe, the vein and artery were separated from each other. The distal end of the vessel was overlapped with a superimposed silk ligature. A ligature is also applied to the proximal end without tightening the knot. After that, the ends of the ligatures are pulled to stop the blood flow to the sides with the help of forceps. In general, and analogous to standards for human interventions, catheters must be flushed and filled with heparin solution beforehand to prevent blood coagulation.

Using surgical micro scissors, a small incision was made on the distal side of the vessel and a catheter was inserted. Then the catheter was fixed using pre-applied ligatures (Jespersen et al., 2012). The wound was closed with a N4 needle with a cutaneous surgical suture. To avoid mechanical displacement of the catheters during further surgical procedures, a surgical tape was applied to the suture area.

After that, catheterization of the urinary bladder is performed. For this purpose, the lower third of the abdomen should also be shaved in advance. Before starting the operation, the skin must be treated with an iodine solution 3 times. Then, with the help of surgical scissors, an incision is made along the midline of the abdomen (around 1.5 cm long). The abdominal muscles are pulled to the side with tweezers. The bladder can then be gently exposed through the surgical opening. The apex of

the bladder must be stitched with a purse-string suture without tightening. A surgical clamp should be placed on the apex of the bladder (above the suture), then a mini incision is made using a micro scissors. The end of the catheter is inserted into the resulting hole, gradually unclamping the clamp. The collapse of the bladder should coincide with full insertion of the catheter. Then the purse-string suture is tightened. The wound is sutured in layers with a surgical suture.

One of the last stages of animal preparation it is endotracheal intubation. For these purposes, a custom-made guide was used, which serves as a laryngoscope. The animal was placed on a plastic platform in such way that the animals head was significantly higher. After that, the tongue was pushed aside and pressed using a mini dental spatula with a curved end. Correctly performed procedure allows visualization of vocal cords and esophagus. A plastic part from an intravenous catheter was used as the orotracheal tube (the size and length were selected individually depending on the weight and length of the rat's body) (Su et al., 2012). As a laryngoscope was used a custom-made guide with LED lighting from one end.

The success of intubation was checked using a dental mirror. The mirror was brought up to the outer end of the endotracheal tube, fogging of the mirror indicated that the procedure was carried out correctly. After that, the animal was placed in an animal bed specially made for MRI scanning. In order to obtain the optimal signal-to-noise ratio for BOLD signals, we modified an opioid-based anesthesia regimen for applications in rats that was previously shown in non-human primates (Goense and Logothetis, 2008a; Lippert et al., 2010; Logothetis, 2002; Logothetis et al., 2001a; Oeltermann et al., 2007). The MEA is then placed in the identical position as described previously for experiments without MRI. The anesthesia is then switched from isoflurane to remifentanil before placement in the MRI machine. While the continuous infusion of remifentanil (approx. 2-4 µg/kg/min) starts, a bolus of mivacurium chloride is given to relax the muscles (~ 1mg/kg), mechanical ventilation is started, a continuous mivacurium chloride injection (~ 2mg/kg/h) provided and isoflurane gradually reduced. Monitoring vital signs ensures that a sufficient depth of anesthesia is guaranteed at all times. With the measurement of the arterial blood gas values, the ventilation is optimized with regard to the arterial CO_2 (or pH) and O_2 content using the ventilation parameters. A custom-made saddle coil integrated with

an animal holder (RAPID Biomedical, Rimpar, Germany) is placed on the prepared skull of the anesthetized rats and the electrode is inserted into the brain.

MRI measurements were performed on a Bruker “ultra shield refrigerated” system BioSpec 70/30 with 7 Tesla magnetic strength (software version ParaVision 5.1). Based on the robustness of these experiments, the imaging parameters were taken identically. First an area of interest was defined and field maps were acquired. The area of interest in our experiments contained the whole rat brain with exception of cerebellum. Subsequently, the local field homogeneity was optimized. To study the time course of the BOLD signal and directly compare it to the neural and neurochemical responses, fMRI was carried out with a gradient-echo echo-planar imaging (GE-EPI) sequence: *field of view (FOV) = 24 × 20 mm^2; slice thickness: 1 mm; matrix = 60 × 50 yielding an in-plane voxel dimension of 400 × 400 µm; segment = 1, flip angle (FA) = 45°, TR = 1000 ms, TE = 17 ms yielding a temporal resolution of 1 s, with interleaved acquisition of slices. An anatomical reference scan was acquired using a* T_2*-weighted rapid acquisition relaxation-enhanced (RARE) sequence: field of view (FOV) = 32 × 32 mm^2; matrix dimension (MD) = 400 × 400, yielding an in-plane voxel dimension of 80 × 80 µm; repetition time (TR) = 6000 ms, echo time (TE) = 40.2 ms*. During the entire experiment the CO_2 and O_2 content are monitored and, if necessary, corrected via the tidal volume. For each animal, three conditions were studied.

Each condition consisted of 10 segments of 6 min length. For the corticostriatal system, first, spontaneous (resting state) activity presented by whole-brain BOLD, and bi-regional neurophysiology and neurochemical signals were measured. Second, an innocuous forepaw stimulation (5 Hz, 1 mA) was applied in a block design (12 periods of 6-s stimulation epochs, followed by resting epochs of 20 s) such that it leads to robust somatosensory activation but does not induce pain or stress(Bosshard et al., 2010; Reimann et al., 2018; Schroeter et al., 2014), thus minimizing co-activation of other neurocircuitries. Third, post-stimulation spontaneous activity was recorded to investigate the potential adaptive impact of the electrical stimulation on the signal dynamics. For the visual system, first, spontaneous (resting state) activity presented by whole-brain BOLD, and neurophysiology and neurochemical signals in LGN, hippocampus and V1 were measured. Second, a

flickering white light stimulation (4 Hz) was applied in a block design (2/10/40, 7 volumes, 50 ms) was applied that has been previously shown (Hinz et al., 2019) to activate the visual system significantly. Third, post-stimulation spontaneous activity was recorded to investigate the potential adaptive impact of the electrical stimulation on the signal dynamics.

2.9 Electrodes & amplifiers for simultaneous fMRI and multi-site amperometry and recordings. The MRI-compatible recording hardware and visual stimulation setup for rats, were developed by Mr. Oeltermann, mechanics and electronics workshops of our institute. Neurophysiological recording and amperometry within the scanner required active compensation of the gradient interference. The early version of the compensation hardware has already been introduced in previous works by Logothetis department (Logothetis, 2002; Logothetis et al., 2001b; Oeltermann et al., 2007).

In order to avoid repetitions of known facts, we only briefly summarize the critical steps that were developed for current experiments. As described above, the electrodes with 16 channels were custom-made design produced by NeuroNexus. To minimize gradient interference, two small iridium paddles (2 mm^2 in size) were placed to the side of the electrode chunk right above the scull; one serving as the ground contact and the other as far interference (FI) sensor. Contact to the brain was made through agar mixed with saline (0.9 NaCl) forming a small bulbus above the burr hole. The FI sensor signal was fed to a proportional-integral (PI) controller, the output (PIout) of which was connected via a low-resistance electrode to the animal's head remotely positioned from the electrode. The FI sensor signal was used to calculate a noise-cancellation voltage so that interference signals detected right above the burr hole for the electrode could be reduced to zero. The response time of the circuit described above was approximately 0.5 microseconds and thus, shorter than the transient slopes of the switching gradient fields.

An important feature of the current hardware compared to commercially available pre-amplifiers is its insensitivity to cross-talk, a critical property for measurements with multiple contact electrodes. Elimination of cross-talk was accomplished by measuring currents at the electrode and converting them – through the pre-amplifier -

into voltage signals under conditions of zero voltage drop across the electrode tips. The amplitude of currents is typically too small (pA) to induce magnetic coupling between contacts. By ensuring that the voltage drop remains zero, the capacitive coupling between the electrode lines is also kept to a minimum. The output voltage of the current-to-voltage converter is subsequently pre-filtered, amplified, and then transmitted to the remote main amplifier. The voltage signal is high-passed at 0.5Hz with a 1st order and low-passed at 5.5kHz with a 3rd order Bessel filter, then amplified with an adjustable gain. The output signal was connected to a 16bit AD card (PCI-6259; National Instruments) set to 31.25 kS/s for collecting broadband neural signals, working electrode (WE) amperometry signal, including local field potentials (LFP), spikes and the residual interference signal used for the final off-line denoising of all neural signals.

The amperometry signal turned out to be largely free from interference signal, so that no subsequent signal correction was necessary. Out of the 16 available electrode channels, up to 4 were designated for amperometry measurements. In order to use the amperometry channels concurrently and simultaneous with electrophysiological recordings on the other channels on the same electrode (while using the same ground contact), we follow a different strategy than classic amperometry electronic circuitry. The new circuit has the advantage that the ‘counter electrode’ (CE) can be used as well by the recording amplifiers as ground contact. Moreover, the different amperometry channels share only one CE and one reference electrode (RE). This adjustment does not induce any measurement errors, since the animal tissue impedance and the impedances of the ground, the CE and RE are orders of magnitude smaller than the impedance of the ‘working electrode’ (WE) channel and the recording channel. Their contact areas on the electrode have approximately 30-35 µm diameter. Therefore, any voltage drop appears only in the proximity of the electrode contacts, which prevents interaction/cross talk between channels. A separate ‘reference electrode’ (RE) can be used to precisely measure the DC voltage of the tissue close to the electrode chunk and correct the WE DC-level accordingly. Another advantage of the new circuit is that the chemistry components are not part of a regulator loop. Thus, no regulator parameter adjustments needed and no speed limits are given. Another feature of the amperometry pre-amplifier is that its ground is floating, therefore this amperometry amplifier can be easily combined without ground

loop problems with commercial electrophysiology recording amplifiers located outside the MRI scanner, whose ground is often internally connected with safety ground. In this case the animal ground can be chaired by the two systems, while the RE can further serve for differential recording.

2.10 Pre-processing the multi-modal data. Analyses of physiology, neurochemical and fMRI data were all performed using custom-written MATLAB codes by Logothetis and colleagues (Maier et al., 2007). To use this package, a description file was provided for each session, which contained experimental parameters such as number of animals, experiment, date, data on positioning and layout of the electrode, grouping of experiments and anatomical scans allocations. Processes for signal denoising, conditioning, band separation and application of general linear model (GLM) using regressors derived from the neural data are the result of many years of work by Logothetis and his co-workers and have been presented in detail in previous publications (Goense and Logothetis, 2008b; Logothetis et al., 2010; Logothetis et al., 2001b). Here, I summarize the basic concepts and main steps of signal-processing and will then focus on the procedures used for the detection and identification of neuronal and neurochemical events and the implementation of neural-event-triggered and chemical-event-triggered fMRI.

The specific design of the electronic circuits (by A. Oeltermann, MPI Biol Kyb) that were described above allow us to minimize the electromagnetic interference on neurophysiological signals but do not completely diminish them. Therefore, additional pre-processing steps are necessary to obtain 'clean' signals. To eliminate the remaining interference, we followed Logothetis and colleagues (Logothetis et al., 2001b) and used principal component analysis (PCA). This is a critical method to significantly reduce the dimensionality of the time-series in an interpretable manner, while it largely allows to conserve the data content. It is the oldest and most frequently used technique that, in general, is comprised by five steps:

1. Standardization of the data: This step is done by subtracting each value from the mean of the data and then dividing it by the overall standard deviation in the data set. This is important since not every dataset is normally distributed. The standardization transforms the dataset (without losing its statistical

features) into a so-called empirical process, which is normally distributed at zero with standard deviation 1. It is noteworthy that for understanding the difference in neurotransmitter concentrations, we used the raw signal without any normalization, since z-Scoring clearly eliminates any differences due to different concentration in different conditions.

2. Computing the covariance matrix: If p is the dimension of the dataset, the covariance matrix is a pxp-matrix, such that each matrix element represents the covariance of the variables.
3. Calculating the eigenvectors and eigenvalues: This step allows us to decompose the dataset into main and independent components.
4. Computing principal components: In this step, the eigenvectors are sorted by their eigenvalues in descending order. Thereby, the eigenvector with the highest eigenvalue is considered the most significant one and therefore, defines the first principal component. The dimensions of the data are then reduced by removing those principal components that have lower eigenvalue and thus are of lesser significances.
5. Reducing the dimensions of the data set: The final step is rearranging the original data according to the highest-ranked principal components.

Here and as expressed previously by Logothetis et al (2001a) [paraphrased from page 156], "*first, the time-series were transformed into an nxm-matrix, with n representing the product of segments and slices and m denoting the length of the time-series. To this end, the signals were aligned along the slice-selection pulse. Subsequenly, PCA was used to eliminate the components that mostly correlate with interference as measured directly by current-monitor output of the gradient amplifiers. The final outcome is a denoised broad-band (0.05 Hz – 7 kHz) signal that is denoted as 'clean' signal (Goense and Logothetis, 2008b; Logothetis et al., 2010; Logothetis et al., 2001b). This time-series formed the basis of subsequent signal domains such as the the local field potential (LFP) and multiple unit activity (MUA).*"

The processes of band-limited power (BLP) separation and signal filtering are best described in (Logothetis et al., 2001a).

Important is to note the following fact: The neurochemical signals are largely free of MRI-interference, yet the recordings from the amperometric channels contained weak traces of low-frequency neural field inductions. Traditionally, techniques such as Fourier- or wavelet analysis are used to investigate periodicities in neuronal time-series. The continuous wavelet transform is a method for decomposition of signals into so-called wavelets that represent temporally localized small oscillations. If the data is non-stationary, Fourier transform is often inappropriate because it largely ignores all time-localization information and only decomposes the time-series into series of sine and cosine functions. Continuous wavelet transform is based on scaled and shifted variations of the time-localized wavelet such as Morse or analytic Morlet/Gabor wavelet families and is therefore utilized not only for reconstruction of a signal with a high temporal and frequency resolution but also to investigate whether a signal is stationary at all. By mapping the alterations of properties of non-stationary signals, it can further characterize stationary and non-stationary components of the time-series.

However, the amperometric signals are non-stationary and non-linear and wavelet analysis alone cannot fully decompose all important features. The Hilbert-Huang transform or HHT (Huang et al., 1996; Huang et al., 1999; Huang et al., 1998) provides an advanced tool to extract local features from such signals. In brief, the HHT first utilizes the empirical mode decomposition (EMD) algorithm to decompose the signal into several intrinsic mode functions (IMF) and by using Hilbert transform on each IMF it obtains several features. The signal then translates into an energy distribution in time-frequency domain (Hilbert spectrum). These features, particularly, instantaneous amplitude (IA), instantaneous frequency (IF), as well as instantaneous energy density (IE) in Hilbert spectral analysis can be used to classify different modes of the neurotransmitter dynamics. In this thesis, the EMD procedure was used to characterize different oscillatory modes of glutamate and GABA dynamics, in order to causally relate the neurophysiological and neurochemical events. As introduced by Norden E. Huang (Huang et al., 1996; Huang et al., 1999), intrinsic mode functions or IMFs are a generalization of the harmonics-base functions and are obtained through an iterative “sifting” process. The IMFs are defined by two criteria (paraphrased from (Huang et al., 1999) [paraphrased from pages 423-426]): “*1) the difference between*

the total number of zero crossings and extrema is either zero or one; 2) the average of mean envelope is zero at each time point."

We used empirical mode decomposition (EMD) in MATLAB (emd(X,'Interpolation','pchip')) to identify intrinsic mode functions (IMFs) without leaving the time-domain. This algorithm automatically provides 10 IMFs. The interpolation step with 'pchip' (piecewise-cubic Hermite interpolating polynomials) is necessary to obtain smooth functions. Since the algorithm is based on the identification of local extrema, the slow, non-stiff physiological overlaps are eliminated from IMF1 and present themselves only in higher IMFs (Figure 6) to different degrees. Yet, a final decision about which IMF to choose depends strongly on the data.

IMF1 and IMF4 present pure neurochemical signals without any interference and was used for further analysis. However, our tests further demonstrate that higher IMFs also contain non-trivial information that cannot be just the result of interpolation process or caused by the iteration over residual signals (Figure 7). Therefore, we did not completely exclude them from the study and used them as complementary signals for characterization of different patterns.

A. The performance of the EMD over time.

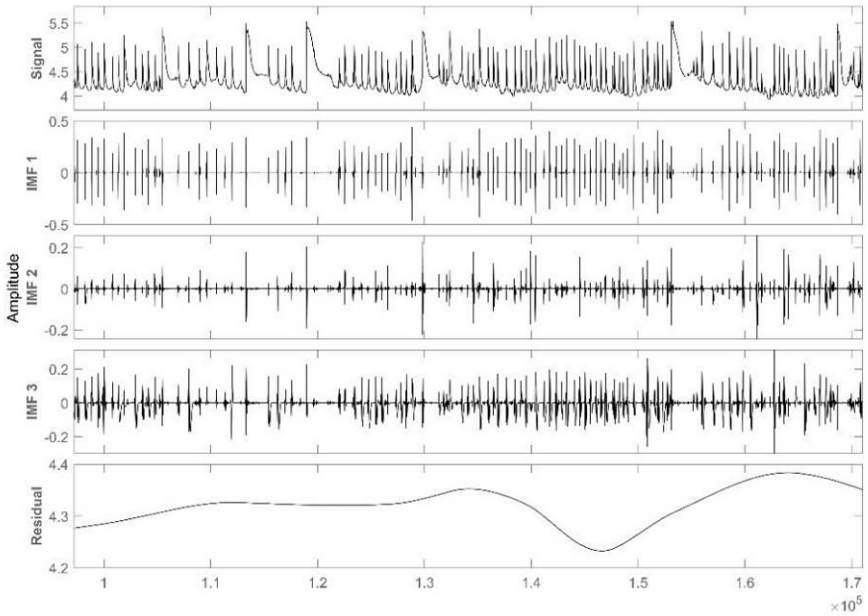

B. A focused view. The red square shows a neurophysiological overlap on the chemistry channel that is filtered out in IMF1 but presents itself and increases in magnitude in all higher IMFs.

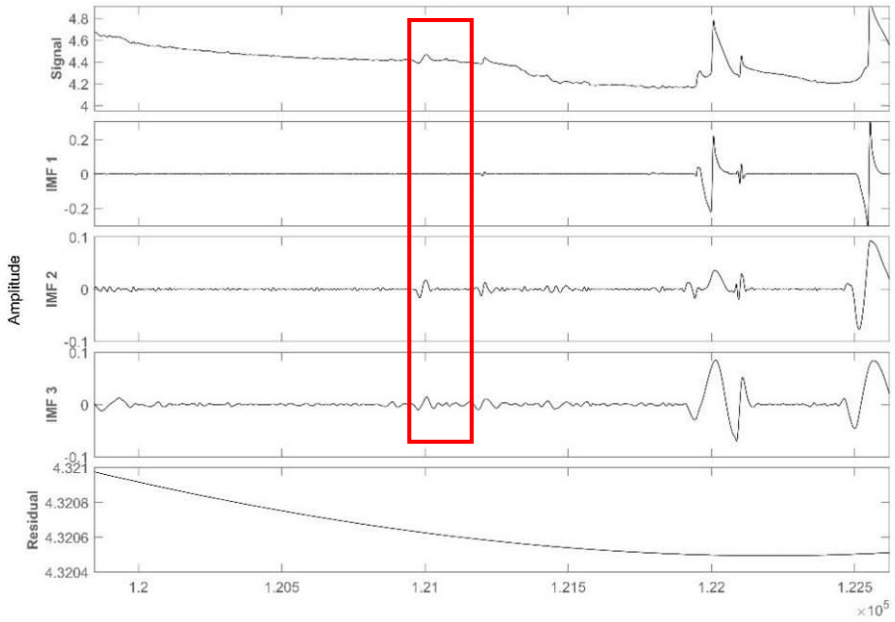

Figure 6. Empirical mode decomposition of glutamate signals into intrinsic mode functions. IMF1 represents a clean neurochemical signal without traces of neural interference. The IMFs were interpolated by cubic splines. A closer look into the IMF characteristics (eg, IMF3) reveals that higher IMFs contain traces of neurophysiological overlap that would significantly affect the interpretations of findings from correlation analyses.

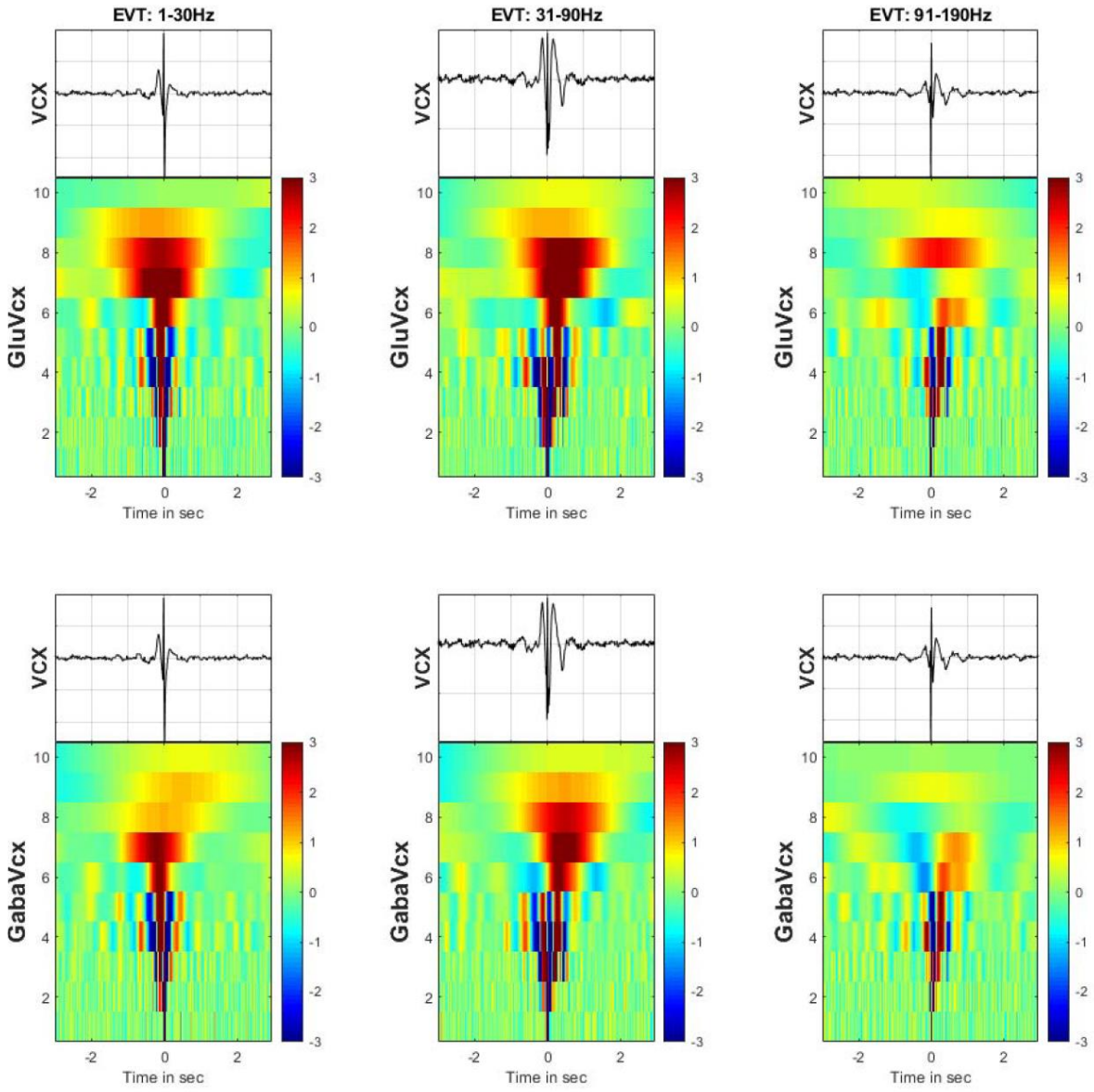

Figure 7. Cortical-Event-Triggered Trials of the IMFs of Chemical Signals. The patterns shown in the time-frequency plots are consistent from session to session and between groups. The y-axis in each image-plot is the number of the IMF(1-10) and the x-axis is the time in seconds around an event, that can be detected by rectifying the bandpass signal filtered in the 1-30Hz, 31-90Hz and 91-190Hz. On top of each image is a plot with the profile of the cleaned signal of the VCX (primary visual cortex , V1) channel.

2.11 Data analysis. The advanced signal processing and data analysis procedures (eg, GLM, correlation and coherence analyses, phase-lock value calculations etc) have been described in detail in our previous studies (Besserve et al., 2015; Ramirez-Villegas et al., 2015). A few of the concepts are elaborated in the following briefly to provide the reader with necessary context of the terms used in the results section.

Correlation analysis. In order to study signal synchronicity within and between the neurochemical, neurophysiological and BOLD time-series, time-lagged cross-correlations were calculated. Cross-correlation is a symmetric normalized estimator of synchrony between two signals. The definition is in the time domain (Hurtado et al., 2004) "*as a function of time lags*", $\tau = -(L-1), \ldots, -1,0,1, \ldots, (L-1)$ (L is the length of the signals). The cross-correlation of signals S1 and S2 is calculated by the equation: for $\tau \geq 0$, $CC_{S1,S2}(\tau) = \frac{1}{L-\tau}\sum_{i=1}^{L-\tau}(S1_i + \tau S2_i)$ and for $\tau < 0$, $CC_{S1,S2}(\tau) = CC_{S1,S2}(-\tau)$. This estimation attains +1 for completely correlated signals and -1 value for completely uncorrelated signals. Value 0 indicates linearly independent signals.

Power spectrum and coherence analysis. There are several techniques that are often used in neuroscience to analyze oscillations of neurophysiological data. The most elementary approach is to use Fourier transform in order to represent the data as a sum of sinusoids curves at different frequencies (f_i) and different phases. The power spectrum is derived from the squared Fourier transform. Intuitively, if the overlap of the data and its Fourier transform is large at a specific frequency, then the power is large at that frequency. More accurately, one can define the power spectrum (Sxx) as: $Sxx = (2Fs^2/L)XX^*$. Here, X is the Fourier transform of time-series x and X* is its complex conjugate. Fs denotes the sampling interval and the length of the measurement is given by L.

In order to investigate how two time-series X and Y, for example glutamate and GABA signals in visual cortex, are associated with each other, one can calculate coherence. Thereby, we need to calculate a so-called cross-spectrum Sxy in addition to the spectrum of each time-series. Indeed, the computation of cross-spectrum is very similar and one only needs to replace the conjugate of X with the conjugate of Y. In order to take the number of trials into account, the cross-spectrum is further divided by the total number of trials (Trial averaging). Coherence is the defined as: $Kxy = |\langle Sxy \rangle| / \sqrt{\langle Sxx \rangle}\sqrt{\langle Syy \rangle}$.

Cross wavelet and cross coherence. In contrast to Fourier transform, wavelet analysis allows us to explore the oscillatory behavior of non-stationary signals. We

used the 1-dimensional continuous Morlet wavelet transform ('cwt' in MATLAB) to investigate neurochemical and neurophysiological oscillatory patterns. Thereby, the continuous wavelet transform represents the signal in a space spanned by time and frequencies (scalogram) and Morlet wavelet provides an appropriate base for extracting features.

From the wavelet transforms of two time-series, we can compute the so-called cross wavelet transform and cross coherence (Bigot et al., 2011). The cross-wavelet transform can be used to find time-frequency domains in which both time-series have high power spectrum and also provides information on how their phases relate to each other. In particular, related time-series show consistent phase-lags. The cross coherence in turn is a correlation analysis of the continuous wavelet transforms of the two time-series and can be used to characterize phase-locking behavior.

Entropy. In order to estimate the amount of information in neurochemical vs. neurophysiological signals, we calculated approximate entropy (*ApEn*). Approximate entropy algorithm requires two parameters m (length of the window of the different vector comparisons) and r (noise filter) to be fixed (Costa et al., 2005; Pincus, 1991; Pincus and Goldberger, 1994; Richman and Moorman, 2000). We set *m=2*, and *r=0.2σ*. Based on the experimental time-series of length *N*, $u = \{u(1), \dots, u(N)\}$ with *2=m≤N*, we define sub-series $x(i) = \{u(i), u(i+1)\}$ and $x(j) = \{u(j), u(j+1)\}$ and calculated the metric *d(x(i),x(j))=max(|u(i+1)-u(j+1)|,|u(i)-u(j)|).* We then use this distance to define $C^m_i(r)$*:=(number of j≤N-1 such that d(x(i),x(j))≤r)/(N-1).* By computing

$$\varphi^m(r) = \frac{1}{N-1}\sum_{i=1}^{N-1} \log C_i^m(r),$$

we can calculate

$$ApEn(2, r, N)(u) = \varphi^m(r) - \varphi^{m+1}(r).$$

General linear models. As it has been described in numerous studies (Poline and Brett, 2012), the general linear model (GLM) approach refers to linear regression models for continuous response variables given continuous and/or categorical predictors. Thereby, the time-series obtained for the voxels are modelled by a

weighted sum of a number of such predictor variables such as on- and offset of experimental condition, and an error. In general, it encompasses multiple linear regressions, analysis of variance and fixed-effect ANCOVA. Thereby, the main goal of GLM is the estimation of the impact of each predictor on the variability of time-series in each voxel. The problem can be expressed as: $Y = X\beta+\varepsilon$, where Y is a nx1-vector (n: length of BOLD time-series and yi, the i-th matrix component being the intensity of BOLD observation in a voxel at time i), and X denoting different predictor variables as an n×p design matrix.

3 Results

3.1 In vitro results

To determine the sensitivity and general feasibility of the system, we first performed *in vitro* experiments. In order to reduce the costs of experiments, custom-made, dummy electrodes were produced and coated with nafion and an enzyme solution. The coating and storage process were identical with the techniques that were described above. In conventional terms, our electrode can be categorized as a so-called first generation amperometric sensor (Qin et al., 2008). These sensors significantly differ from second generation by having the protection layer (ie, nafion) directly on the surface of the electrode instead of over the complex solution made of glutamate oxidase and horse-radish peroxidase as redox mediator. The main advantage of our sensors is the easy fabrication and far faster response times. Here, we first conducted linear sweep voltammetry, to identify the optimal working potential. Thereby, the electrode potential is changed at a fixed rate and the current is measured. For platinum, the peak was reached at approximately 0.6 V, whereas for iridium the optimal working potential was achieved at approximately 0.9 V.

3.1.1 In vitro characterization

To evaluate the sensitivity of our sensors, we then measured the current in response to different neurotransmitter concentrations (1, 5, 10, 15, and 20 µM). Previous studies have demonstrated a wide range of sensitivity and response times for sensors made of different materials and different sizes. Most studies (Day et al., 2006; Hu et al., 1994; Kulagina et al., 1999; Oldenziel et al., 2006; Rahman et al., 2005; Schuvailo et al., 2006) that dealt with only measurements of glutamate concentrations used carbon fiber electrodes, platinum or platinum/iridium with surfaces ranging from 0.005 to 0.183 mm^2. The majority of these sensors show relatively low sensitivities of 0.0034 to 0.03 nA/µM. The only exceptions are studies by Rahman et al (2005) and Hu and colleagues (1994), which present sensitivities of 14 and 0.1 nA/µM. However, the sensor characterized by Rahman and colleagues has a very long response time of ~10 s, which makes it unfeasible for our experiments. In our study, we used a similar strategy as suggested by Hu and colleagues (1994), yet we were able to significantly improve the sensitivity of the

enzyme and achieve a seven-fold increase in sensitivity to glutamate compared to earlier publications.

In addition, our novel signal amplification systems allow the observation of alterations in lower pA scale, which enhances the sensitivity of the sensors with respect to small fluctuations. In particular, our glutamate sensor (with a diameter of ~ 30-35 µm) showed a sensitivity of 0.44 nA/µM (Figure 8a,c). The actual response time was less than 0.01 s (as reported in Burmeister et al., 2020).

In light of the fact that our electrode not only measures glutamate but also electrophysiology, we also compared its performance with previous attempts of simultaneous measurements of the two factors (Wei et al., 2015). Since, we optimized the process of coating the electrode, we could significantly reduce the size of the contact surface without reducing the sensitivity (35 µm vs 343 µm in Wei et al). Reducing the contact surface of the electrode is an important step for investigating smaller brain structures (such as LGN) and can significantly reduce tissue injury.

Glutamate measurements using amperometry are well-established, however *in vivo* quantification of GABA levels remains challenging. The adjacent GABA-responsive electrodes show a sensitivity of 0.38 nA/µM (Figure 8b,d) for GABA and negligible sensitivity to glutamate in light of basal glutamate concentrations of 1-2 micromolar. While one recent study (Burmeister et al., 2020) presented an attempt to simultaneously measure glutamate and GABA concentrations in vivo, our approach still provides more benefits as it additionally provides scale-consistent measures of neural activity. Furthermore, in contrast to the majority of amperometric studies that are concerned with absolute glutamate and GABA concentrations, our main focus is to characterize how relative changes in concentration relate to neural activity and BOLD signals. Therefore, the interpretation of sensor sensitivity in this thesis differs from the traditional style in the field of electrochemical neurotransmitter detection.

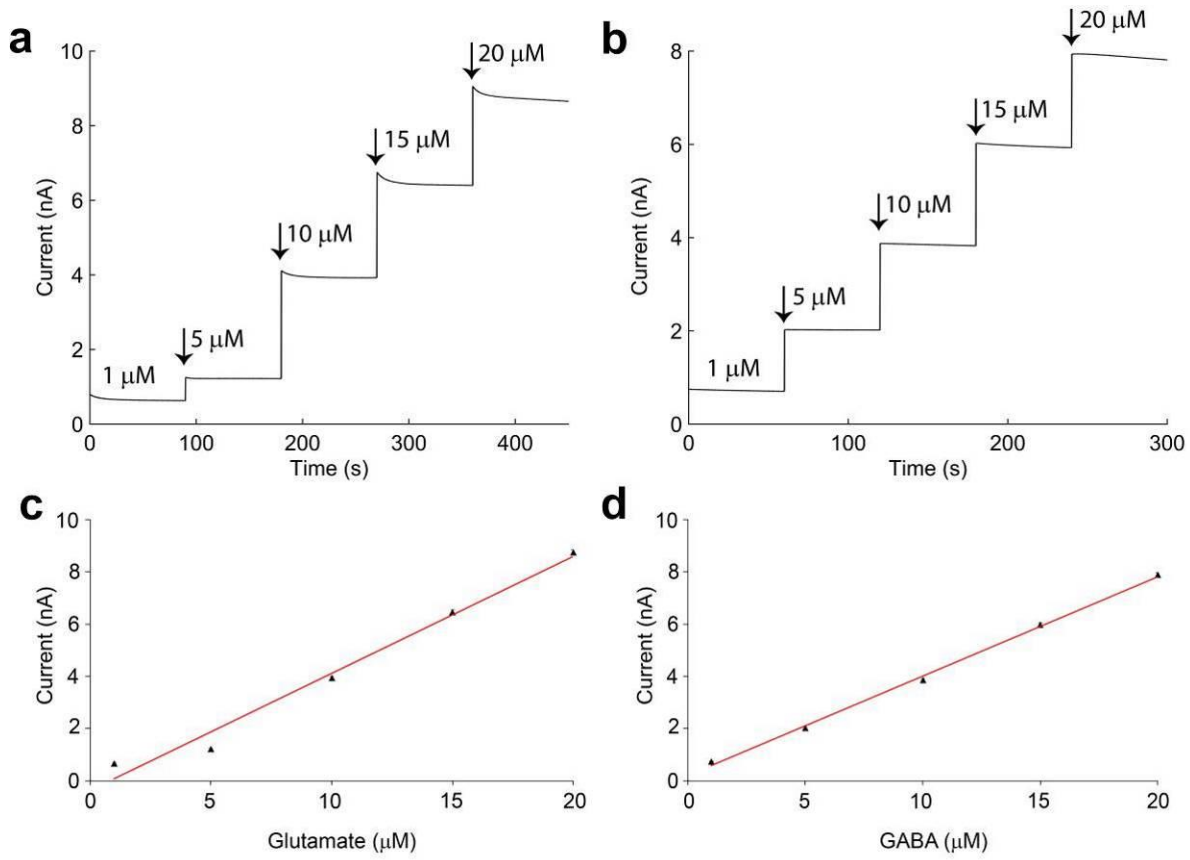

Figure 8. In vitro sensitivity of the electrochemical channels for glutamate and GABA. Both peroxidase-based amperometry sensors show high sensitivity (glutamate: 0.4486 nA/µM with 95% confidence interval [0.3394, 0.5578]; GABA: 0.3813 nA/µM with 95% confidence interval [0.3517, 0.411]) and a robust linear dose-response relationship (glutamate: R-square = 0.983; GABA: R-square = 0.998).

3.1.2 Storage stability. As mentioned above, the glutamate oxidase is a rare and expensive enzyme to work with. Therefore, it is more efficient to use the same enzyme preparation for coating several electrodes. Although, in our experiments only freshly prepared solutions were used, we still investigated how long the coated electrodes maintain their sensitivity. This allows other scientists to apply our methods at a lower cost. This step was also conducted using dummy electrodes *in vitro*. Several dummies were coated identically on the same day and were stored either in PBS overnight or kept dry at 4°C in an air-tight container in a refrigerator. Identical to our previous *in vitro* sensitivity tests, we evaluated the sensitivity of the sensors of different post-preparation age (24 hours, 3, 7, 14, 21 days) at different concentrations of glutamate. Although, there were no significant differences (F=0.16; p=0.95) between the sensitivity of the sensors (Figure 9) we observed a clear time-

dependency as older sensors tend to be less sensitive to lower glutamate levels. Since the stimulus-induced events are normally associated with larger neurotransmitter changes, the stored electrodes may be appropriate for usage under such conditions and to a lesser degree for resting-state observations.

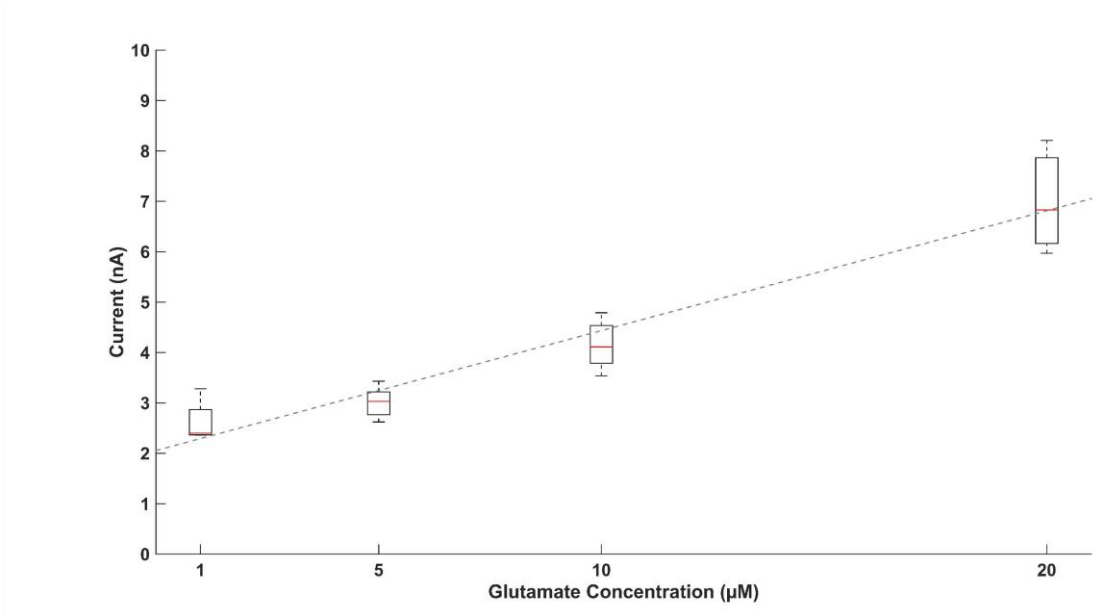

Figure 9. Storage stability of the modified electrodes for amperometric measurement of neurotransmitter concentrations. There are no significant differences between the dose-response sensitivity of the sensors kept overnight in PBS or kept at 4°C for 1, 3, 7, 14 and 21 days.

3.2 Concurrent in vivo measurements of neurophysiology and neurochemistry

As briefly elaborated in the methods section, the MRI-gradients produce strong electromagnetic noise on neurophysiological signals. Although we have improved the hardware (particularly the amplifiers) and software (cleaning algorithms) to reduce such undesired interference, it was yet unknown how the gradient noise is expressed on neurochemical signals. Moreover, experiments outside the MRI environment would allow us to optimize experimental parameters such as frequency and intensity of light stimuli for activating thalamic regions.

Therefore, we conducted a series of experiments without MRI and analyzed basal properties of our methodology such as in vivo sensitivity, biofouling (gradual reduction of the sensitivity of the sensor due to accumulation of cells on electrode surface) and temporal stability of the sensors. Furthermore, we investigated how

neural activity and neurochemistry are correlated and considered it as a reference for MRI experiments.

3.2.1 Resting-state measurements in somatosensory pathway

Basal ganglia form a brain network that has been shown to largely regulate motor coordination and response to somatosensory stimuli. The main input structure of this cluster is the caudate-putamen or striatum, which by continuously receiving and integrating sensory data, produces and selects adaptive motor behavior. Numerous cortical regions project massive glutamatergic neurons to caudate putamen following strict a topolographical organization, such that functionally similar information from diverse cortical areas is converged in specific subregions of caudate putamen.

In particular, the dorsolateral part of caudate putamen received major glutamatergic input from neurons in primary somatosensory cortex (S1) that are uniformly distributed across layer 5. In general, S1 like other neocortical regions is comprised of 6 layers, with a granular layer IV and unremarkable boundaries between the second and third layers. Functionally, it can be divided into three sections associated with the head (Par1 according to Paxinos terminology), fore- (FL) and hindlimbs (HL).

This pathway is especially relevant for processing environmental cues that guide the rat's exploratory behavior. The glutamatergic input from S1 is processed by GABAergic medium spiny neurons in caudate putamen, which form the main population (~96%) within this structure. These aspects make the somatosensory pathway an excellent framework for studying the interaction of glutamatergic and GABAergic systems.

The recording of glutamate, GABA and neural activity simultaneously in both regions at rest not only allowed us to determine basal levels of the transmitters but it further enables us to investigate the dynamical features of these systems (Figure 10).

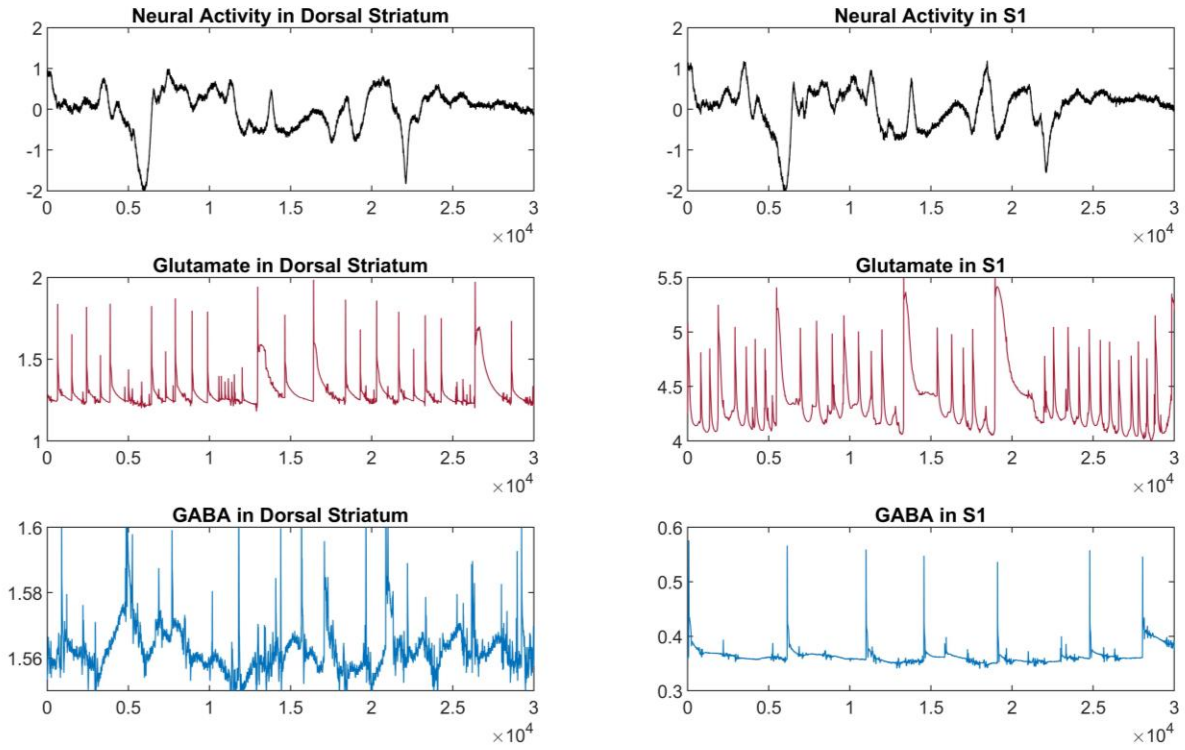

Figure 10. Baseline communication within corticostriatal, somatosensory pathway (recorded with 6-fold gain on amplifier). Three seconds of measurements are shown as an example of observation accuracy.

Although the basal levels of glutamate in S1 (~1.63 µM) was almost four-fold higher than in caudate-putamen (~0.47 µM), the average magnitude of glutamatergic peaks were in both regions largely comparable. An interesting feature of the glutamatergic signals is the presence of small glutamate bursts (3-8 events within 100ms). In both brain areas, glutamate events occur with a frequency of 10-15 Hz. In contrast, GABA levels in dorsal striatum (~0.68 µM) were significantly higher than in somatosensory cortex (~0.17 µM) and less frequent (2-8 Hz). Interestingly, GABAergic peaks in caudate putamen were two-fold stronger than in S1. In addition, the peaks in cortex show a certain regularity and local dissociation from glutamatergic events.

3.2.2 Correlations of neurophysiological and neurochemical time-series

While the comparative characterization of neurochemical signals in each brain region is important, it is critical to investigate how the signals within the network relate to

each other. To address this question, we computed cross-correlations of all signals. Defining a correlation above 2 x (n - |τ|)-1 (n: number of observations and τ the lag) as significant, our analysis suggests that all time-series are weak to moderately and significantly correlated (Figure 11). As briefly elaborated in previous section, the GABA signals at rest in S1 appear regular, almost dissociated from other events in the systems. Thus, the correlation of cortical GABAergic signals with other variables were weak. In contrast, glutamatergic events in caudate putamen and S1 show relatively strong correlations with small delays, suggesting a high level of synchronicity. As expected by the anatomy of the somatosensory pathway, there are further relatively strong correlations between glutamate in S1 and GABA in caudate putamen with a delay of 150-200 ms. Correlations of neurophysiological and neurochemical signals largely depend on the neural event types and will be discussed in the next sections.

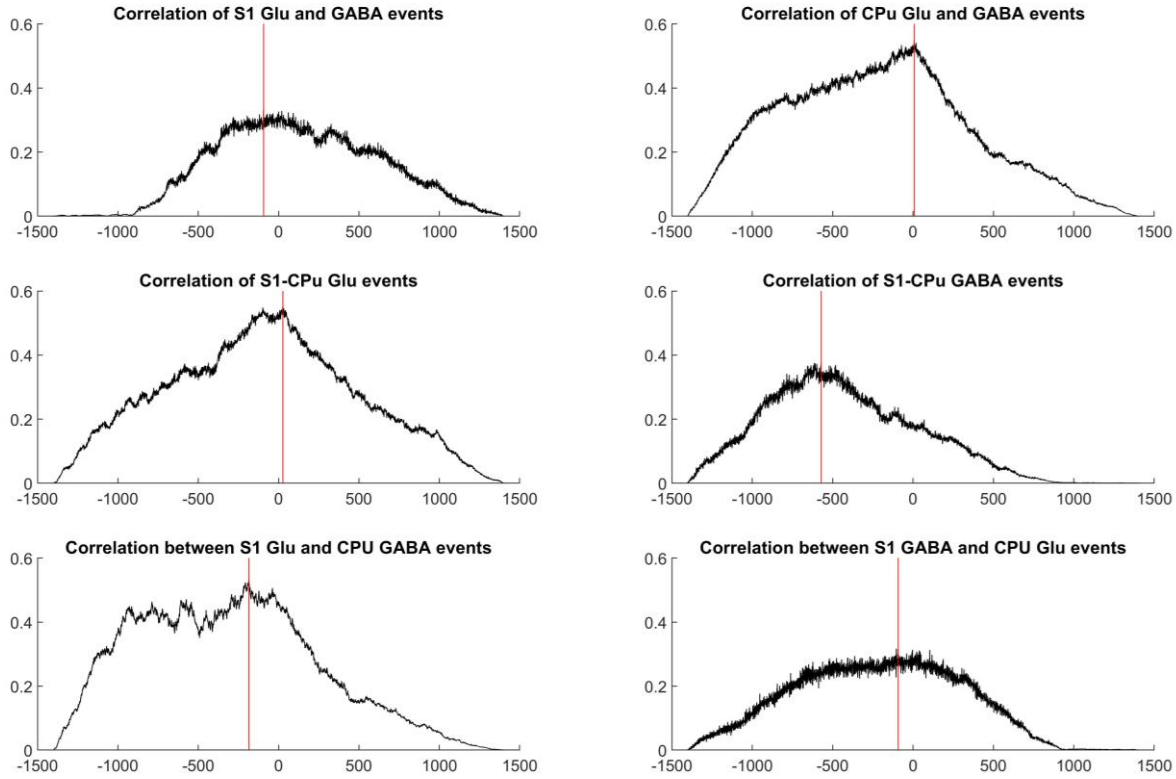

Figure 11. Normalized cross-correlation (xcorr) of neurochemical time-series in different brain regions.

3.2.3 Parameter adjustments for visual stimuli

Rats are nocturnal animals with advanced visual systems. The lateral positioning of the eyes provides panoramic view and considerable depth of focus. The rat retina is

works in different (scotopic and photopic) conditions since it not only contains photoreceptors but also cones. Indeed, so far two cone types have been classified, with the majority of them containing photopigments with peak sensitivity of approximately 500 to 520 nm (Deegan and Jacobs, 1993). In this study, we used albino Wistar rats. Differences in light sensitivity of albino and pigmented rats (for example, more myelinated fibers in optical nerve and thicker visual cortex in hooded rats) have been the subject of countless discussions, yet recent studies (Herreros de Tejada et al., 1992) suggest that the evoked potentials in cortex are largely identical among the different strains. Indeed, the retinal fibers in both strains converge into the same brain area. Thus, for our investigations the retina light sensitivity plays a minor role. Visual stimulation of retina is known to induce a significant response in dorsal lateral geniculate nucleus, superior colliculus and primary visual cortex. In albino rats, signals arriving from the ipsilateral eye are largely relayed over callosal projections from contralateral visual cortex (Diao *et al.,* 1983a; Silviera *et al.,* 1989). The visual cortex also receives topographically-ordered inputs from raphe and locus coeruleus (Waterhouse *et al.,* 1993).

The main goal of this sub-experiment was to identify optimal visual stimulation paradigms such that they lead to considerable response in lateral geniculate nucleus (LGN) while the activation of other circuitries originated from raphe and locus coeruleus remain subthreshold. LGN is a thalamic subregion that is reached first by retinal ganglion cells. The LGN itself is comprised of dorsal and ventral sections, separated by a plexus, that both receive retinal and cortical efferents, while only the dorsal components projects to visual cortex. LGN is small (~0.6 mm dorsoventral, 1.1 mm mediolateral with anterior and posterior extensions of 1.5 and 0.5 mm, respectively in an adult rats), non-laminar (based on Nissle-straining), kindey-shaped structure and in addition to other thalamic nuclei, it also borders hippocampus. Its dimensions and location make it a difficult target for electrode placements, however its connectivity makes it an excellent candidate for preliminary investigations of the visual system.

Here, we used a custom-made, programmable LED stimulation source to characterize the effect of different parameters such as wave-length (red, green, blue and combinations thereof), stimulation frequency (1-10 Hz) and light intensity.

Interestingly, even 1Hz stimulation frequency leads to significant neuronal response in LGN for all colors (Figure 12), including the red-light spectrum, which is largely assumed to not activate the retina in rats. Following discussions with experts on retina, this response is presumably due to an overlap in the green and red spectra and is captured by green cones on rat retina. Since all spectra and frequencies lead to significant activations of LGN, we chose an intermediate frequency level of 4Hz and white light for fMRI stimulations. The intensity of light was adjusted in the MRI setting to avoid a harmful overstimulation and co-activation of other neurocircuitries (Figure 13).

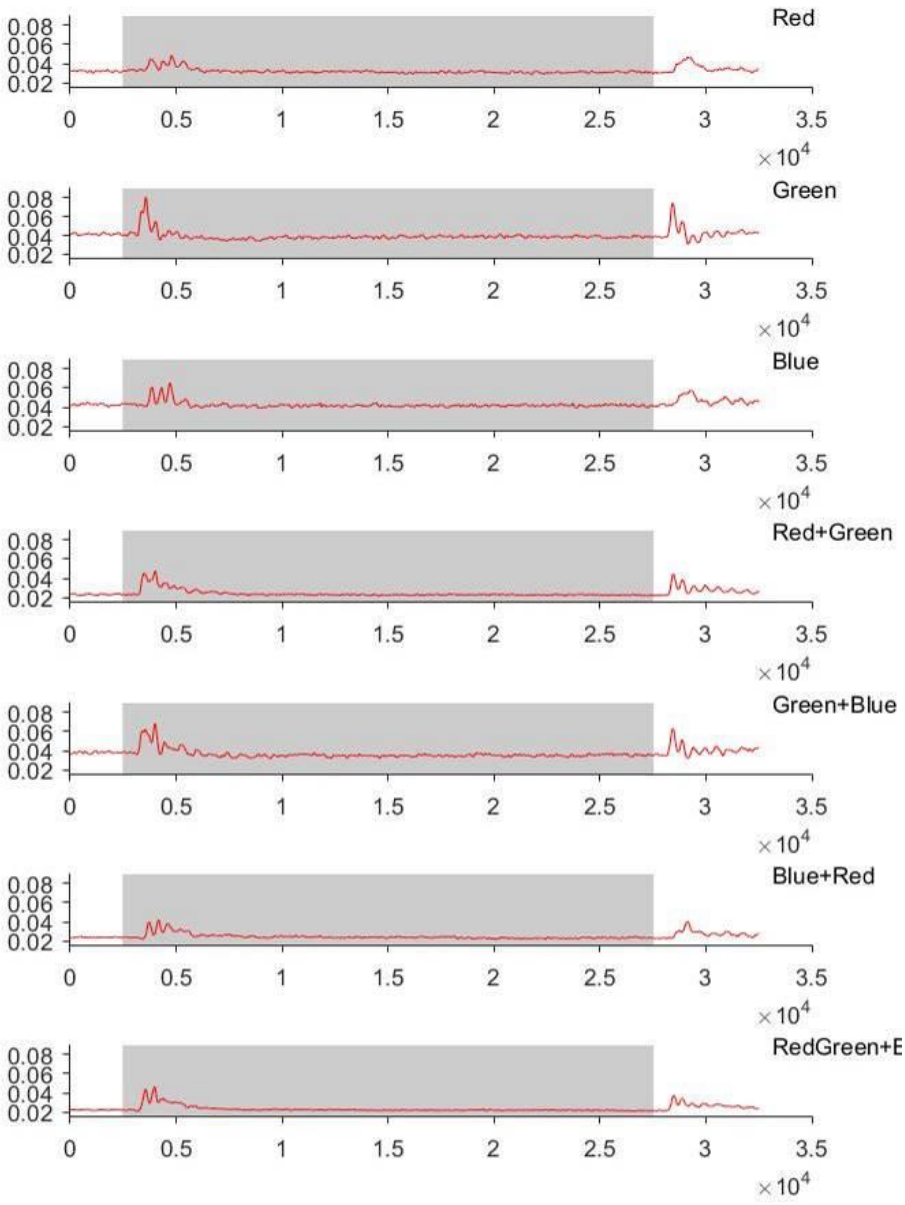

Figure 12. Average spiking in LGN in response to different light wave-length projected contralaterally at 1Hz to retina.

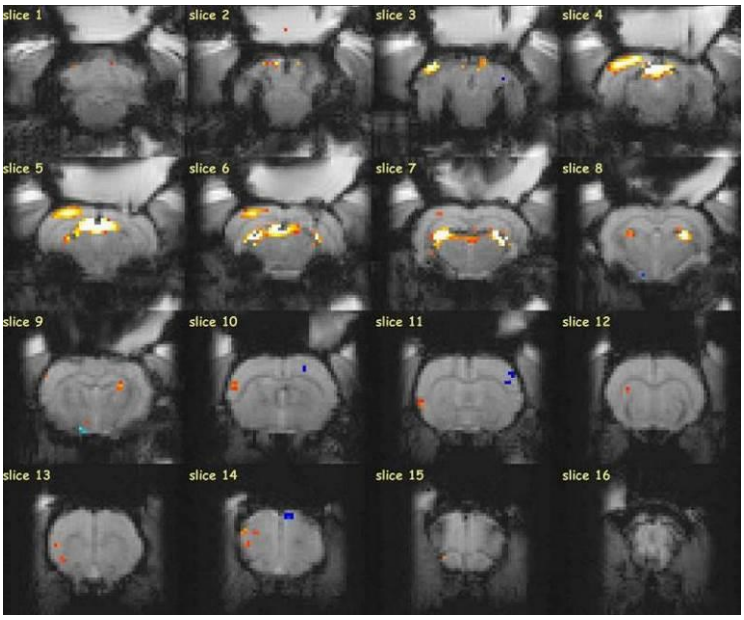

Figure 13. Adjusting the intensity of visual stimulation such that co-activation of other circuitries could be minimized. Here, both retinae were stimulated leading to an activation of visual systems in both hemispheres.

We further used the retinal stimulations to investigate the in vivo response time and sensitivity of our modified MEA. The recordings clearly demonstrate that neural response to visual stimuli in LGN is directly associated with glutamatergic response (Figure 14).

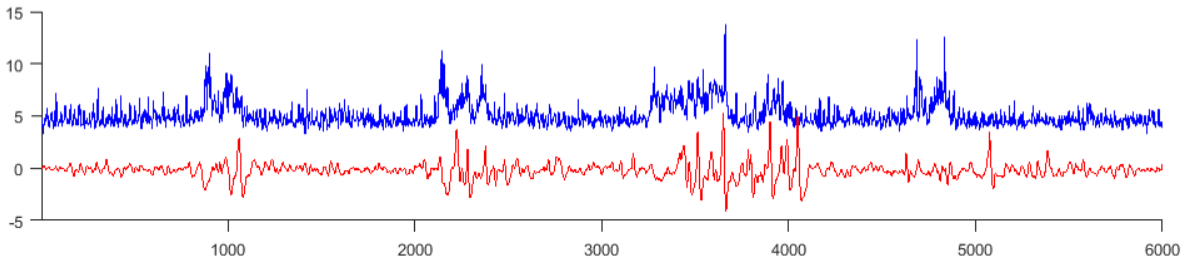

Figure 14. Simultaneous neuronal (blue) and glutamatergic (red) response to visual stimuli in LGN is largely synchronous. The technology allows a comparison with high temporal resolution.

While most (70–80%) neurons in LGN are projecting glutamatergic signals to primary visual cortex, up to 30% of LGN neurons are GABAergic interneurons that modulate/inhibit the activity of the thalamocortical neurons. Therefore, to decode the neural signals in LGN it is of outmost importance to investigate the complex relationship of not only glutamate and neural activity but also GABA release.

Interestingly, GABA signals in LGN are not directly associated with neural response to retinal input and present a more complex relationship (Figure 15). The exact nature of this relationship and the association of different neuronal signal types with changes in glutamate and GABA signals will be discussed in the next sections.

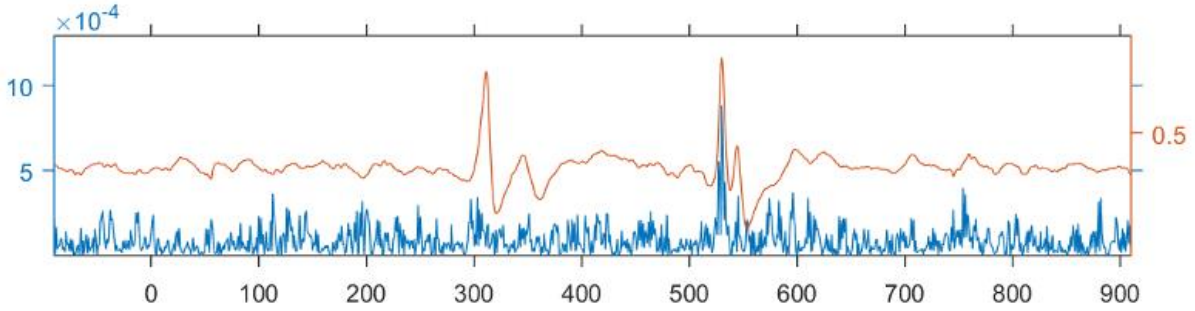

Figure 15. Simultaneous neuronal (blue) and GABAergic (orange) response to visual stimuli in LGN.

A general view of all sites recorded simultaneously with either standard - or chemo-electrodes for amperometry is presented in Figure 16. The angular implantation of the multi-channel electrode allows us to measure the neurochemical and neurophysiological signals concurrently along the primary visual pathway and even record in hippocampus, which helps us analyze the data in light of different brain states.

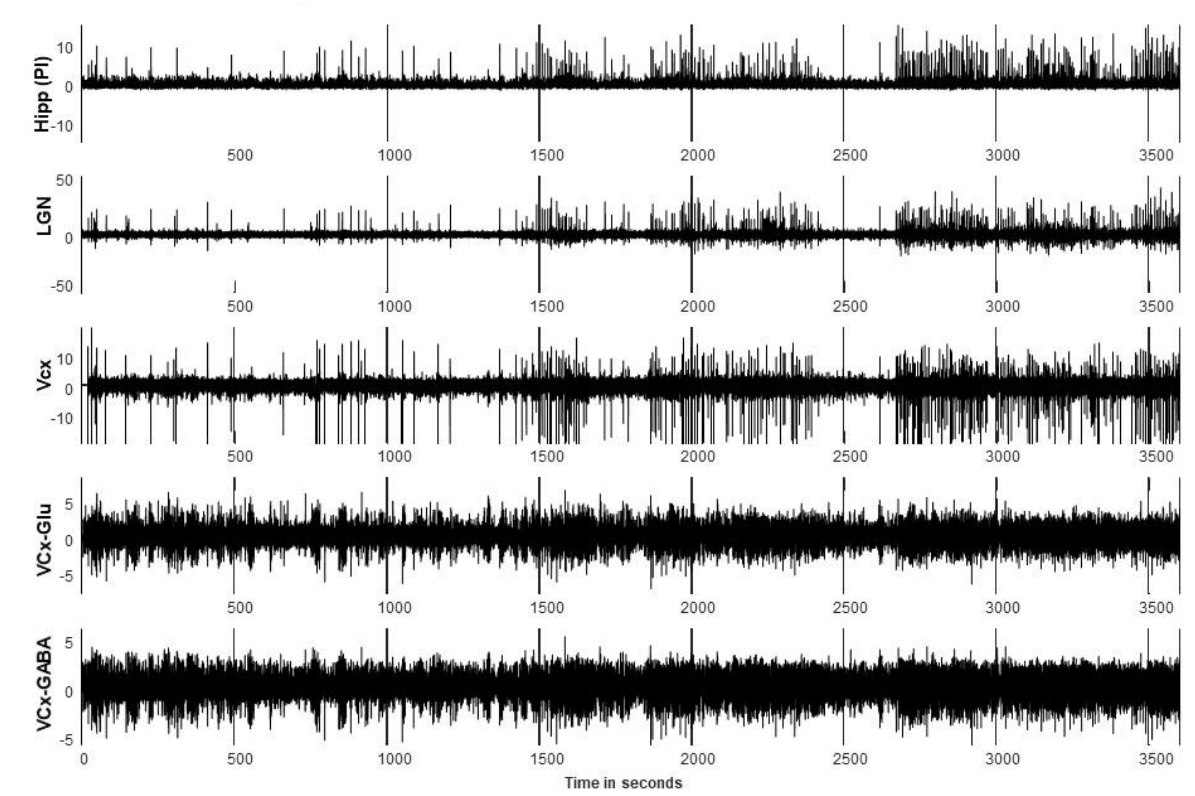

Figure 16. Data are from concatenated files of an entire sessions (acquisition-duration of ~1 hour).

3.2.4 Decoding neural signals into neurochemical components

Canonical microcircuits rely strongly on continuous excitation and inhibition (E-I) and to a lesser degree on feedforward inputs from thalamus. Thereby, cortical regions assess the context of the information through significant interactions within and across different structures. What follows prior to the presentation of the results in this subsection, is an introduction of the concept of excitation-inhibition networks, which largely reflects the content of the review article by Logothetis (2008).

Studies using intracellular injections of markers into single neurons have determined the projection patterns of different neuronal types in the visual cortex. An important and surprising finding was that the greatest part of the input (approximately 85%) to the pyramidal neurons is from other pyramidal cells in cortex, with only a minority of synapses devoted to thalamic input, which innervates both the pyramidal and the smooth cell populations. Excitatory and inhibitory cortical neurons show a remarkably similar laminar and tangential organization with respect to their morphology and interconnectivity patterns along the entire neocortical sheet.

The cells communicate using connections within and between different layers with horizontal and vertical orientations such that the ultimate neuronal response is a cumulative consequence of various feedback and -forward synapses. Thereby, the recurrence is the outmost critical feature of cortical networks that largely affects the energy metabolism and hemodynamics. For instance, pyramidal cells form positive feedback loops through axonal branching towards more superficial layers, while also propagating glutamatergic excitation at the same layer and thus presenting a recurrent excitatory network. Such pyramidal networks are however heterogeneous in the sense that they integrate GABAergic interneurons. Interneurons have by definition only local connections but receive diverse excitatory and inhibitory inputs.

Different types of inhibitory interneurons are capable of targeting different subdomains of neurons (i.e. dendritic regions, somata, or axons). In particular, depending on how the interneurons target the pyramidal cells, they can either adjustment the response gains or override the neuronal integration.

The diversity and synaptic organization of the inhibitory network and its connectivity patterns with the projection neurons suggest that the steady-state activity of the recurrent pyramidal network can, in principle, be regulated by balancing E-I. The response to stimuli, on the other hand, may lead to transient imbalances in the coupled excitatory and inhibitory interaction patterns.

The balanced E-I hypothesis recently received support from experimental work examining conductance changes during states of high and low spontaneous activity. Intracellular and extracellular recordings in animals had long demonstrated the presence of two distinct activity-states alternating with a period of about 10 seconds. In cerebral cortex, these states are readily observed during slow wave sleep or anesthesia.

Our technology readily provides the proper framework to study the “balanced” excitation-inhibition with a high temporal resolution. It is critical to note that balance is not a static feature and how two systems maintain coupled state equilibrium depend cannot be described by a snap-shot observation. Most measurements presented in this section were conducted within the MRI. Before we investigate how different types of neural activity relate to different patterns of excitation and inhibition, there are already many questions that must be answered correctly to start building a concept of how can measurements of neurotransmitter dynamics can help us understand the state of micro- and macro-circuits, and how can be potentially used to understand the neurovascular coupling and improve our interpretations of BOLD functional MR imaging data:

1. What is the Time-Frequency Profile (TFP) of each neurochemical signal following visual stimulation?
2. What is the TFP of each neurochemical signal around strong spontaneous signal deflections, as of now dubbed as Chemical-Event-Triggered (CET) Trials.
3. Can we successfully detrend the Chemical Signals from the Induction of the corresponding electrophysiological signal?
4. Does the degree of cross-correlation of CET-Trials depend on brain-state?
5. What are the CET-BOLD and CET-LFP profiles?

6. What is the Glu and GABA TFP in CET-Trials triggered by well-known events, such as thalamic/cortical Spindles, Sharp Wave Ripples, or Gamma-Frequency- or Gamma-Amplitude Increases, along the lines of research with fMRS-fMRI?
7. What is the relationship of Glu/GABA to the positive & negative BOLD (PBR, NBR)?
8. What is the multi-structure activity pattern in the case of CET-fMRI?

We first analyzed how sensitive our technology can decode the neural activity into glutamatergic and GABAergic events. More accurately, in our efforts to examine the nature of the neurotransmitter (NT) signals measured with amperometry, we used two complementary approaches. Sensory – in this case visual – stimulation, as well as studies of spontaneous activity. Figure 17 shows changes in electrophysiological activity and neurotransmitter-release during Visual Stimulation with a 4Hz-Flickering Pattern. As can be instantly observed, both glutamate and GABA respond to visual stimulation, but importantly with distinct correlated, anti-correlated or utterly independent dynamics and in a potentially different manner.

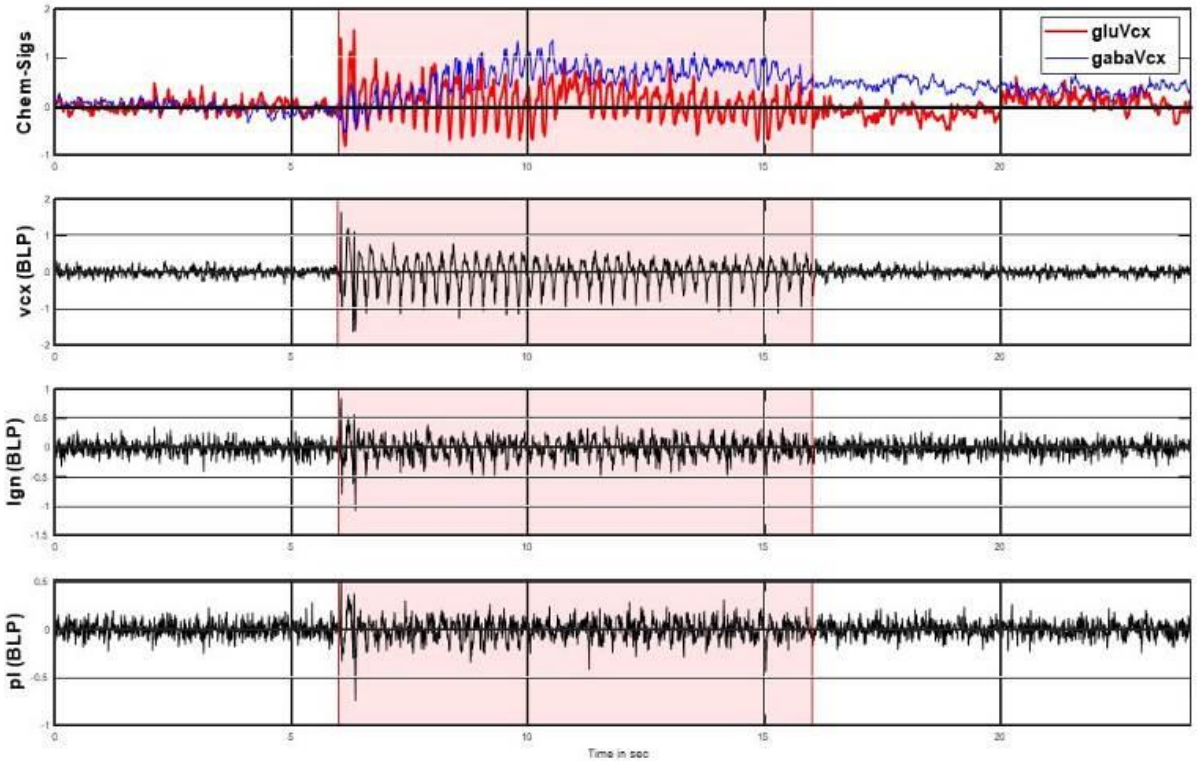

Figure 17. Distinct neurotransmitter dynamics in primary visual cortex during and after stimulation. Both glutamate and GABA respond to visual stimuli.

The excitatory response of glutamate, for example, has been often characterized by high amplitude potentiation in release. The inhibitory (GABAergic) interneurons show a characteristically different behavior. By decreasing GABA secretion in response to each light pulse but – at the same time – potentially reducing the reuptake-process, they lead to an accumulation of extracellular GABA levels and a long-term depression of neural activity. Not surprisingly, these first findings reveal a complex feature of the excitation-inhibition network, suggesting that the investigation of this system should not only be focused on immediate response to stimuli but also on adaptive, long-term inhibitory dynamics. For that matter, numerous studies have shown that GABA play a far more critical role than being 'just' the primary inhibitory neurotransmitter in the adult brain. The GABAergic neurotransmission is generally finalized by either neuronal or glial re-uptake through specific transporter proteins, and the overall non-synaptic activity of GABA may well be perceived as circuit-regulated neuromodulation.

The stimulus-induced transition in neurotransmitter dynamics and mean levels can be observed in more detail in z-score representation (Figure 18).

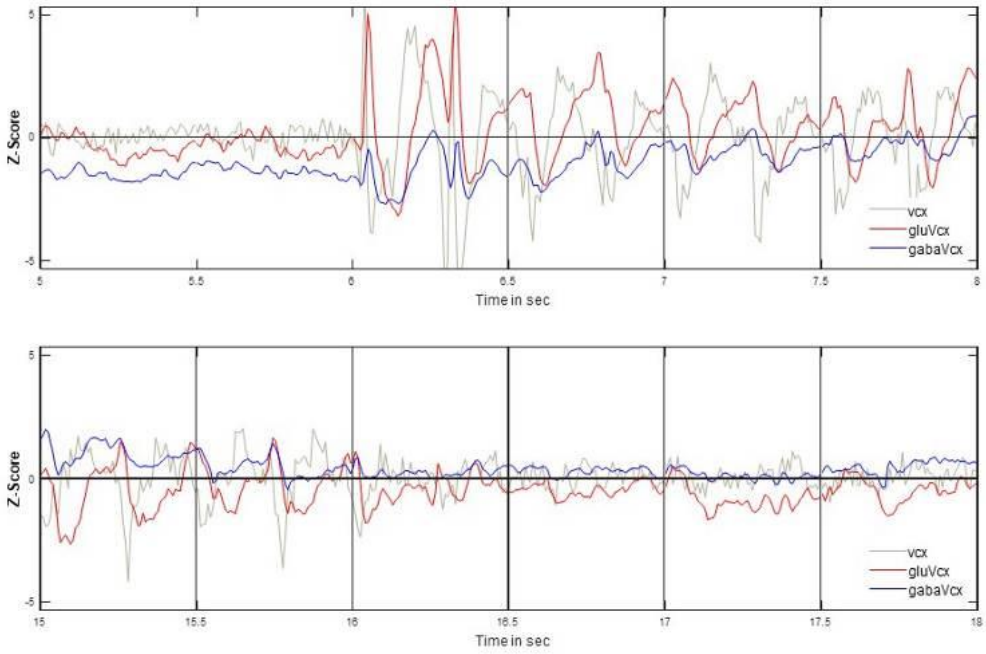

Figure 18. Standardized (z-score) representation of neural and neurochemical activity in visual cortex, in response to light pulses.

The first stimulus induces an instantaneous glutamate response and a small GABAergic reaction. However, as shown in PLV analysis, neural activity leads the

response of both transmitter systems afterwards. Interestingly, while the GABA response to each pulse remains weak throughout the stimulation period, GABA levels gradually increase to a level higher than their basal levels prior to the stimulation and even temporarily higher than mean levels of glutamate post-stimulation. Both basal processes converge back to initial pre-stimulation states within 1-2 seconds.

A closer look at the behavior of the NT dynamics during stimulation further demonstrates the distinct response of glutamate and GABA to visual stimulation (Figure 19).

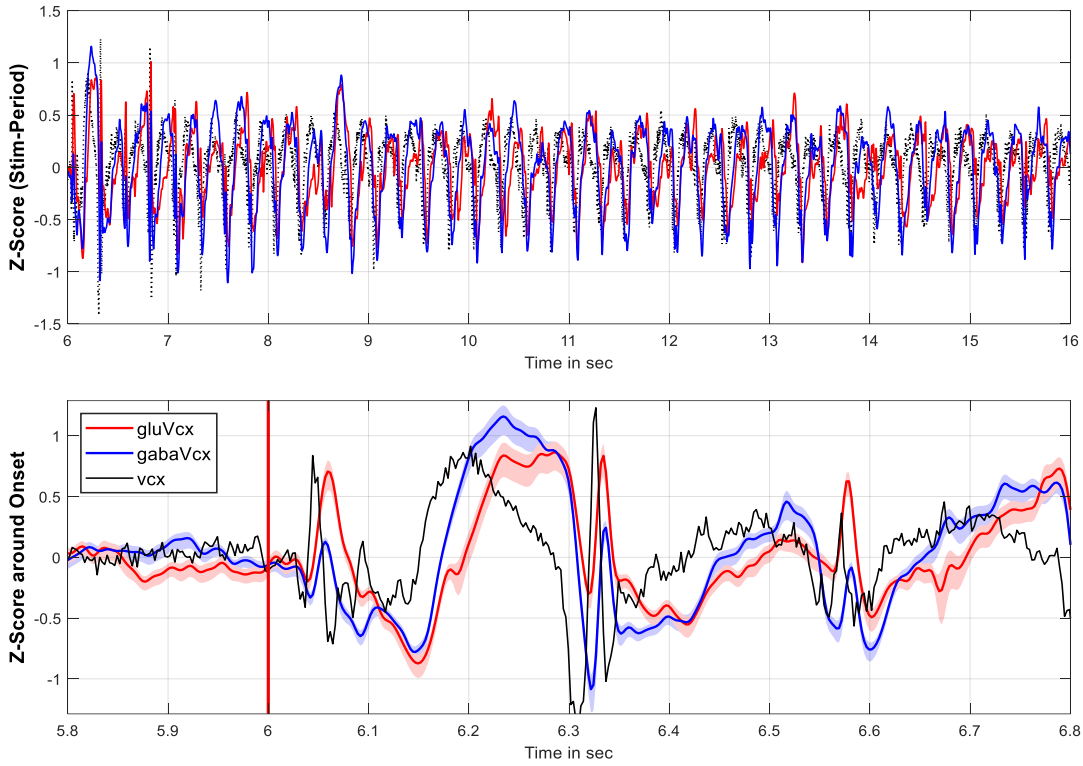

Figure 19. The top plot shows the visual-stimulation-induced 4Hz Oscillations in the electrophysiological signal (dashed-line) of the visual cortex and in the Glu and Gaba Signals in the same area. The bottom plot is a “zoom-in” display of the epoch 0.2 s before and 0.8 s after the onset of the first visual stimulus. The time courser of signals clearly demonstrated NT-related signal, rather than electromagnetic induction, etc. Importantly in the first pulse, Glu-Increase is consistently higher than GABA. As can be seen in the bottom plot, the very first stimulus-flash induces an instantaneous glutamate response and a small GABAergic reaction. However, as shown in PLV analysis (see below), neural activity leads the response of both transmitter systems afterwards. Interestingly, while the GABA response to each pulse remains weak throughout the stimulation period, GABA levels gradually increase to a level higher than their basal levels prior to the stimulation and even temporarily higher than mean levels of glutamate post-stimulation. Both basal processes converge back to initial pre-stimulation states within 1-2 seconds.

This complex interaction of the excitation and inhibition components suggests the non-stationary nature of the E-I balance. The glutamatergic signals are not always accompanied with an immediate GABAergic event. While every larger neuronal event is associated with glutamatergic signaling, simultaneous GABA release seems to relate only to specific type of events and occur often in the early stages of excitation. In order to systematically investigate such phenomena, we first need to process the signals to identify state-specific neuronal events which in turn can relate to characteristic patterns of neurotransmitter dynamics.

In general, the analysis is conducted on three main types (larger scale) of signals (Figure 19). From top, (1) the raw (Cln) amperometry signals of Gaba (first from top) and Glutamate, (2) the Cortical and LGN electrophysiological signals, and (3) the area-plot of the hippocampal pyramidal layer in the theta-range that can give some hints related to the REM and NREM sleep-states.

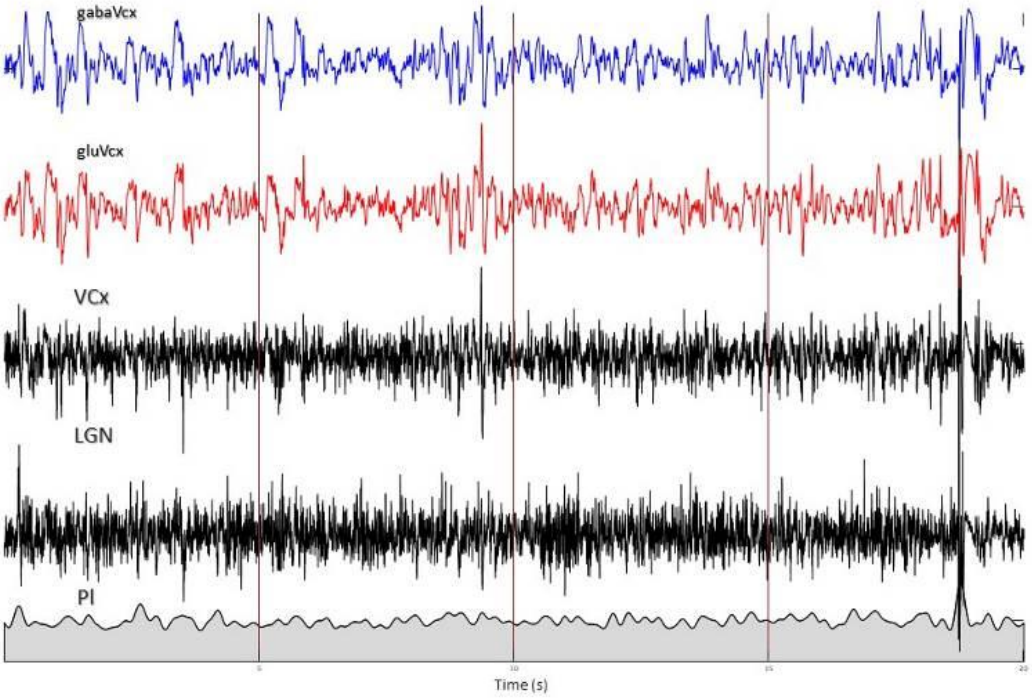

Figure 19. Alignment of neurochemical and neurophysiological signals for state-dependent characterization of events.

As mentioned above, time-series of neurotransmitter concentrations are non-linear and non-stationary. Therefore, we used empirical mode decomposition and extended the signal alignment with all intrinsic mode functions (Figure 20). Thereby, smaller

scaled blueish (Gaba) and reddish (Glu) signals from top to bottom they represent the 1 through 10 Intrinsic Mode Functions (IMF) obtained with the empirical mode decomposition (EMD) method.

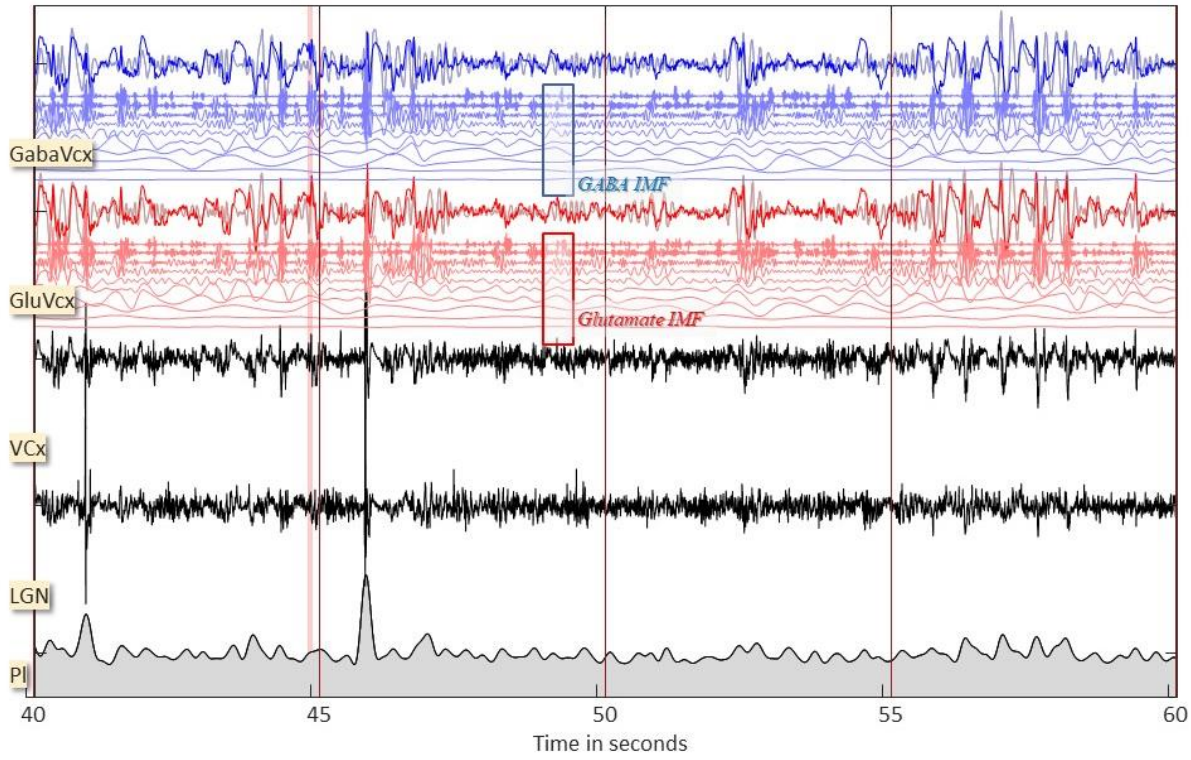

Figure 20. Extended signal alignment by inclusion of intrinsic mode functions. The plot shows the time course of the physiology (Cortical, LGN and Hippocampal Pyramidal Cell Layer) and Neurotransmitter Signals (Glu and GABA). The top lines in the upper two time-course-sets are the amperometry signals of GabaVcx and GluVcx superimposed by the Glu-IMF(4) and Gaba-IMF(4) respectively (gray). The ten signals below the aforementioned ones are the 10 Intrinsic Mode Functions estimated by the Empirical Mode Decomposition method. Empirically the IMF(4) has been the signal most correlated with the electrophysiological one.

To better understand the nature and relevance of each IMF, we have also used Tensor-Clustering, considering both the peri-event time courses and the IMF (vertical) profile at any given time point. The Time X IMF matrix can be technical seen like the Time-Frequency patterns observer in the usual Spectrograms for neural activity, e.g. Wavelets (Figure 21 & 22) or neurochemical signals (Figures 23-26).

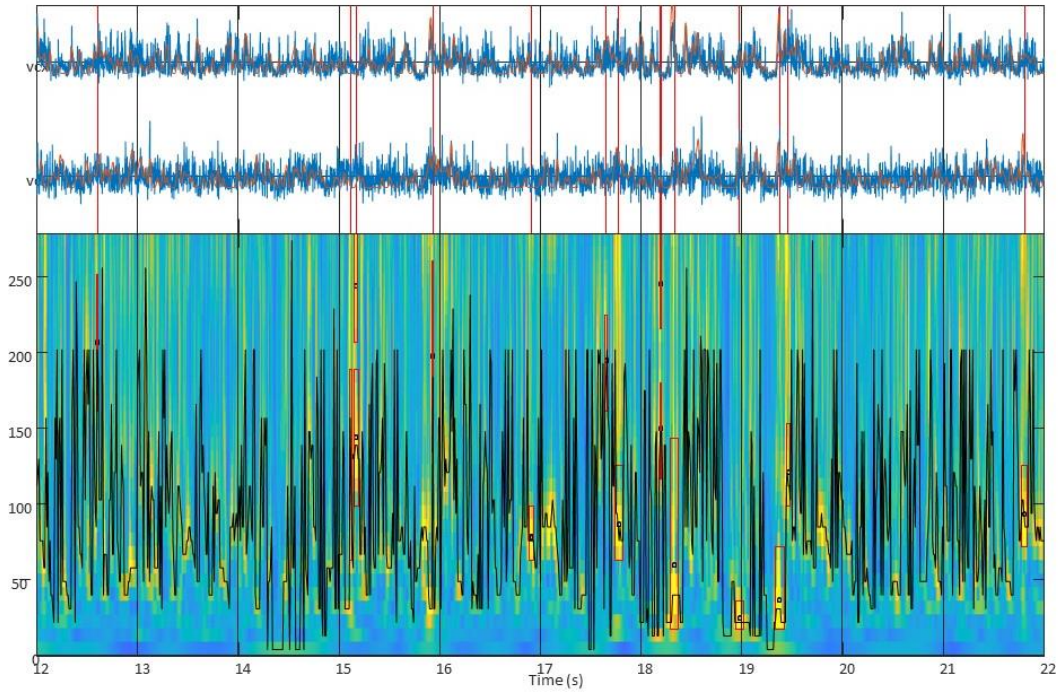

Figure 21. The scalogram refers to the time-scale power distribution of signal, which simply the square of a continuous wavelet transform (CWT) of that signal. Important for our study of spontaneous activity is the fact that based on a scalogram one has a running max amplitude for each single time point together with the frequency at which the max-amplitude is observed. The running Amp-Freq variables can help estimate important large deflections of the extracellular field potential without a priory selecting frequency ranges hypothesize to be important for a given question. The running amplitude can be z-scored and used for detection of “chemical” events as much as one can do with the neural ones. (on the top subfigure, blue marks multi-unit activity [MUA] and red marks spike density function [SDF]).

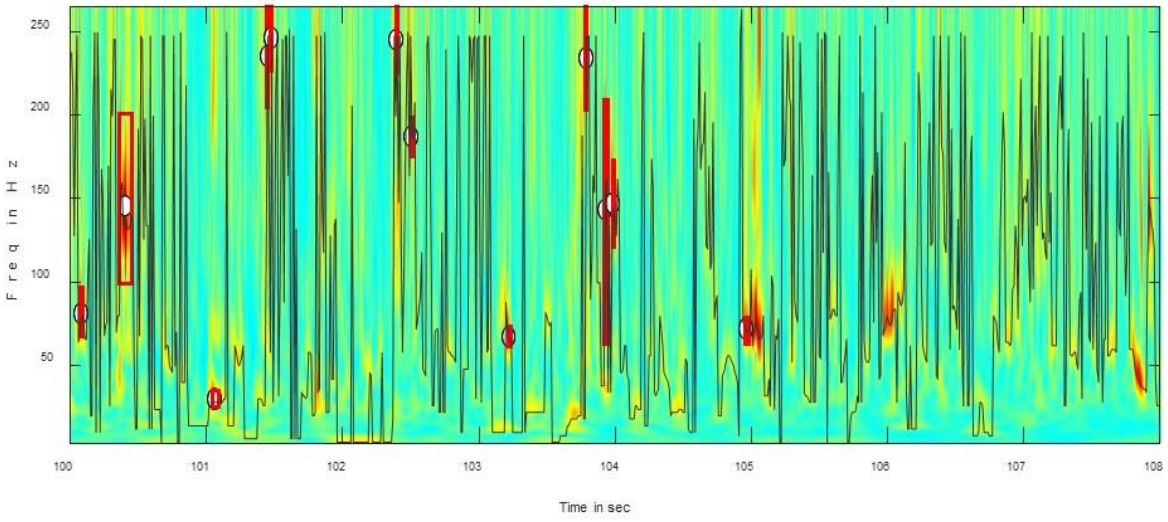

Figure 22. A clearer example of the scalogram. The circles show events above threshold for any time-frequency, and the rectangles the statistically significant activation of time-frequency ranges. Events can be detected by simple suprathreshold activity or on the basis of “blobs”, namely above amplitude and area threshold. The second yields very good results.

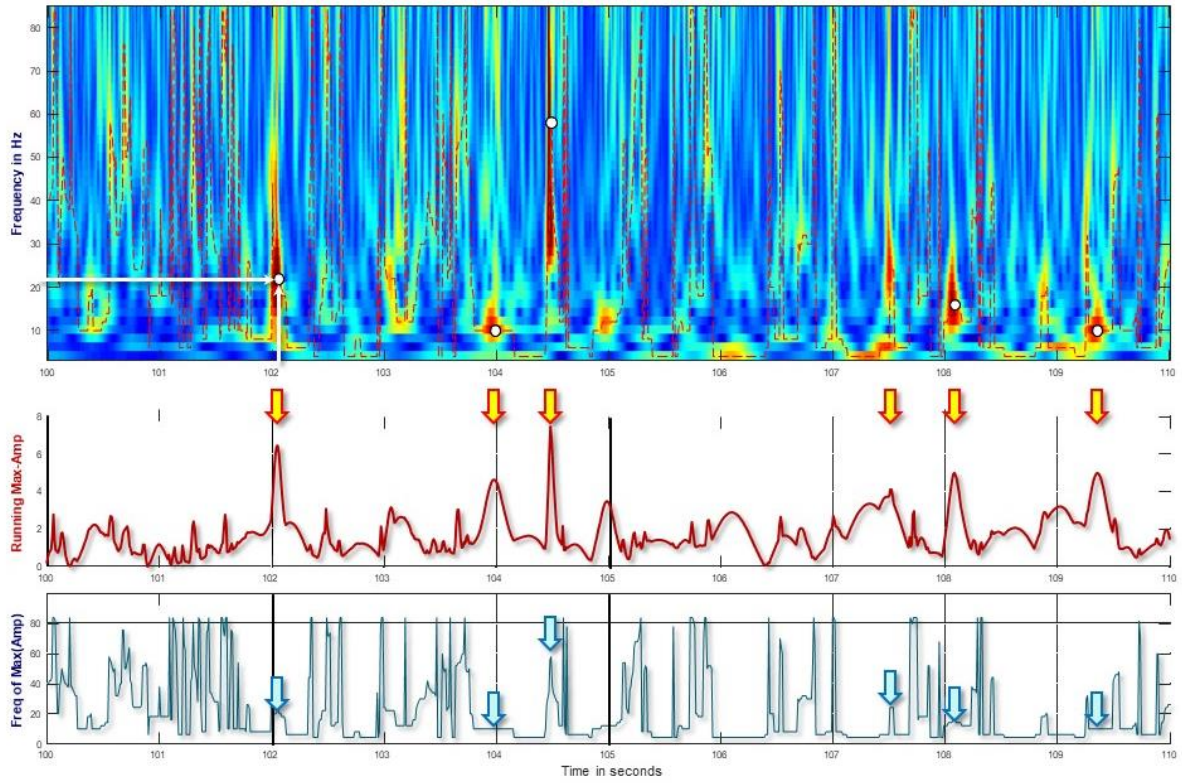

Figure 23. Examples of neurochemical scalograms used for event detection.

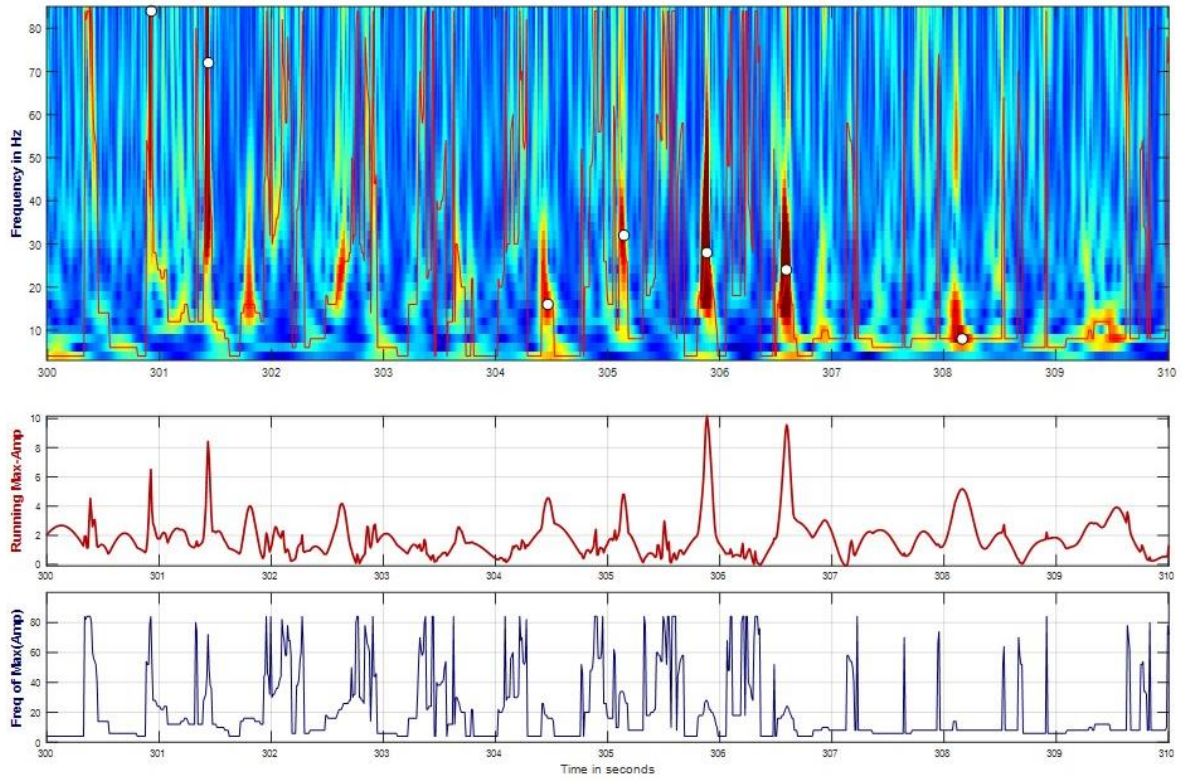

Figure 24. Examples of neurochemical scalograms used for event detection.

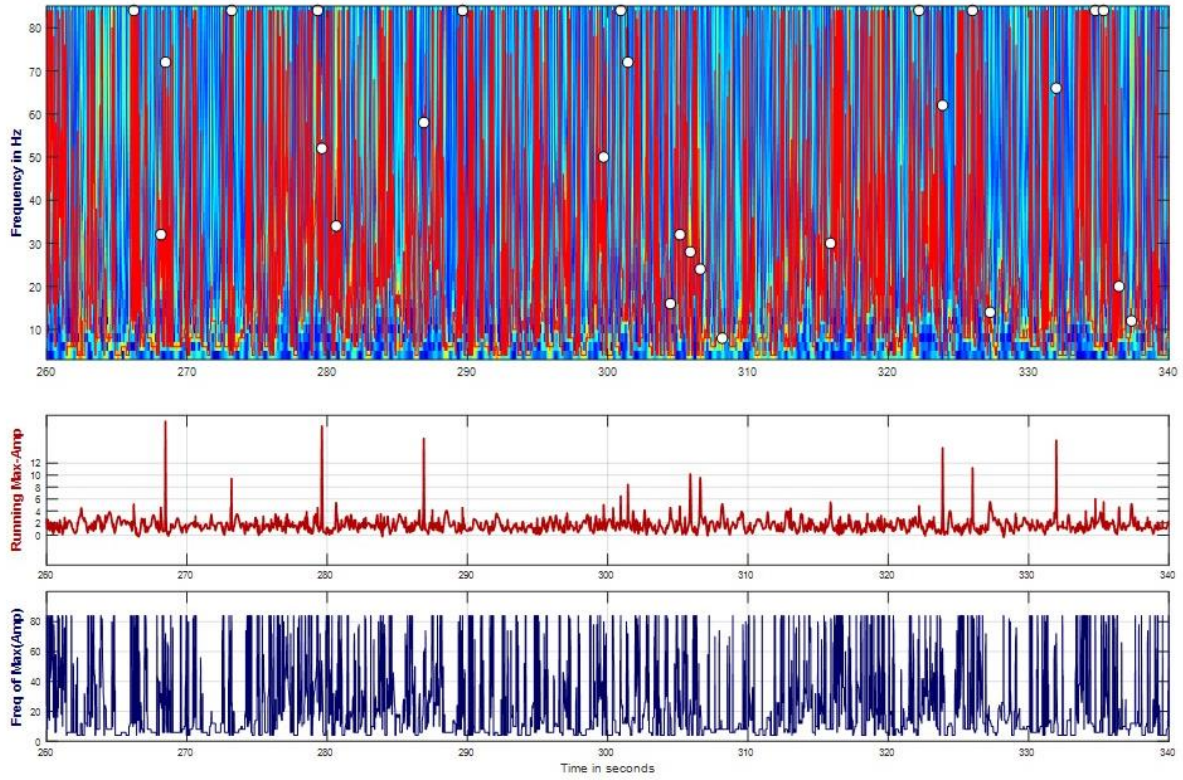

Figure 25. Examples of neurochemical scalograms used for event detection.

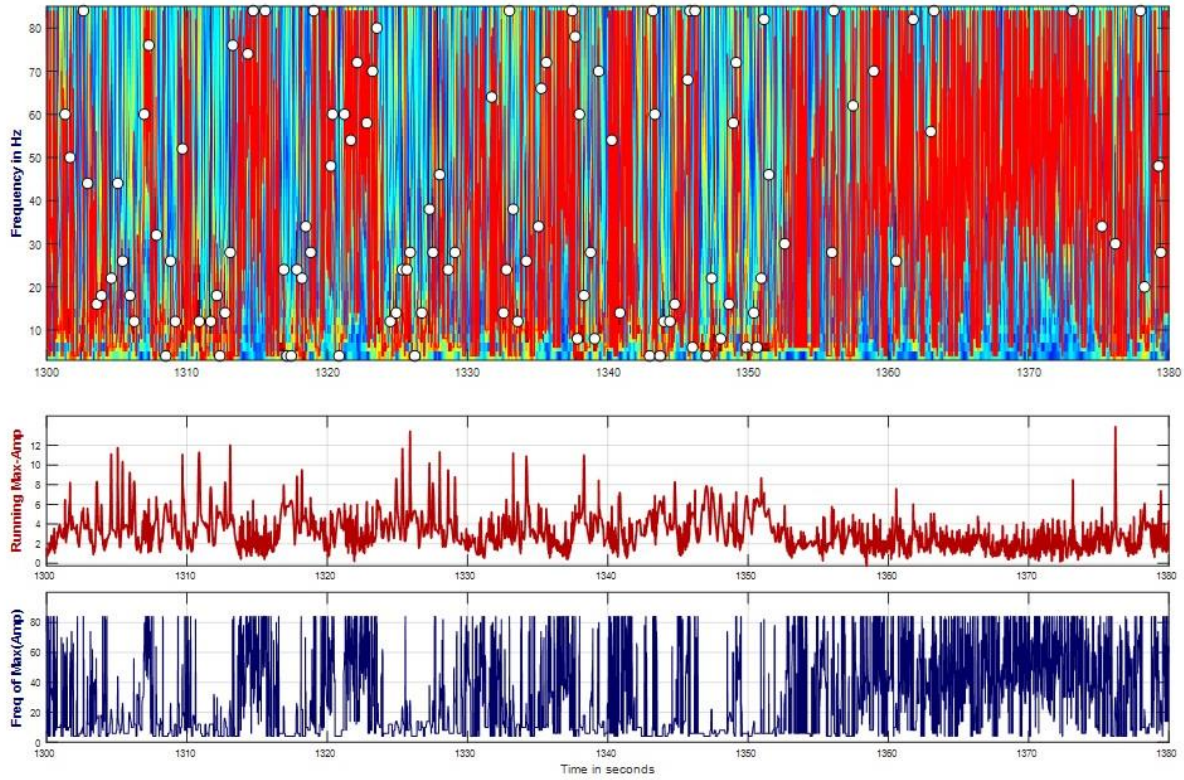

Figure 26. Examples of neurochemical scalograms used for event detection.

Based on these scalograms, one can further identify perievent time-frequency profiles for all recording sites around the cortical events (Figure 27).

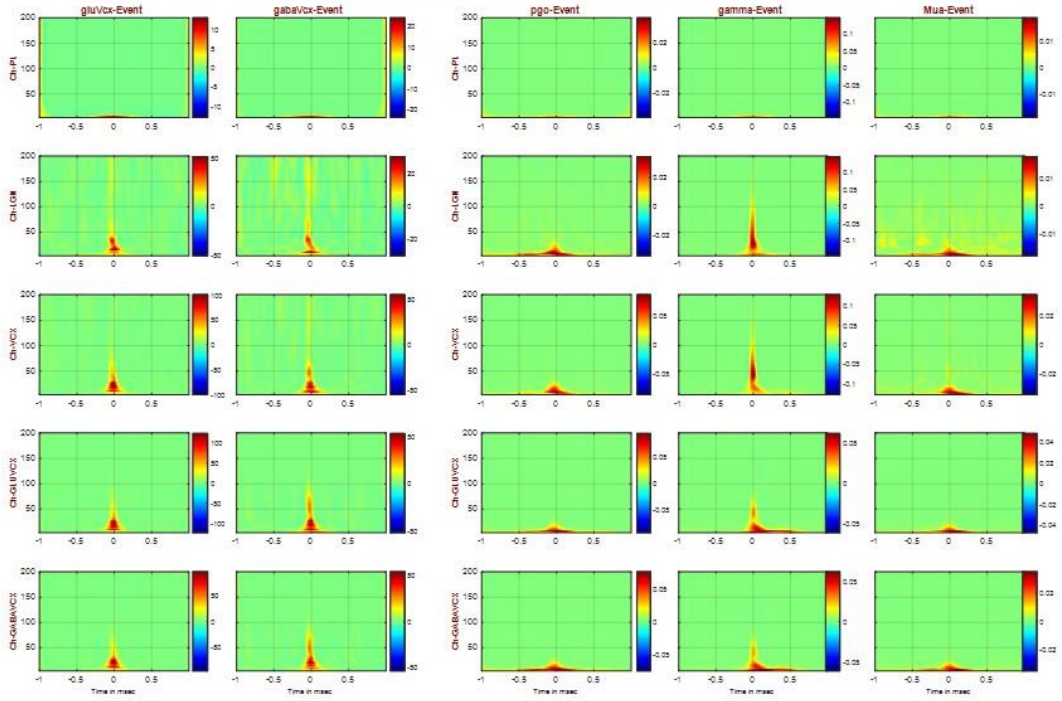

Figure 27. Perievent trial time-frequency profiles for glutamate, GABA and neural activity patterns.

In general, each IMF may have a physical meaning and since such interpretations are not set a priori, it is not justified to exclude any IMF without a systemic investigation. More importantly, it is critical to investigate whether the findings generated based on empirical mode decomposition of RAW neurochemical signals are consistent. To this end, we analyzed the cortical-event-triggered trials of the IMFs of chemical signals (Figure 28 &29).

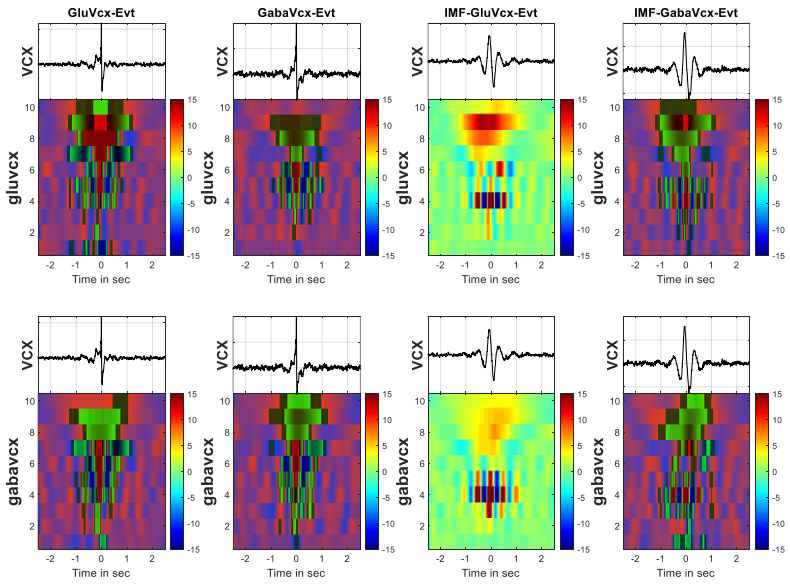

Figure 28. Cortical-event-triggered trials of the IMFs of chemical signals.

The patterns shown in the time-frequency plots are consistent from session to session and between groups. The y-axis in each image-plot is the number of the IMF(1-10) and the x-axis is the time in seconds around an event, that can be detected by rectifying the bandpass signal filtered in the 1-30Hz, 31-90Hz and 91-190Hz. On top of each image is a plot with the profile of the cleaned signal of the VCX (primary visual cortex, V1) channel. As expected, the VCX centered, while the chemical signals GluVcx and GabaVcx can be around, before or after the event-time. The first IMF captures a very brief deflection of the mEFP. The IMF(2:5) have the small oscillatory profile, while the 6th IMF appears to be consistently around the VCX-Event occasionally surrounded by negative deflections.

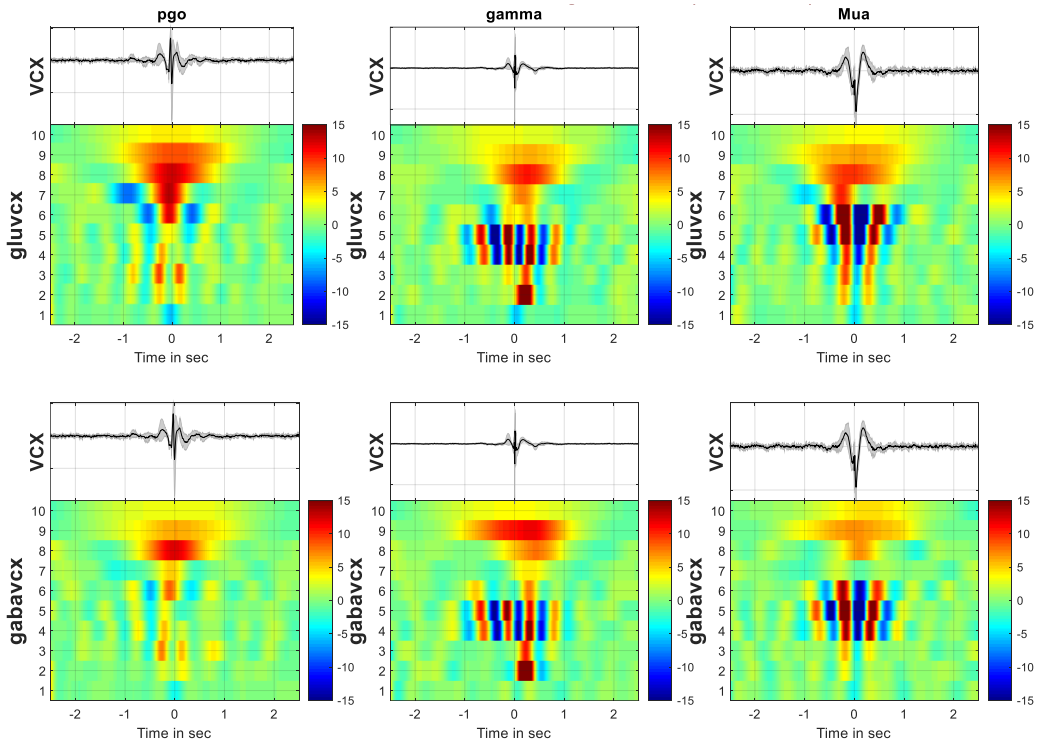

Figure 29. Cortical-event-triggered trials of the IMFs of chemical signals.

As mentioned before, the best strategy for understanding deeper the nature of the chemical signals we observe is to use their time-frequency profile and split them in groups on the basis of both their “frequency” and “temporal” profiles.

The so-called time-by-frequency non-negative matrix factorization is just a variant of the traditional and well established non-negative matrix factorization (NNMF) that effectively decomposes tensors rather than vectors. Depending on the complexity of

the question, one can use the “smallest” possible tensors (w/ two associated vectors), or more than two, depending on the question. The Tensor components (vectors), here dubbed as “modules”, represent the number of clusters. Per default two vectors per Module will result into 4 clusters (Figure 30). More specifically, the core underlying assumption of the decomposition model is that all time-frequency modules can actually be factorized into nonnegative time and frequency modules.

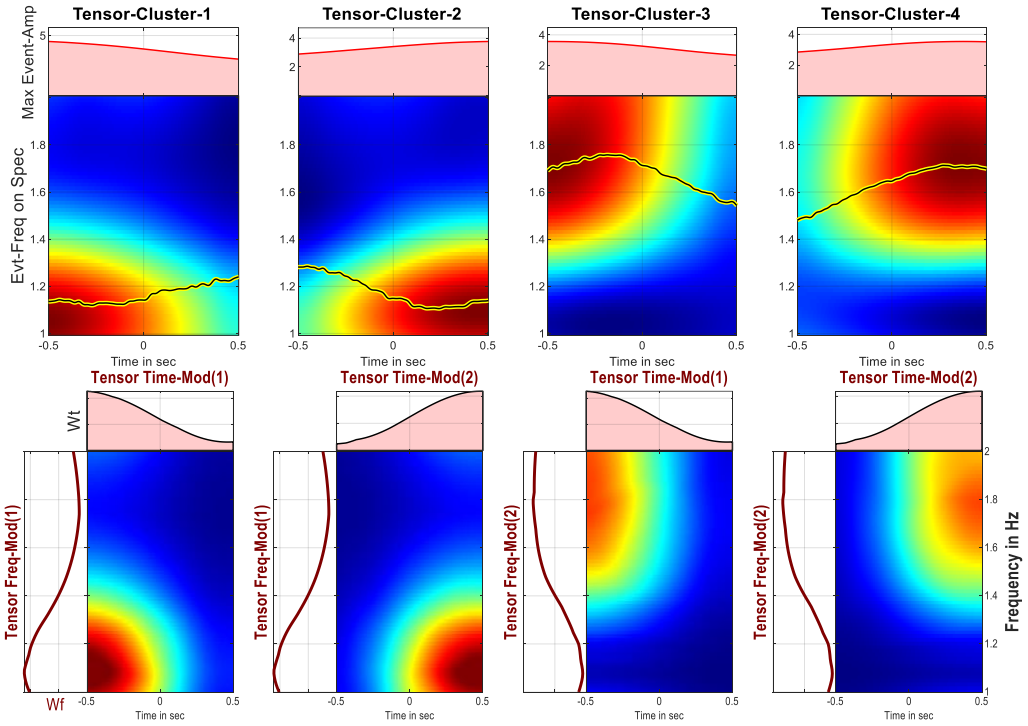

Figure 30. Characterization of tensor clusters.

While this method was initially implemented for clustering wavelets, i.e. Time-Frequency representations, in this particular case we used the Intrinsic Mode Function (IMFs) rather than the “usual” frequencies obtained with the spectrograms. In the upper raw one can see the characteristic response profile in all sessions, dominated by the IMF-4 and 5. The modules for glutamate (Figure 31) are characterized by increases/decreases of the IMF-number 4 & 5, and dominating amplitude is the average of both (top). The tensor clustering results for GABA are presented in figure 32. We further demonstrate one possible decomposition of time-frequency spectra of a set of events into modules and activation coefficients (Figure 33 & 34).

Moreover, averaging the perievent trials for each cluster obtained with the Tensor-NNMF (Figure 35) yields the responses observed here for Glu (up) and GABA (down).

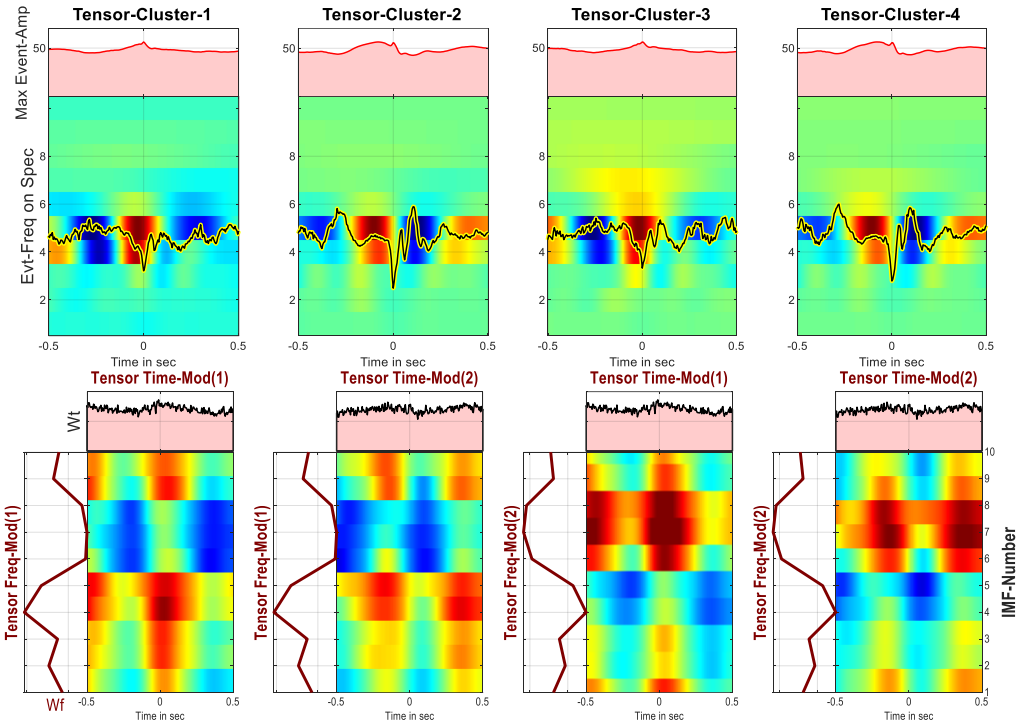

Figure 31. Tensor clustering for glutamate deflections.

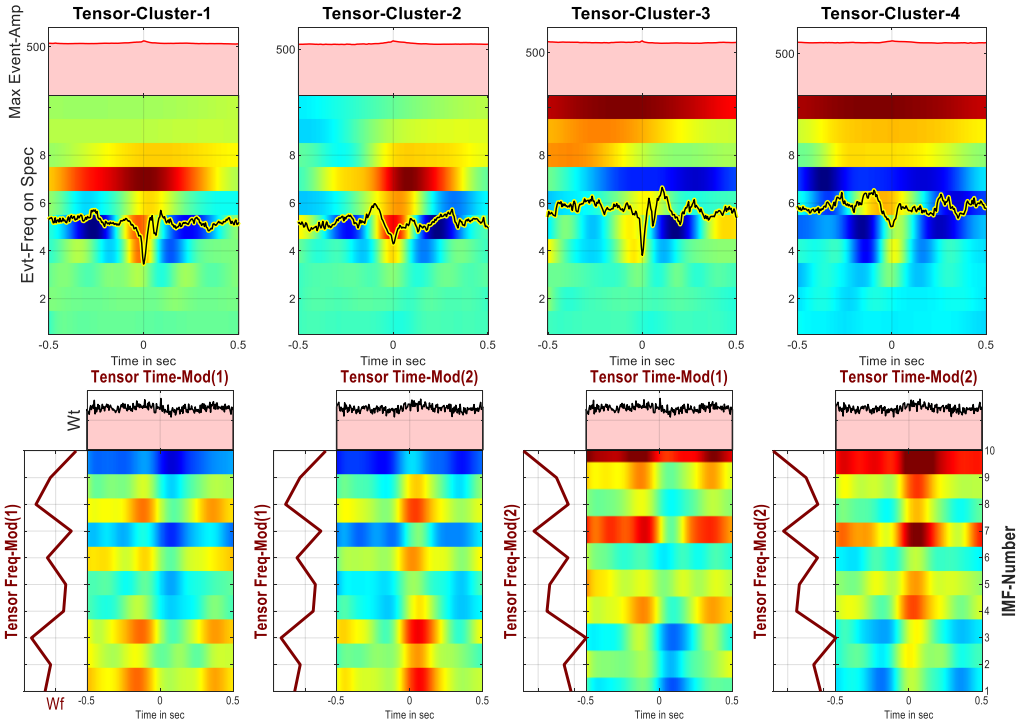

Figure 32. Tensor clustering for GABA deflections.

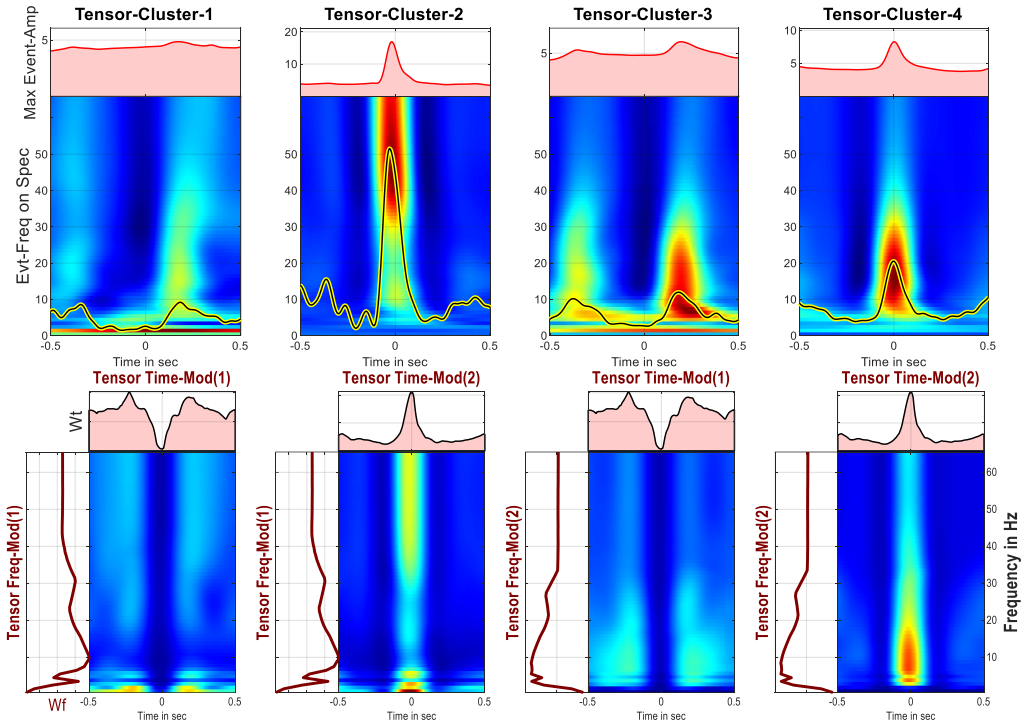

Figure 33. The input spectra form a 3D tensor (glutamate). The time and frequency modules are used to calculate product modules that characterize the event spectra. The upper row shows the centroid of each cluster. The first cluster has week post-event activation, the second one strong activation at the time of occurrence of a Glutamate deflection, and somewhat similar but also different are the two last clusters. To help the figure visualization the top row has the running max-amp of the wavelet on top, and the frequency of each max-amp superimposed on the spectral image. The bottom row shows the two types of modules, one varying in the temporal and another in the frequency domain.

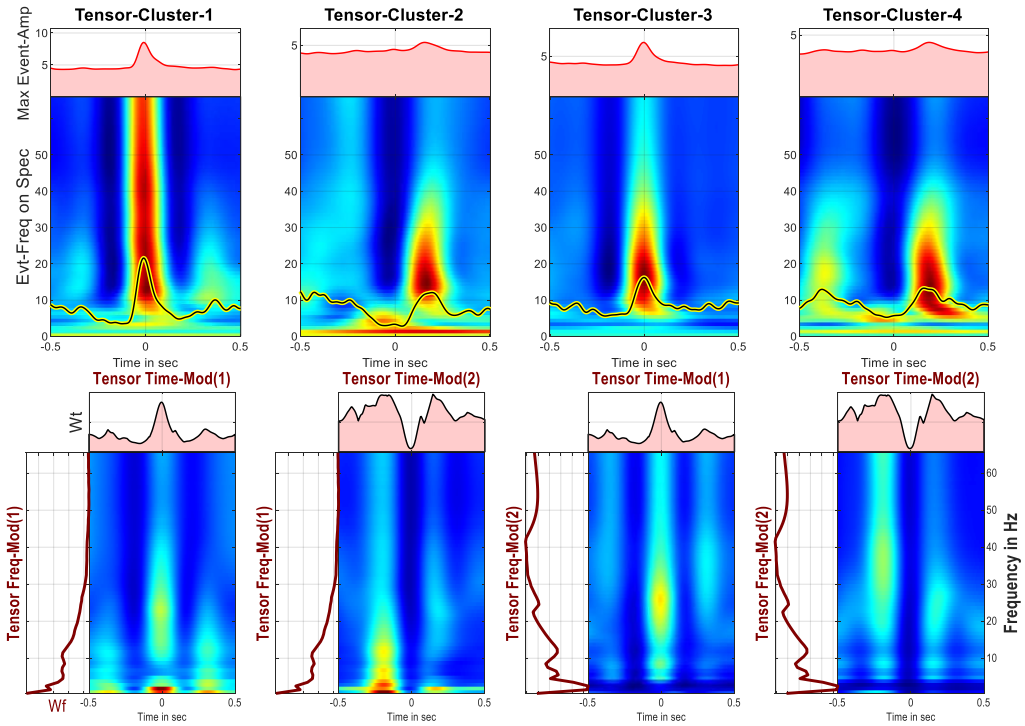

Figure 34. The input spectra form a 3D tensor (GABA signals).

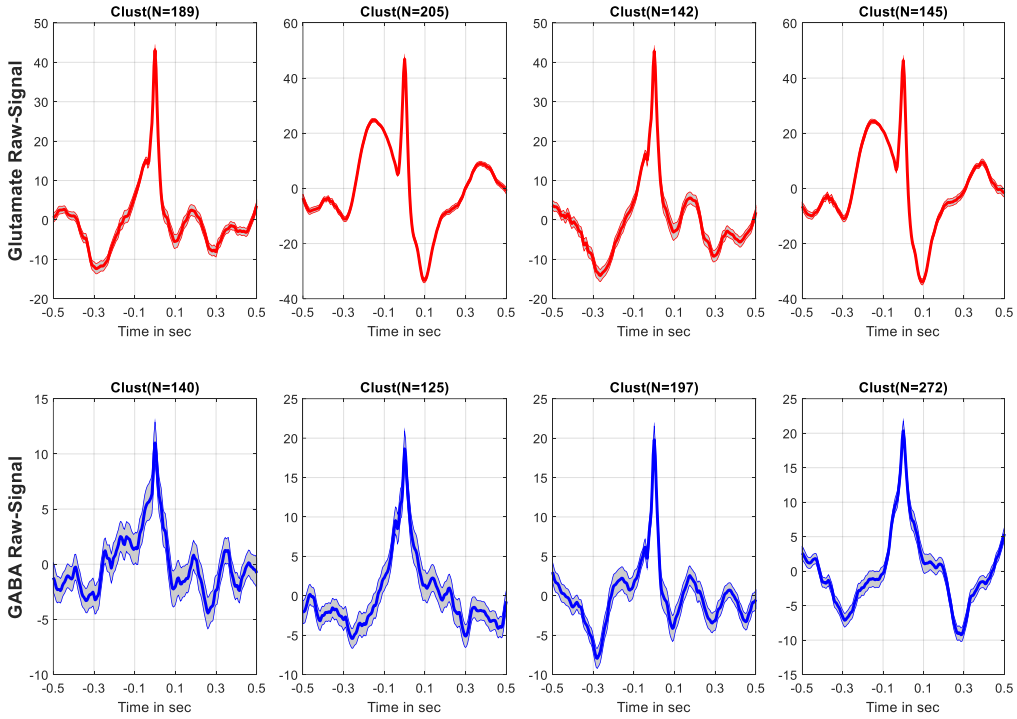

Figure 35. Results of averaging the perievent trials for each cluster obtained with the Tensor-NNMF.

The previous figures show the peri-event responses for different types of events in different structures. Important is to see the time series of the electrophysiological and chemical signals. There is nothing unexpected, yet all figures support the notion of measuring true chemical signals, rather than reporting a slightly filtered version of the electrophysiological one.

In order to relate the neurophysiological observations, it is critical to estimate of occurrence-probability of a set of events with respect to given reference events. For this purpose, the conditional intensity function (CIF) was calculated for signals in different brain regions (Figure 36-38).

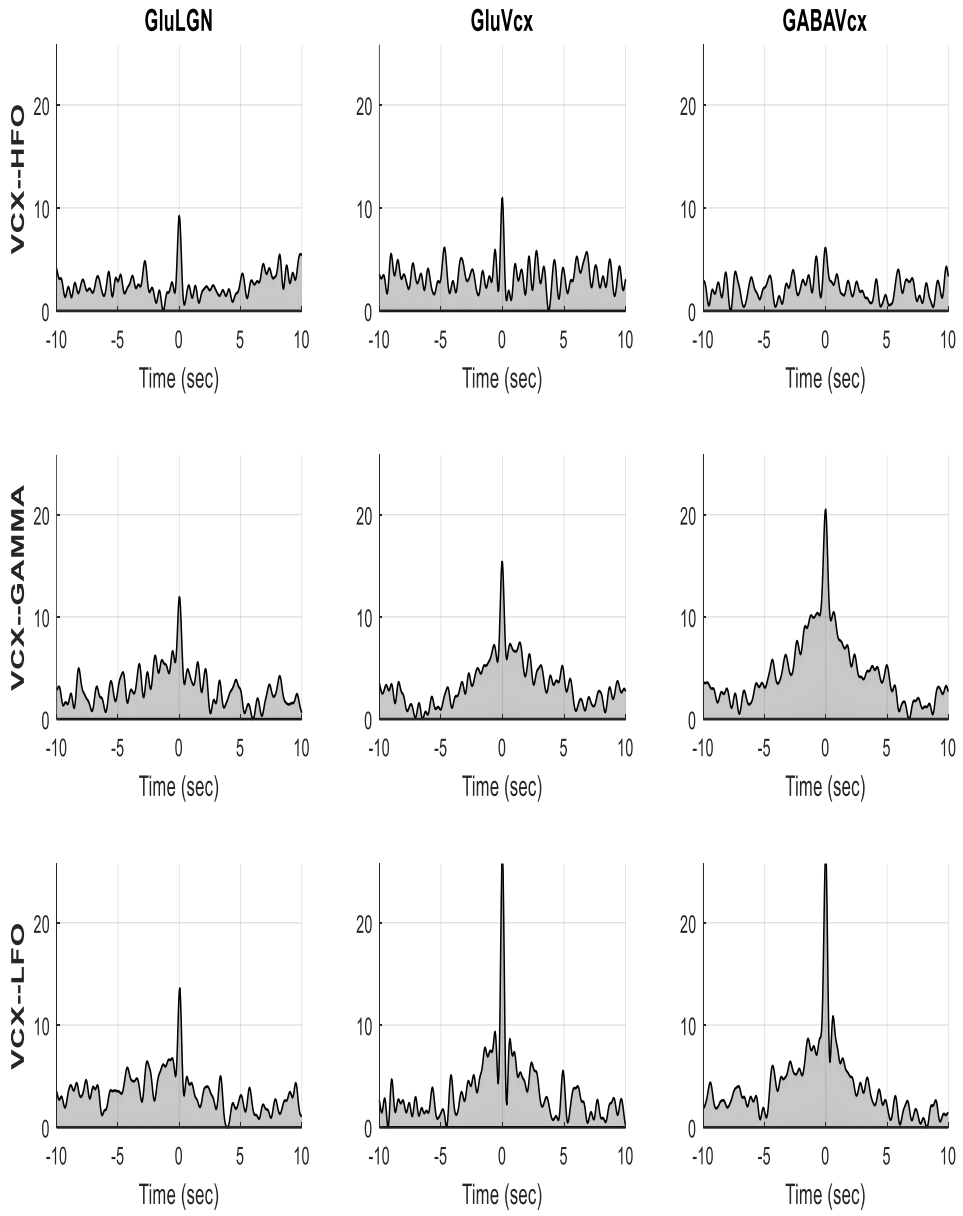

Figure 36. Conditional intensity function (CIF) between neural signal (VCX) and chemical signals. The occurrence probability of high-frequency oscillations (HFO) in primary visual cortex is lowest in comparison with gamma and low-frequency oscillations (LFO) and nearly exclusively to glutamate events. Gamma and even more strongly LFO in visual cortex are co-occurring with GABA and glutamate in VCX and with a lesser degree with glutamate in LGN.

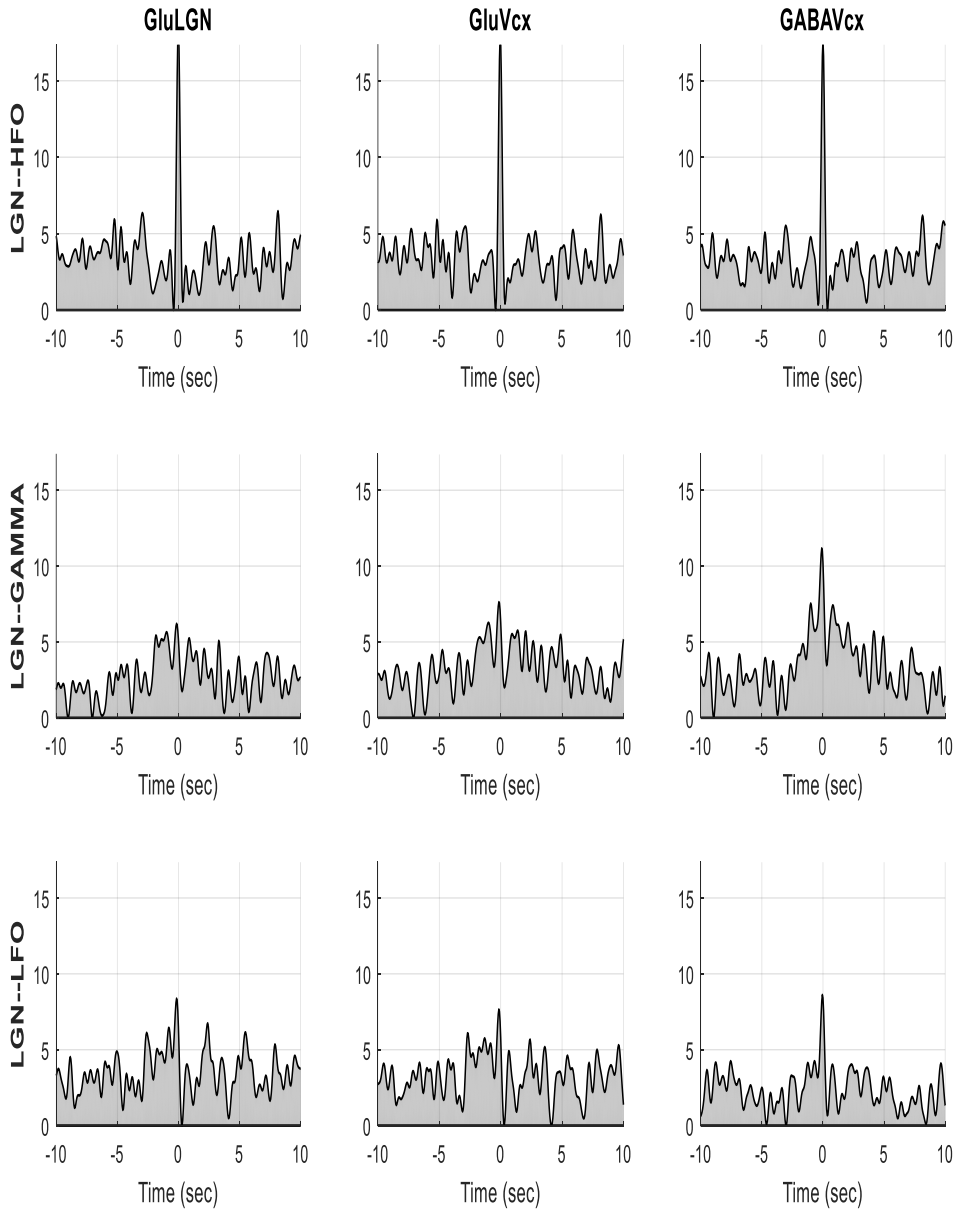

Figure 37. Conditional intensity function (CIF) between neural signal (LGN) and chemical signals. In contrast to cortical signals, HFO in LGN has the highest occurrence probability with all neurochemical signals, yet gamma and LFO show low and non-specific occurrence probability with GABA.

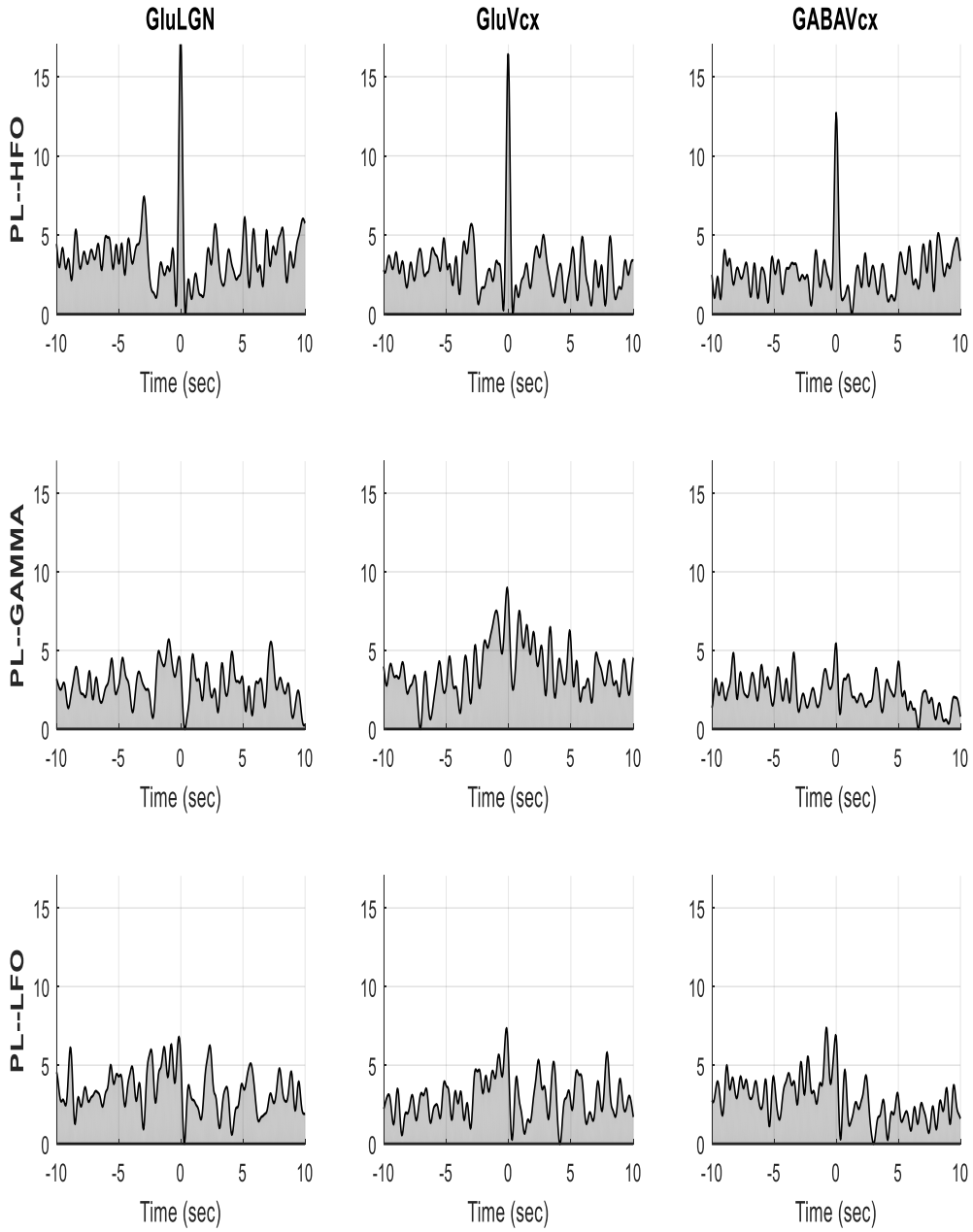

Figure 38. Conditional intensity function (CIF) between neural signal (hippocampus) and chemical signals. Similar to LGN, only high frequency neural oscillations in pyramidal layer of hippocampus have a notable occurrence probability with glutamate in thalamus and cortex and GABA in cortex. CIF suggests that occurrence of gamma and LFO seems to be largely unrelated to the E-I cortical network.

The robustness between groups and sessions as well as anatomical specificity of conditional intensity function between neurophysiological and neurochemical signals enable us to identify different spatiotemporal excitation-inhibition patterns that relate to different neuronal events in a consistent manner (Figures 39-41).

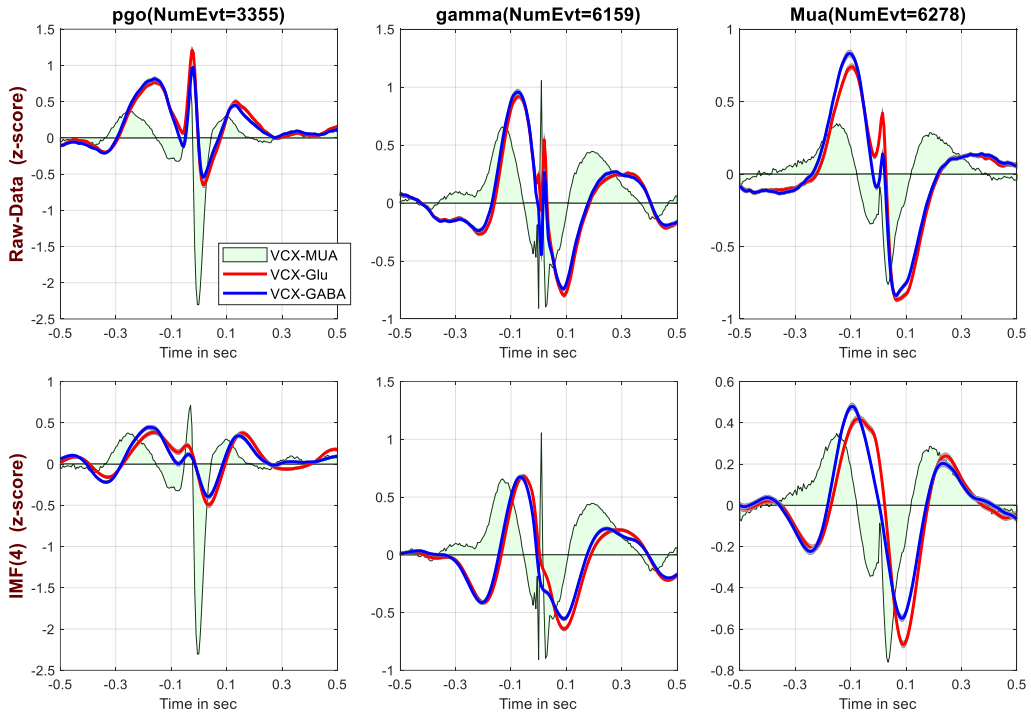

Figure 39. VCX-events: Peri-Event Raw-Data- (top-row) and IMF-Trials (bottom-row) for Cortical Events, i.e. PGO, Gamma + High Gamma and MUA area-Plot is the Multiunit activity in Cortex, Red Glutamate and Blu GABA (population data).

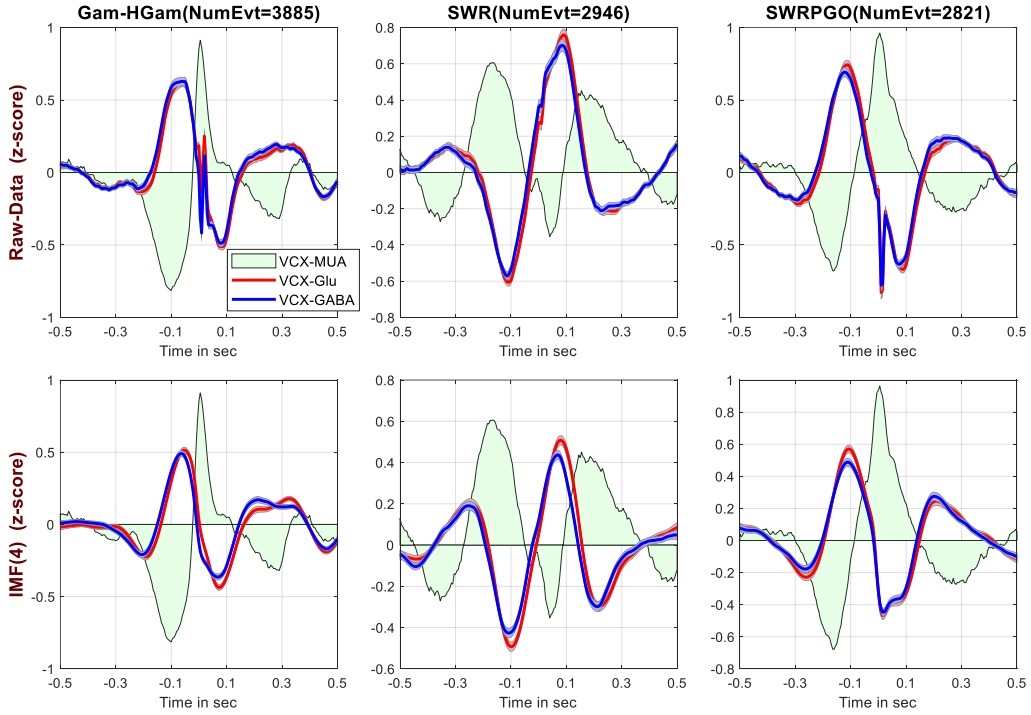

Figure 40. Peri-Event Raw-Data- (top-row) and IMF-Trials (bottom-row) for hippocampal events.

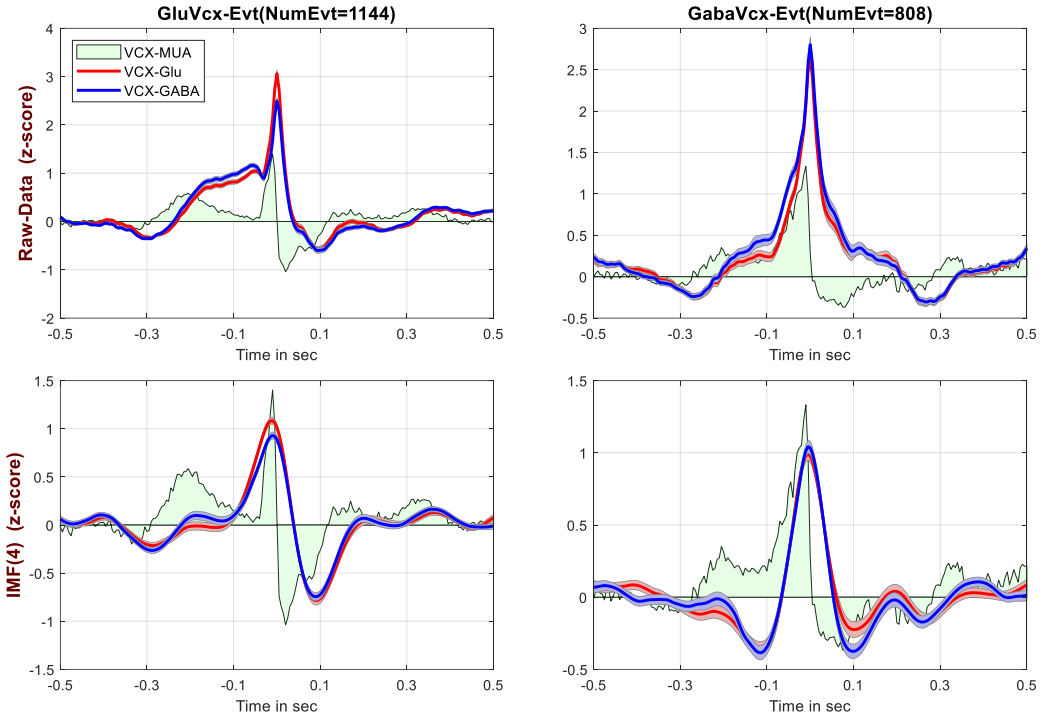

Figure 41. Peri-Event Raw-Data- (top-row) and IMF-Trials (bottom-row) for neurochemical events.

The overall findings suggest that our technology allows us to characterize the neural events in terms of diverse patterns of glutamatergic and GABAergic activity that relate to the structure of canonical circuits. Thus, the recordings can potentially be utilized to characterize the functional structure of such networks. The temporal relationship between the electrical and chemical signals was further investigated by calculating the phase-lock-values (PLV) for different animals and the findings remained consistent. The PLV is a normalized measure of phase synchronicity and allows us to evaluate how the distribution of phase differences between two signals is spreading (Lachaux et al., 1999). Thereby, the PLV values increase, when the distribution of phase difference decreases ranging from no phase dependence to complete phase lock.

Here, we present the distribution of phase differences and phase-locking-values of three representative animals (Figures 42-44) for neural activity, glutamate and GABA signals in the primary visual cortex and LGN. The results suggest that neural activity is always advancing neurochemical signals during visual stimulation. Cortical glutamate and GABA alterations present themselves approximately 19 ms after the neural response in VCX (0.48 ± 0.1 rad and 0.47 ± 0.05 rad, respectively), while as

expected, the neurochemical phase difference with activity in LGN is larger, namely 19.7 ± 3.8 ms for glutamate and 21.3 ± 4.5 ms for GABA.

Although these findings are already encouraging, numerous previous studies have indicated that the modes of operation of the excitation-inhibition network are state-dependent and ignoring the state-specificity of neurotransmitter dynamics may likely lead to non-sensical results. We will focus on state-identification and the interpretation of neurotransmitter dynamics in section 3.3.1.

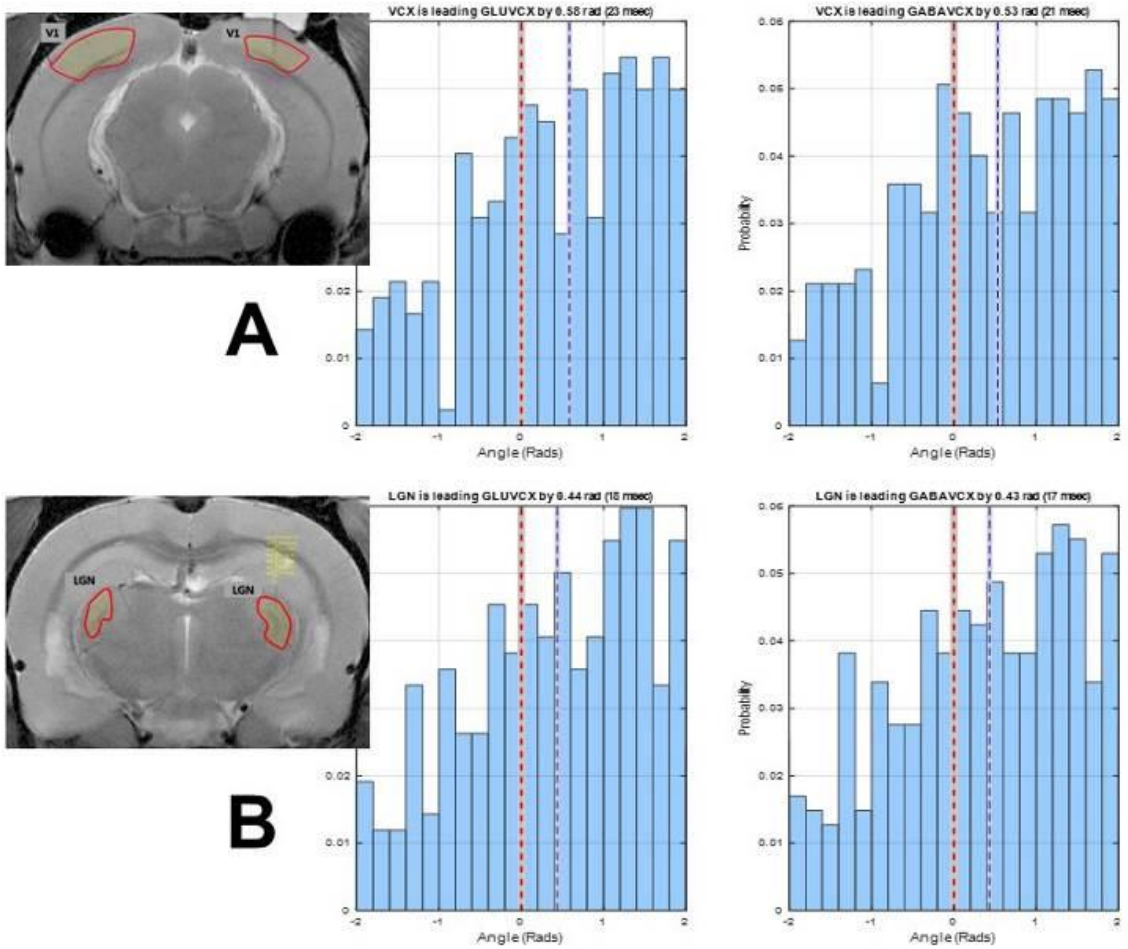

Figure 42. Phase distribution and phase-lock-values (PLV) between neural activity in primary visual cortex (A) and LGN (B) and main cortical excitatory/inhibitory neurotransmitters (glutamate: left, GABA: right) show that neural activity in response to visual stimuli is leading neurochemical response by 19 to 21.3 ms.

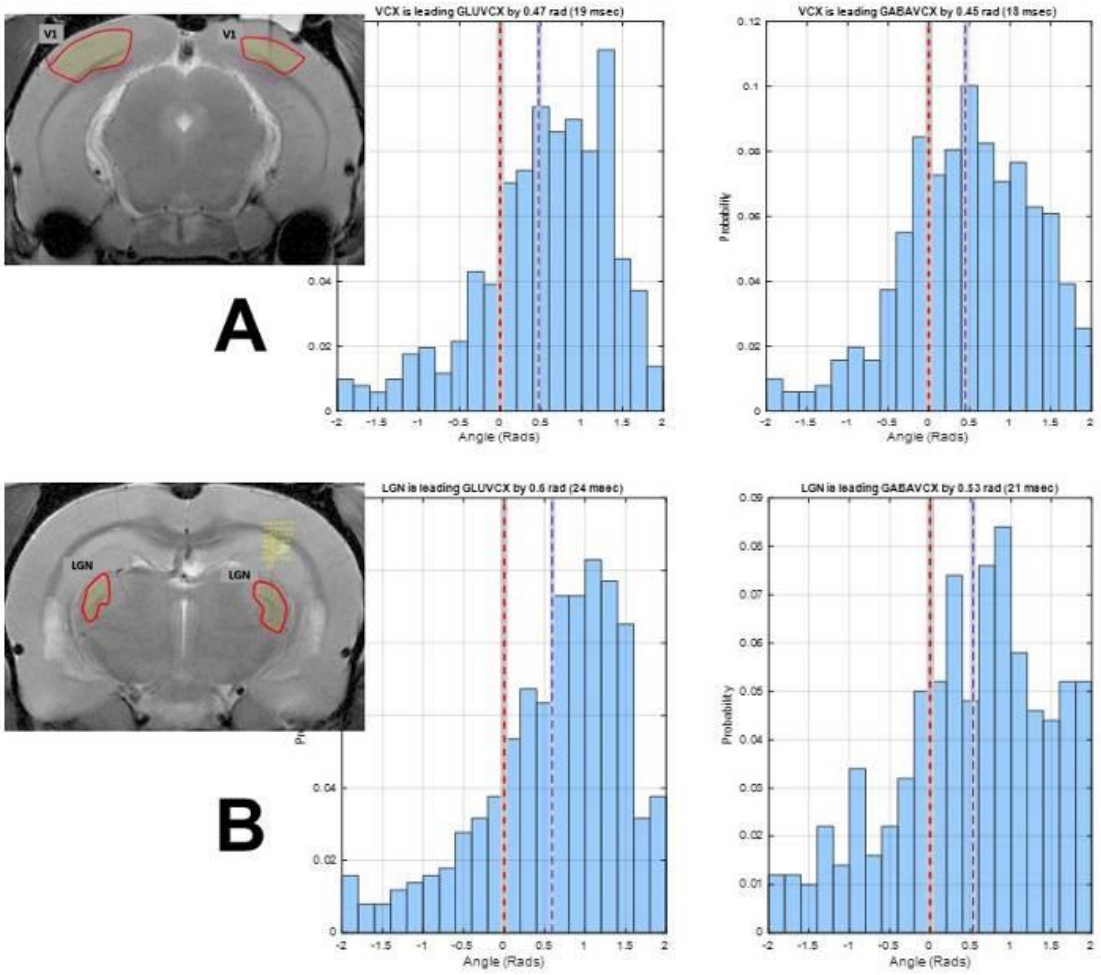

Figure 43. Phase distribution and phase-lock-values (PLV) between neural activity in primary visual cortex (A) and LGN (B) and main cortical excitatory/inhibitory neurotransmitters (glutamate: left, GABA: right) show that neural activity in response to visual stimuli is leading neurochemical response by 19 to 21.3 ms.

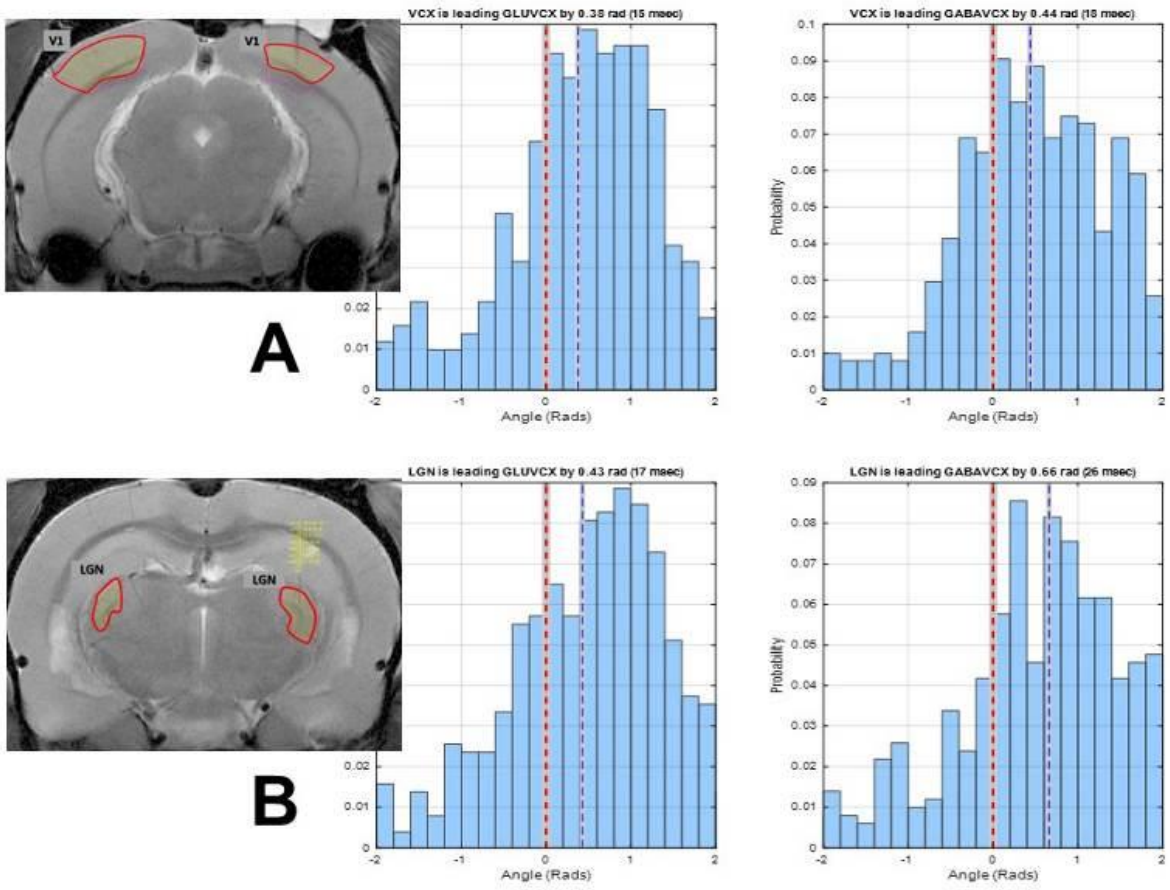

Figure 44. Phase distribution and phase-lock-values (PLV) between neural activity in primary visual cortex (A) and LGN (B) and main cortical excitatory/inhibitory neurotransmitters (glutamate: left, GABA: right) show that neural activity in response to visual stimuli is leading neurochemical response by 19 to 21.3 ms.

Last but not least, we characterized the temporal profile of the clustered neurotransmitter responses (Figure 45). Top row is for glutamate and bottom row for GABA. Glu and GABA have distinct profiles, even when raw-data are used without the Empirical Mode Decomposition. The right most Tensor-Cluster shows the most frequent response profile for Glu and GABA. Typically, glutamate deflections have three “phases”. Glu-Concentration increases before and decreases – below baseline – after the peak activity of each “onset”. Thereby, the before-peak activity of Gaba is characterized by a concentration-drop. Interestingly the opposite profile is observed in the third subset.

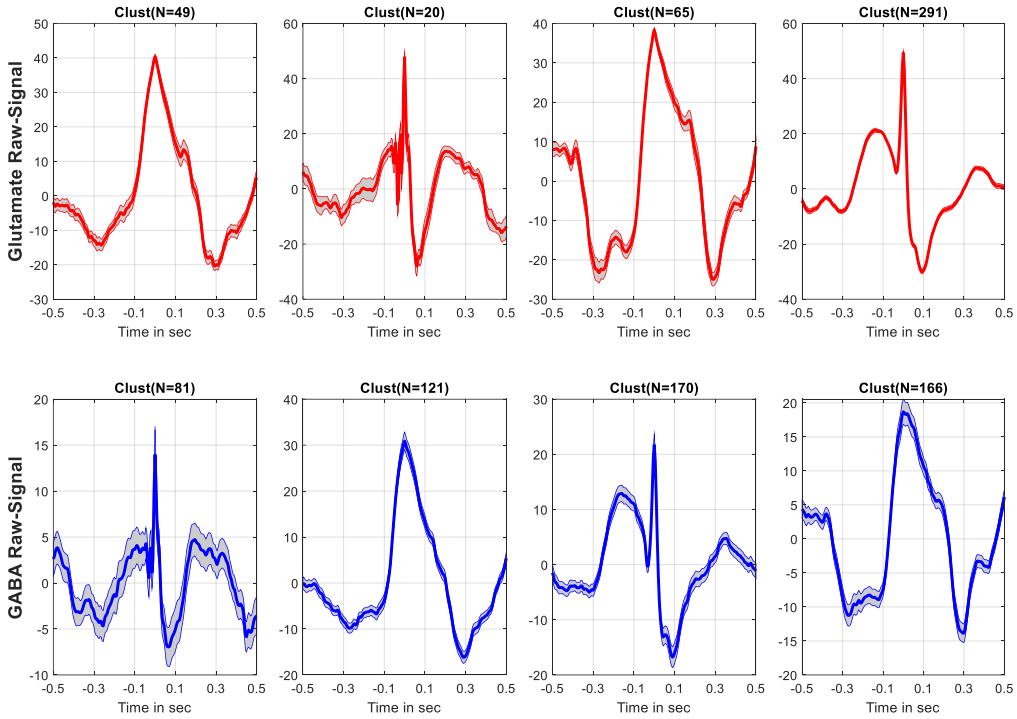

Figure 45. Temporal profile of glutamate and GABA associated with different clusters.

Following the profile characterization, we decided to check systematically the relationship of Glutamate and GABA concentration-changes to the modulation of the cortical signal in the Gamma range, as more than 5 studies did in the past, by mostly using fMRI/fMRS etc. One of them (Kujala et al., 2015), reported the most "specific" relationship between neurotransmitters and gamma, albeit by measuring NT-receptor density, rather than signal modulation. The authors claimed that increases in GABA are associated with decreases in Amplitude and increase in Frequency of visuo-cortical gamma-field potentials. In fact, we have shown here exactly the opposite (Figure 46 & 47).

Firstly, one cannot possibly examine correlations between GABA and Gamma, assuming that all peri-Gamma-Deflection trials are the same. They are not. Clustering the trials of peri-GABA-deflection, by using more than 4 different algorithms, one of which can estimate the optimal number of clusters as well, consistently yielded two patterns of physiological responses, which are displayed in the top and bottom rows respectively. In the left column you see the perievent GABA-Responses, as well as the IMF-ones, for the two clusters of the scalogram, namely

the running max-amplitude and the corresponding frequency changes within the gamma-range of the cortical signal.

Increase in GABA-concentration (left column) can yield – in about 80% of the cases – to an increase of the Max-Amp signal associated to mild decreases of running frequency. In 20% of the cases one has the Kujala-reported result.

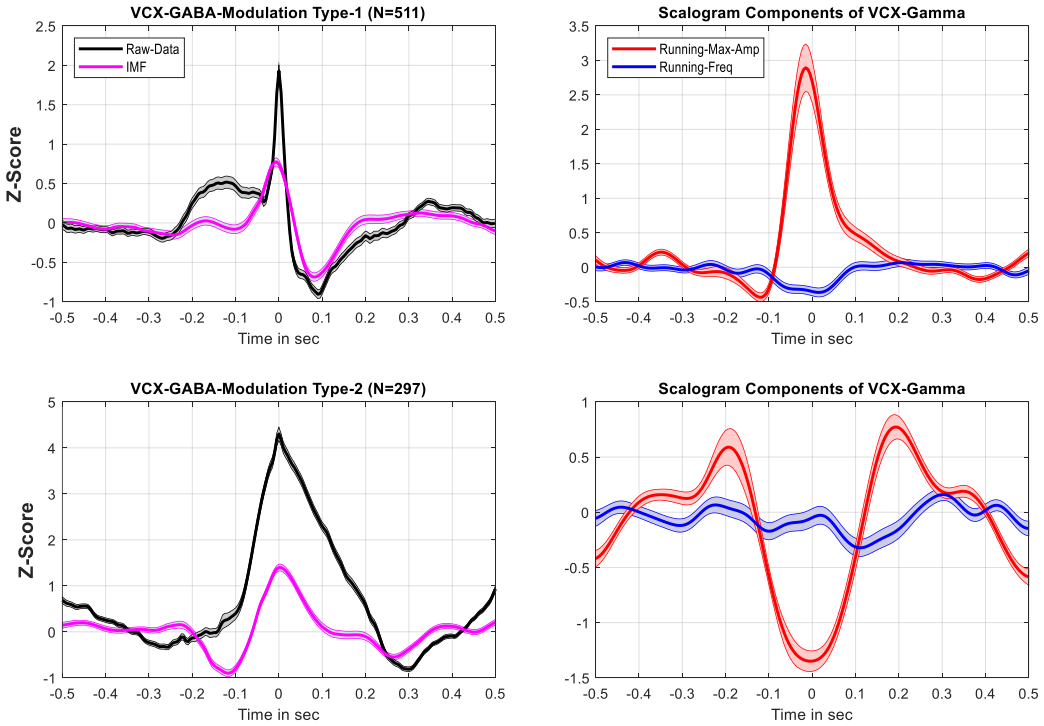

Figure 46. Modulation of cortical gamma oscillations by GABA dynamics.

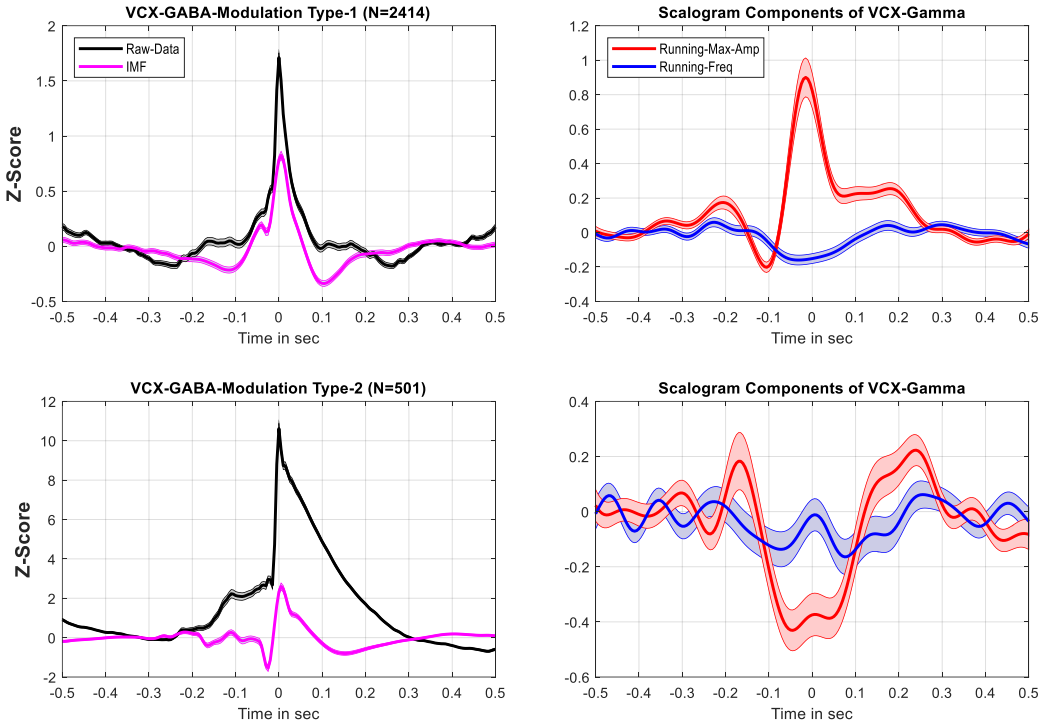

Figure 47. Modulation of cortical gamma oscillations by GABA dynamics.

Notably, the relationship of the GABA to the Gamma Cortical Signal is not specific to "GABA", but applies also to the glutamate (Figure 48 & 49).

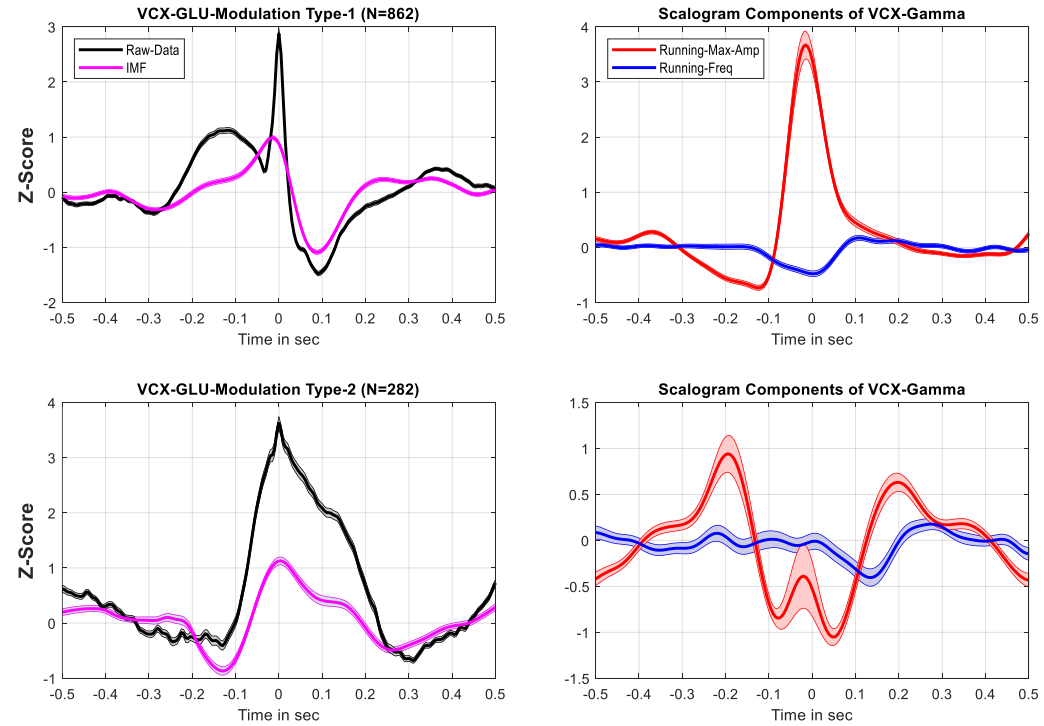

Figure 48. Modulation of cortical gamma oscillations by glutamatergic dynamics.

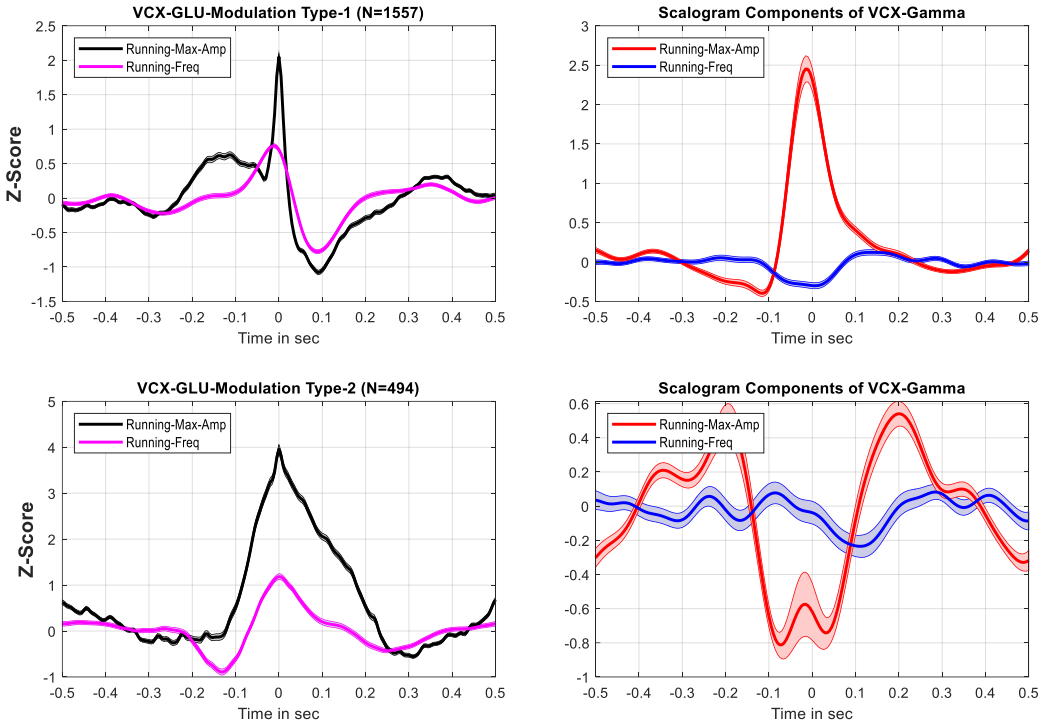

Figure 49. Modulation of cortical gamma oscillations by glutamatergic dynamics.

The anti-proportional dynamics clearly shows the independence of the amperometric signals from (removed) electromagnetic induction. Moreover, anti-correlated Glu-GABA (Figure 50) are typically seldom and usually reflect local events, rather than general (partly neuromodulatory) activity that characterizes the nested recursive cortical microcircuits.

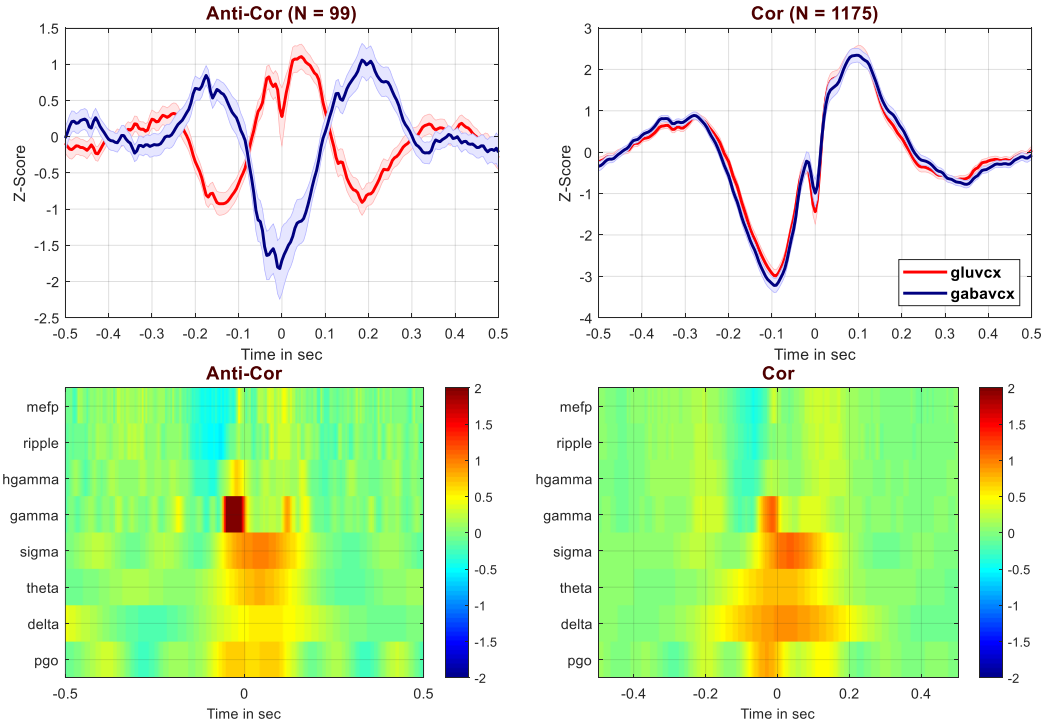

Figure 50. Rare, yet significant, anti-correlated behavior of glutamate and GABA systems in VCX.

3.2.5 The contribution of astrocytes in glutamatergic time-series

For many years, glia cells were considered as silent participants of information processing of the central nervous system. However, over the past few decades more and more studies demonstrated that glia and particularly astrocytes actively release neurotransmitters such as glutamate and modulate synaptic processes. The effects of astrocytes on glutamate levels have also a large impact of BOLD signal. Therefore, it is critical for us to understand the origin of the glutamatergic signals that our technology observes. Here, we used a selective P2X antagonist, namely PPADS, that has previously been shown to significantly reduce and almost eliminate glutamate release from astrocytes. By infusing this drug right next to the recording channels of the electrode (~500 µm distance), and comparing pre- and post-infusion conditions, we were able to analyze the contribution of astrocytic glutamate in the measured time-series (Figure 51).

Prior to the drug administration, the glutamate release in S1 at rest presented itself with a frequency of 12.7±2.9 Hz and was weakly ($r=0.3$) yet significantly correlated with neuronal spikes. The application of PPADS gradually diminished glutamate release for ~30-40 minutes. However, it is not possible to designate the elimination of glutamate signal solely to active drug effects. It is as well possible that the dilution of the extracellular fluid and not the pharmacodynamic action of the drug caused the signal reduction.

Therefore, we also observed the recovery period of the signals to estimate true drug effects. Our analysis suggests that the frequency of glutamate release was decreased significantly ($F_{1,14}=7.33$, $p<0.05$) by 74.2±23.9%. Thereby, the signal amplitude was largely unaffected ($F_{1,14}=0.19$, $p=0.67$). As a proof of concept, we could demonstrate that the neuronal firing rate was as well not altered significantly ($F_{1,9}=0.49$, $p=0.5$). Yet, a small 27% increase of neuronal firing frequency was observed. In addition, the cross-correlation of neuronal spiking and glutamatergic time-series was decreased by 60.1±18.1%, from 0.3 between spiking and gluatamatergic events to 0.13. The overall findings suggest that PPADS actively reduced glutamate release but more importantly that approximately 70% of the measured glutamate signals by our electrodes may not be neuronal.

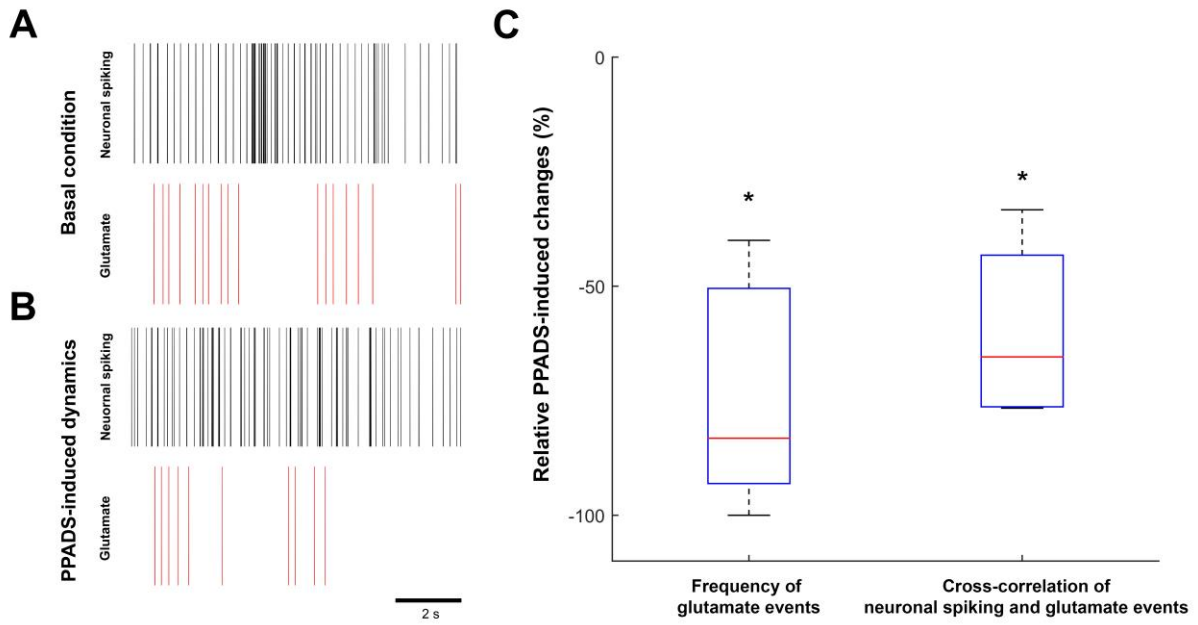

Figure 51. Investigation of the impact of glia cells on simultaneous measurements of neural activity and glutamatergic signals in S1. The intracerebral infusion of selective P2X antagonists significantly alter the baseline properties of the signals (A) by reducing the frequency of the glutamatergic events (C), while keeping the firing rate of neurons unaltered (B).

3.3 Underlying biology of BOLD signal

The main advantage of functional MRI experiments is the fact that they provide a whole-brain estimate for hemodynamics response to different stimuli. We decided to investigate two major and widely studied pathways, namely the somatosensory and the visual systems. The rationale for this choice was two-fold: 1) the existing data and information obtained in seminal previous experiments can be used as reference. This allows us to optimize stimulation and measurement paradigms; 2) In the first step of methodological developments, it is critical to provide a robust proof-of-concept. This can be achieved by demonstrating that our technology advances our understanding of well-known systems at mesoscopic level and shines a new light of existing hypotheses and theories.

For example, numerous studies have used retrograde tract-tracing and electrophysiological techniques to explore the internal organization and connectivity of the sensorimotor system in rat brain, revealing a general map of projections between somatosensory cortex, basal ganglia and the thalamic. In order to further investigate the functional connectivity of this map, a large number of studies focused on the effects of electrical stimulation of the rat paw on cortical information

processing (Boussida et al., 2017). Although, the effects of such sensory peripheral stimulations should also present in basal ganglia and thalamic regions, functional MRI experiments often cannot observe the activations of these subcortical brain areas. This could be a consequence of the choice of anesthesia. These compounds often significantly affect the cerebral blood flow and metabolism and therefore, can reduce the hemodynamic response. In addition, the choice of stimulation parameters such as pulse width and electrical current can significantly alter the pattern of brain activation. In our study, we used an innocuous forepaw stimulation (5 Hz, 1 mA) and a pulse width of 1 ms to avoid the co-activation of pain centers in the rat brain. Although, anesthesia with remifentanil as applied in our study is known to provide excellent signal-to-noise ratio, the reaction of animals to the anesthesia during the experimental process can vary and lead to instabilities.

The stimulation paradigm induced in the majority of the animals the expected pattern of activation in sensorimotor, basal ganglia and thalamic regions (Figure 52) and the results remained robust throughout the averaging process (Figure 53).

The observed BOLD response around the electrode provides excellent settings, since a main goal of our study is to characterize the causal relationship between BOLD, neural activity and neurochemistry and would optimally analyze data from the same voxels, as it would be possible in this case.

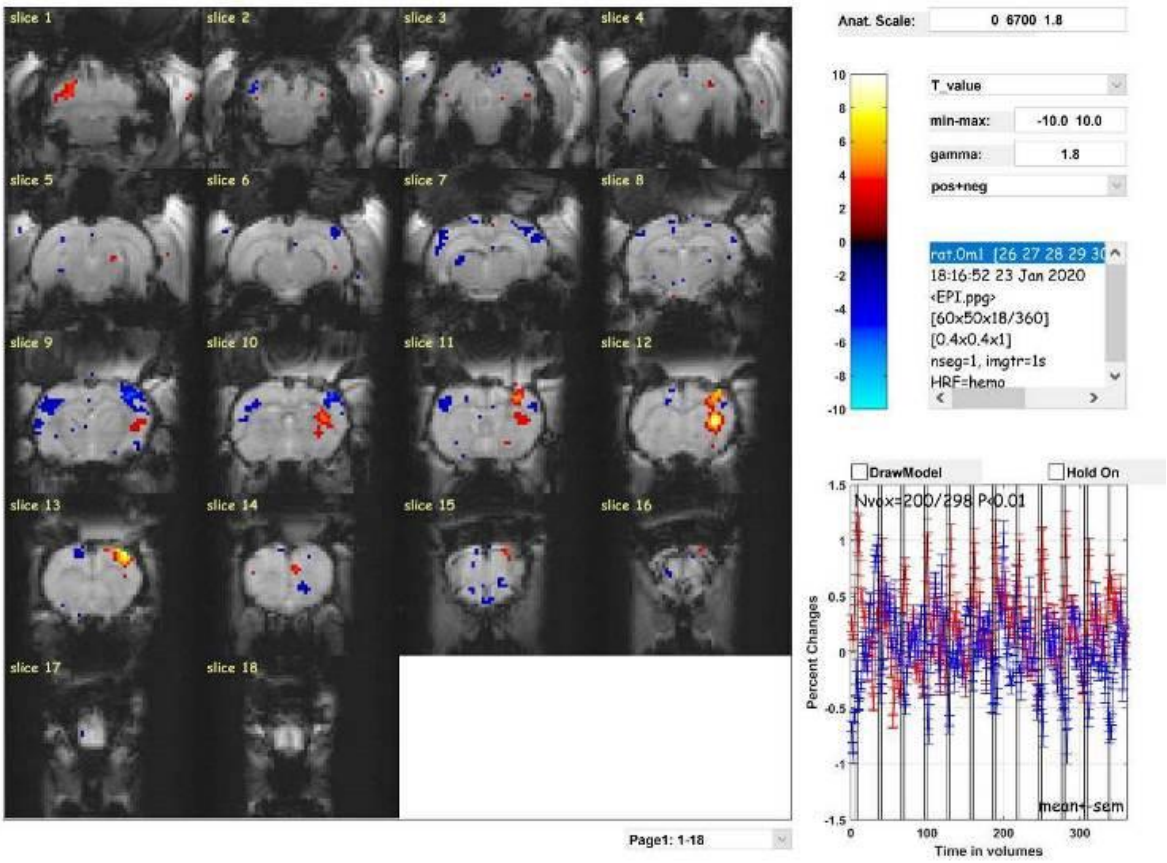

Figure 52. Coronal view of cumulative (all segments) hemodynamic response of sensorimotor system to unilateral paw stimulation in a rat under remifentanil anesthesia from posterior to anterior. The echo-planar imaging maps present statistically significant voxels (uncorrected ($p<0.01$)) with positive and negative BOLD. Overall, positive BOLD was observed in parts of cerebellum, somatosensory and motor cortex as well as caudate putamen, while negative BOLD was forming clusters in regions of S1 not-related to paw stimulation such as Barrel cortex. Slide 11 and 12 show large cluster activations in S1 and caudate putamen where the electrode was implanted.

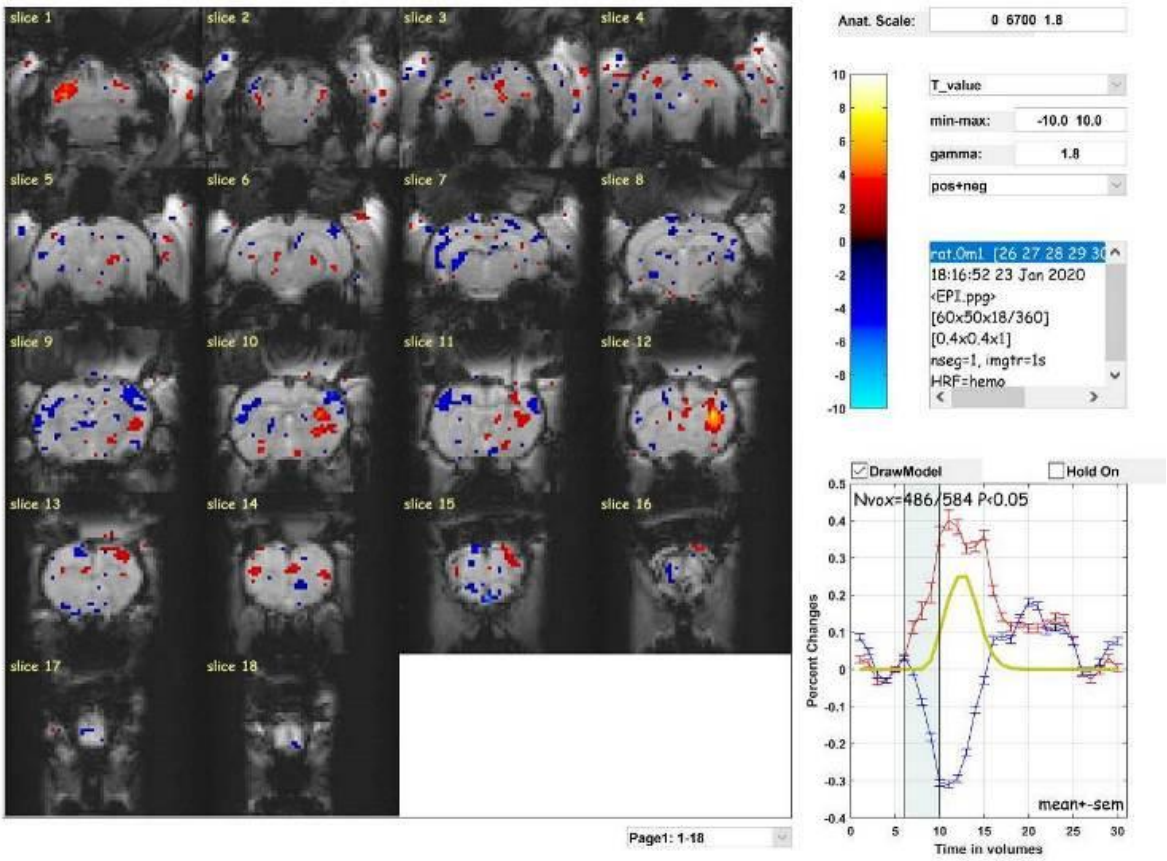

Figure 53. Coronal view of the averaged (all segments) hemodynamic response of sensorimotor system to unilateral paw stimulation in a rat under remifentanil anesthesia from posterior to anterior. The echo-planar imaging maps present statistically significant voxels (uncorrected ($p<0.01$)) with positive and negative BOLD. The results are consistent with the cumulative presentation. Moreover, the efficacy of the stimulus in generating positive (number of voxels=486) and negative (number of voxels=584) BOLD responses is shown in subfigure (lower right corner).

However, in a few cases, the averaged BOLD response does not survive a correction for multiples comparisons eg, False Discovery Rate (Figure 54). This issue can be interpreted from two different perspectives. Since the uncorrected BOLD maps largely reflect the expectations from previous studies, the elimination of signals due to FDR corrections may mean that this specific multiple comparison technique is too strict and conservative. Alternatively, the choice of the opioid remifentanil, which also acts as an analgesic compound may lead to weaker response to peripheral stimulations.

Indeed, a recent study (Renaud-Roy et al., 2019) suggest that there is an inverse correlation between the levels of nociception and remifentanil doses. Although, a

non-noxious paw stimulation paradigm was chosen in our experiments, it cannot be excluded that the use of an opioid may have suppressed the brain responses.

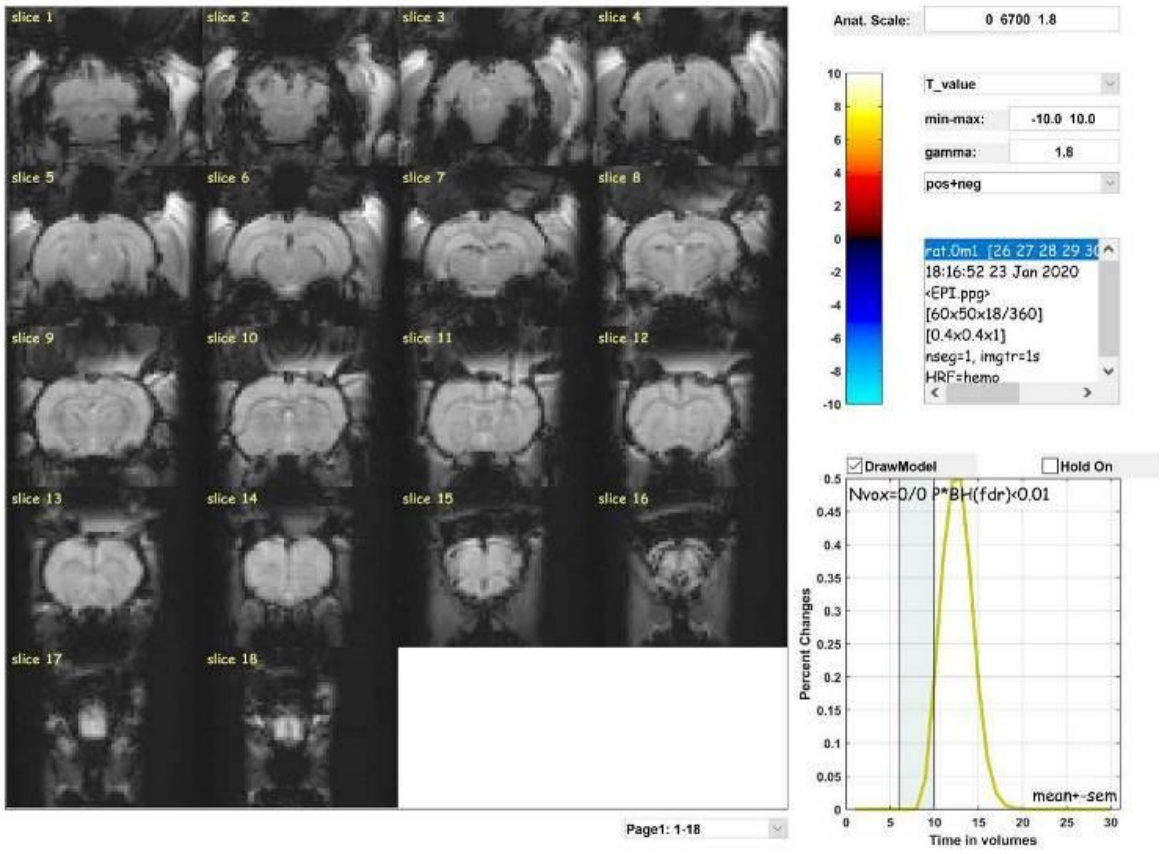

Figure 54. Correction for multiple comparisons (FDR-corrected ($p<0.01$)) on average BOLD responses to paw stimulation eliminates the signal in a few cases. In contrast to other correction techniques such as Bonferroni, false discovery rate does not control the possibility of false positives but rather controls within the set of suprathreshold voxels the proportion of false positives. Its threshold is adaptive and relates to the distribution of the observed p-values.

Our observations also indicate a certain degree of variability in the BOLD response between different animals under identical conditions. While the paw stimulation consistently leads to a positive BOLD in cerebellum, somatosensory cortex and basal ganglia, particularly in the immediate proximity of the electrode placement (Figure 55), some animals present massive and diffuse negative BOLD in numerous cortical and subcortical areas that remains significant even after a correction for multiple comparisons (Figure 56). Interestingly, the negative BOLD is largely present in the somatosensory cortex (S1) contralateral to the stimulation side.

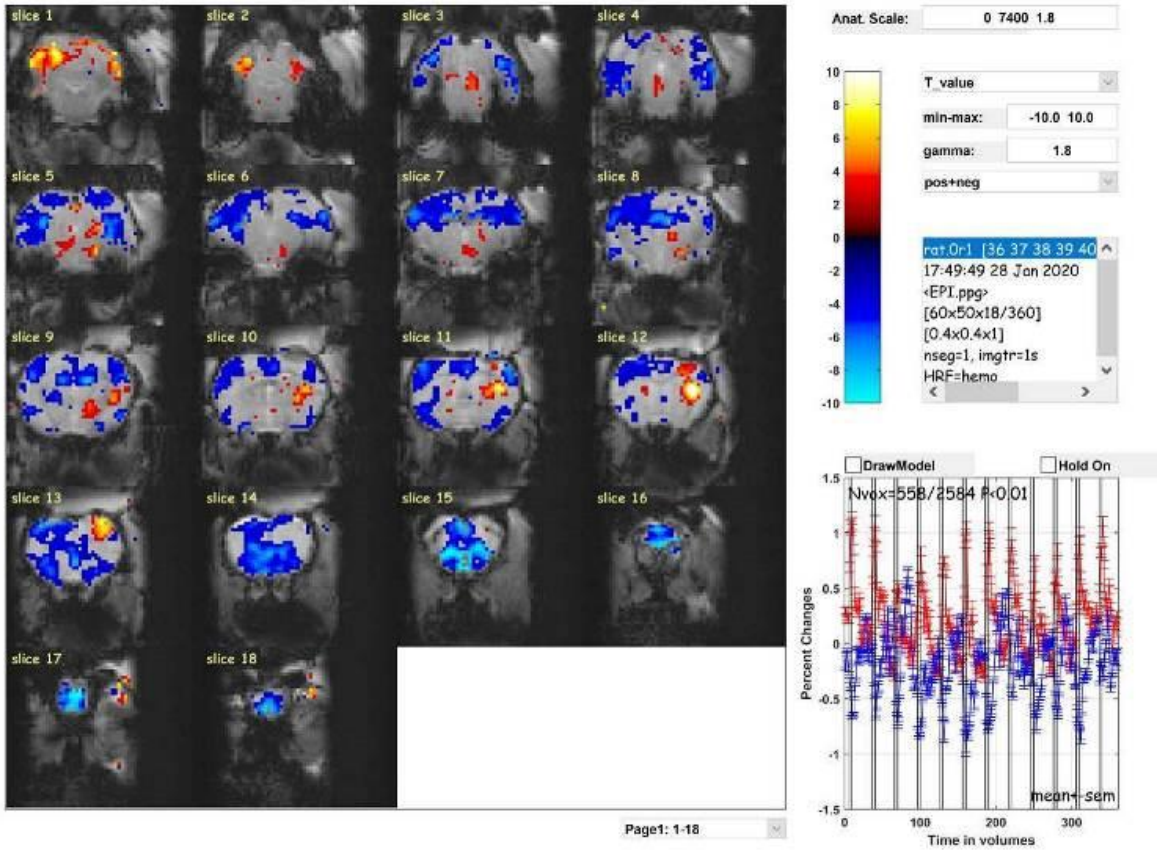

Figure 55. Coronal view of cumulative (all segments) echo-planar imaging maps (uncorrected ($p<0.01$)) of sensorimotor system to unilateral paw stimulation in a rat under remifentanil anesthesia from posterior to anterior. The positive BOLD response was largely identical among all animals and was present in cerebellum, S1 and caudate putamen. Although all stimulation parameters and anesthesia regimen were kept identical, some rats showed a diffuse and more massive negative BOLD than positive (number of negative BOLD voxels = 2584, number of positive BOLD voxels = 558). The negative BOLD was bilateral and increased in intensity from posterior to anterior. Large negative BOLD responses were further observed bilaterally in thalamus and contralateral to the stimulation side in somatosensory and motor cortex areas.

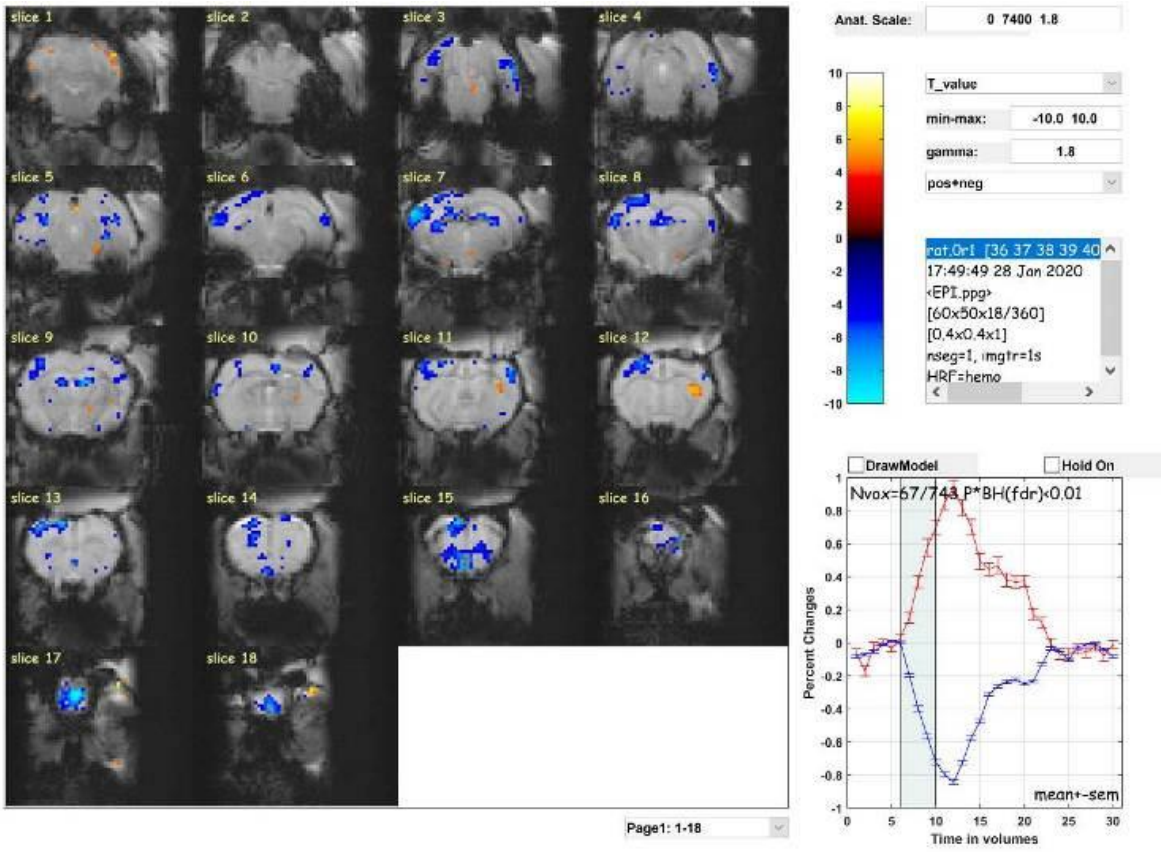

Figure 56. Correction for multiple comparisons (FDR, p<0.01) indicates that the negative BOLD is largely present contralateral to the stimulation side.

The primary visual system is one of the most studied brain pathways and numerous studies can be used as reference for setting up the appropriate stimulation paradigms. The main concern in this part of our study was to not overstimulate the retina and thus, induce activation of deep subcortical brain areas such as locus coeruleus and dorsal raphe. These regions innervate intensively cortical and subcortical regions with neuromodulators serotonin and norepinephrine and thus can lead to significant (uncounted) changes in excitation-inhibition network dynamics.

Our stimulation paradigm led to a clear, yet bilateral activation of lateral geniculate nucleus, hippocampus and primary visual cortex (V1), and diffuse negative BOLD in largely anterior and subcortical areas (Figure 57). The bilateral positive BOLD in visual system may seem surprising at the first sight, since the LED light was placed unilaterally and contralateral to the electrode implantation side. However, it can be safely assumed that the activation of ipsilateral hemisphere is caused by the light stimulation in the extremely dark environment of the MRI hole. Even when the

ipsilateral eye is covered, there is still a chance of stimulation of its retina by residual light penetrating the eye cover. All findings remain robust following an FDR-correction for multiple comparisons (Figure 58).

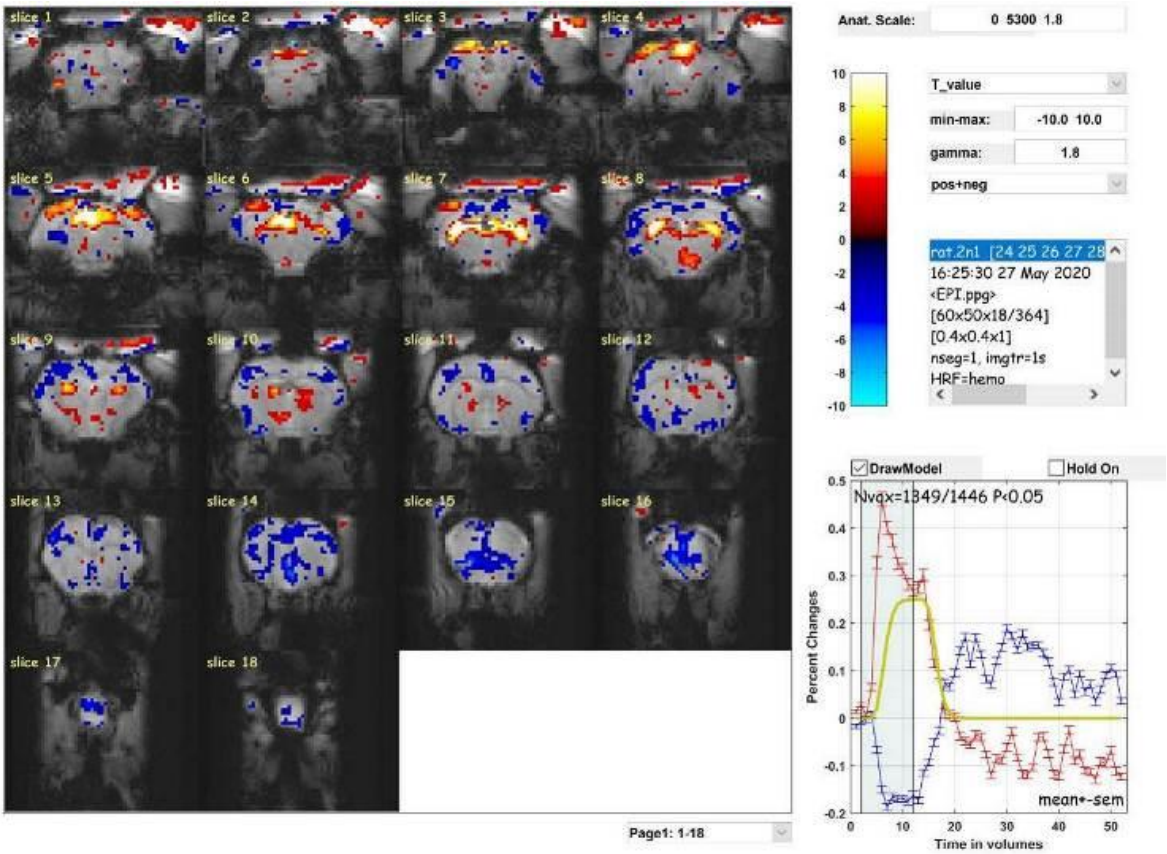

Figure 57. Coronal view of averaged (uncorrected ($p<0.05$)) hemodynamic response to visual stimulation. The main elements of primary visual system, namely LGN, SC and V1 show significant positive BOLD response. Negative BOLD was in this case largely present in anterior subcortical brain areas.

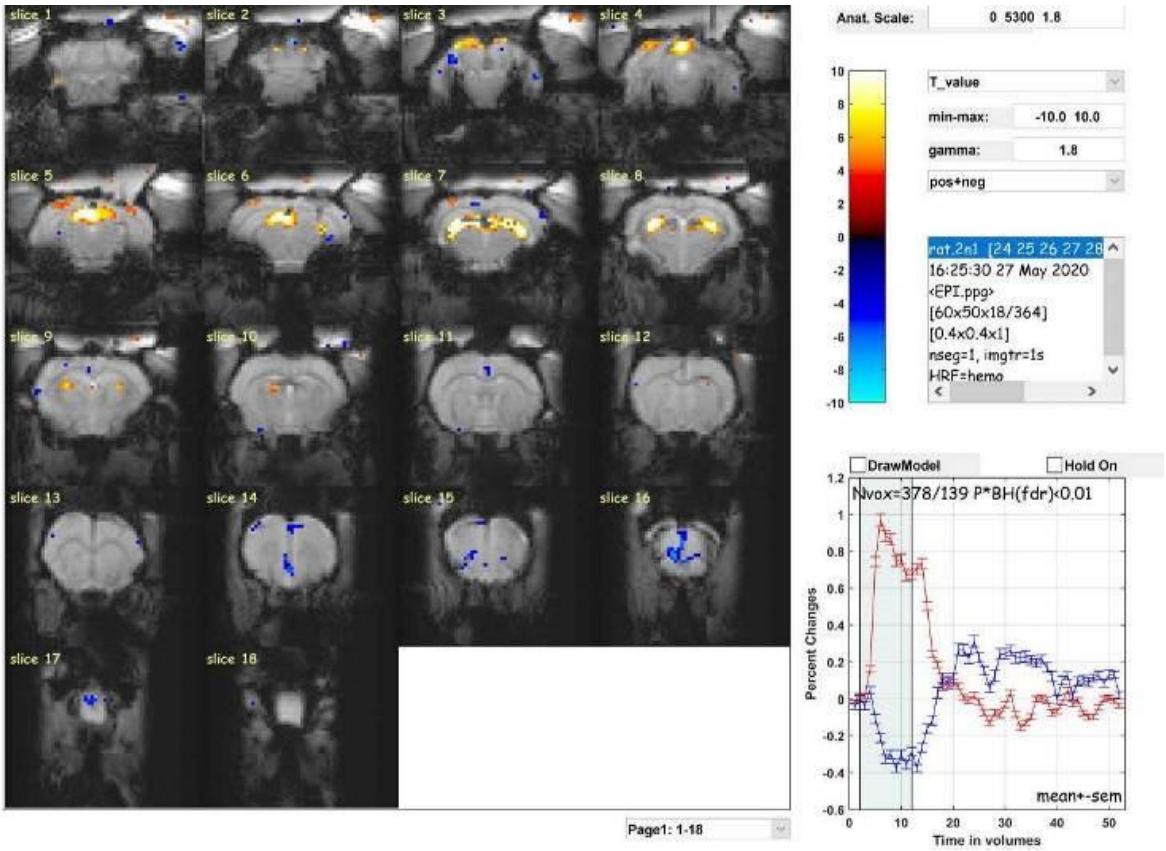

Figure 58. Average FDR-corrected (p<0.01) BOLD response to visual stimulation. The primary visual system robustly responds to the stimulus, most dominantly in SC and lateral geniculate nucleus.

In one animal, visual stimulation led to an unusual pattern of positive and negative BOLD. While the lateral geniculate nucleus was consistently associated with positive BOLD response, in contrast to other cases, BOLD in the entire cortex including primary visual cortex was significantly (FDR, p<0.01) negative (Figure 59). Consistent with all animals, negative BOLD is largely associated with an increase in GABA events and additional analyses of the data from the animal indicated predominantly GABAergic processes.

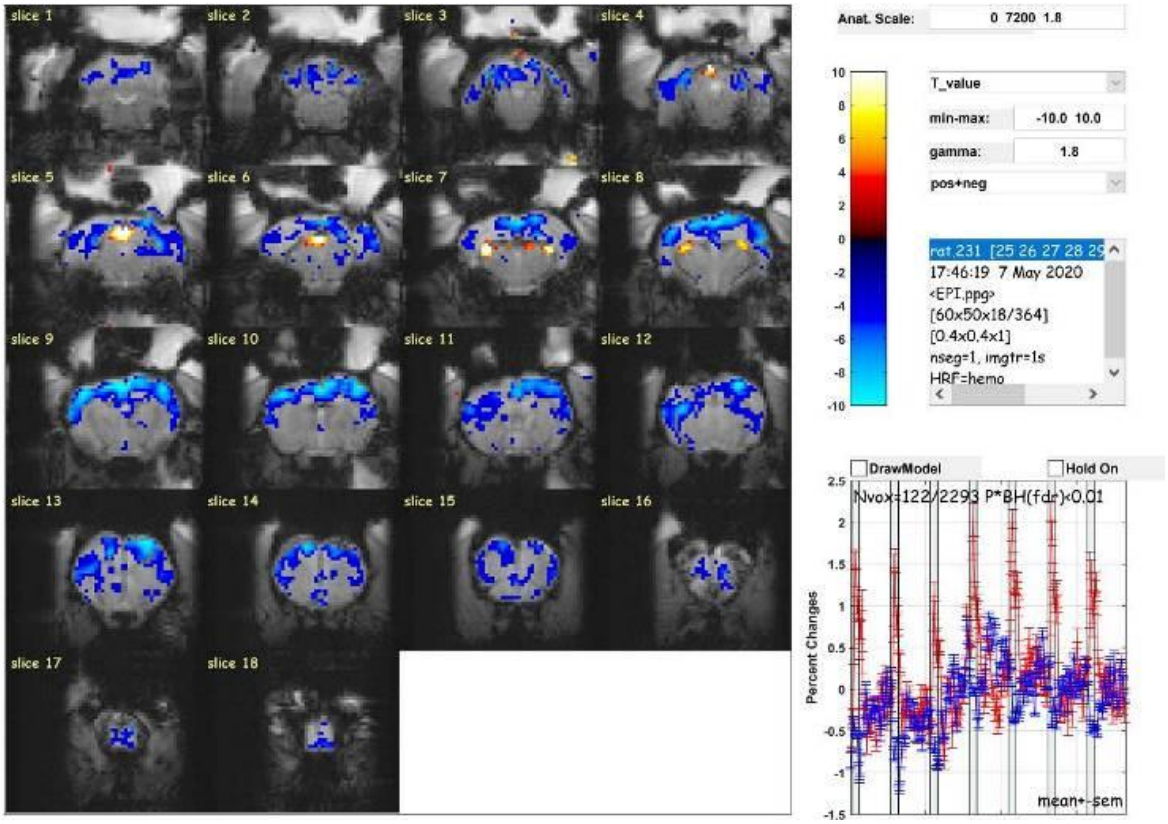

Figure 59. Visual stimulation activates LGN (FDR-corrected ($p<0.01$)), while induces a wide-spread cortical negative BOLD as a consequence of GABAergic hyperactivation.

As it was previously demonstrated in non-human primates (Logothetis et al., 2012), ripples are associated with both positive and negative BOLD responses that clearly show an anatomical gradient (Figure 60). In average, positive BOLD is largely manifested in cortical areas and olfactory bulb, while the suppression of activity is characteristically present in subcortical brain regions. The middle section of the figure reveals the time course for different regions of interest, which have been arranged based on their anatomical location from ventral to dorsal and anterior to posterior directions.

In contrast to non-human primates, ripples did not induce a deactivation of V1 in rats. Moreover, there is an interesting pattern of sign change from cortical to subcortical areas with an earlier positive response in cortex and a subsequent deactivation of subcortical regions. The fractions of activated/deactivated regions of interests (right column) further emphasizes the presence of two anatomical clusters, however far less pronounced as presented in primates (Logothetis et al., 2012).

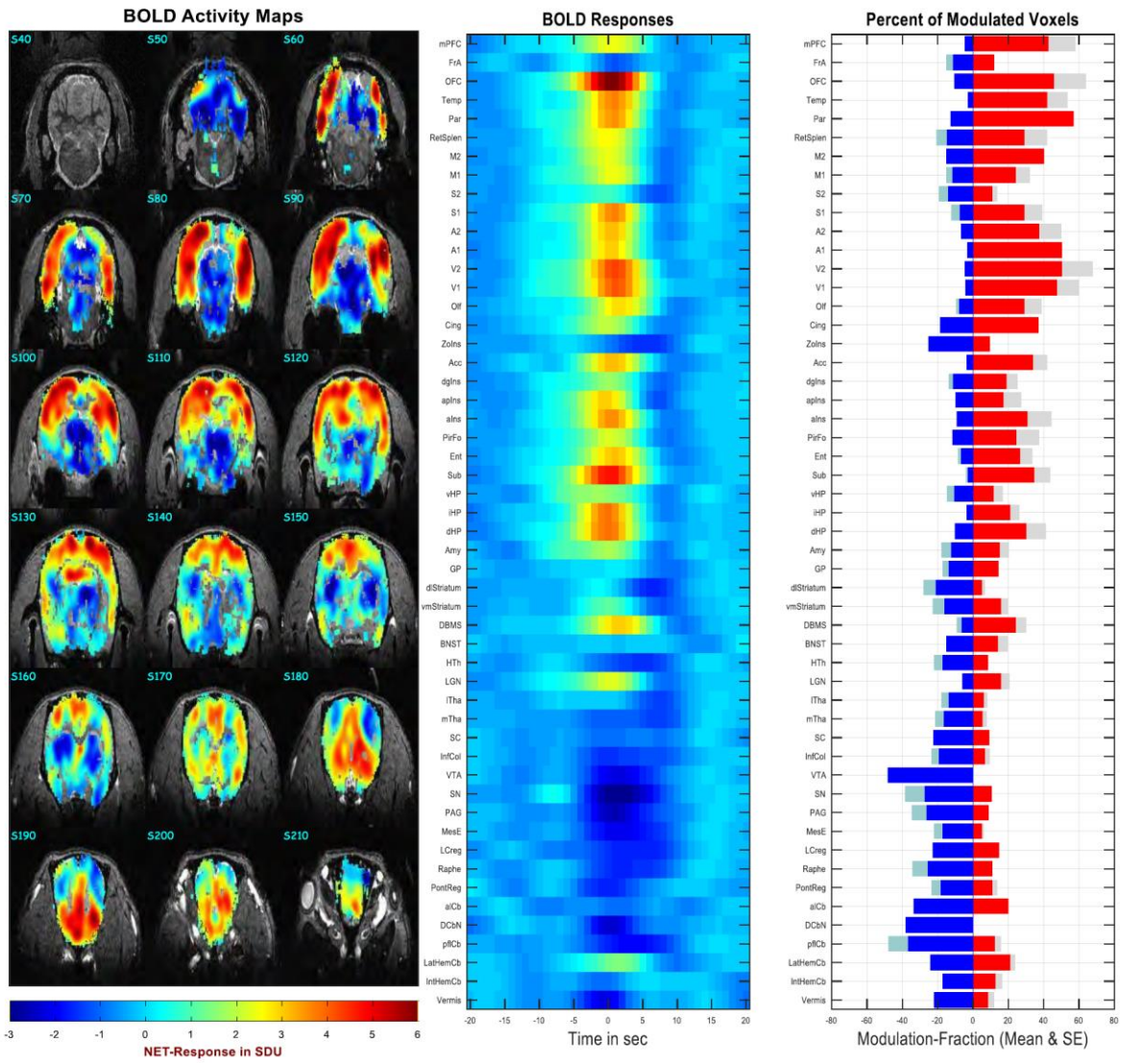

Figure 60. BOLD response maps as induced by ripples in space and time. Here, we present the average maps of activation over all measured sessions. The positive BOLD response is present in all cortical regions with the exception of frontal association cortex (FrA) and secondary somatosensory cortex (S2).

3.3.1 State identification

A main application of our technology is to describe different states of the brain in a more precise manner. As shown above, BOLD responses in hippocampal region is in average negative. Such offline states are related to characteristic (large deflections in LFP), aperiodic recurrent events such as the sharp wave-ripples (SWR) (Buzsaki et al., 1992; O'Keefe and Nadel, 1978). The sharp waves are associated with ripples (fast field oscillations) that are sensitive to numerous factors including state of consciousness, strain and morphology of hippocampal subregions (Axmacher et al., 2008; Buzsaki et al., 1992; O'Keefe and Nadel, 1978; Skaggs et al., 2007; Ylinen et al., 1995).

Although largely associated the hippocampus, the SWRs are caused by a complex interaction of several neurocircuitries such as thalamocortical pathways that generate slow oscillations (McCormick and Bal, 1997; Steriade et al., 1993) and information transfer between ensembles in cortex and hippocampus (Isomura et al., 2006; Siapas and Wilson, 1998; Sirota et al., 2003; Wierzynski et al., 2009). This cortical, hippocampal and thalamic framework is also the targeted by our technology during the investigations of response to visual stimuli. Indeed, we analyzed both resting, pre-stimulation, stimulated, and resting post-stimulation periods and thus, could use the data to examine whether the SWRs alone, or in combination with phasic field potentials spanning over brain stem (pons), through thalamus (LGN) to primary visual cortex (V1), the so-called ponto-geniculo-occipital (PGO) waves, is the cause for the presence of anatomically distinct states.

Here, we analyzed whether different multi-unit activity (MUA), ripple event densities and theta-band event densities can generate characteristic population patterns in rat brain (Figure 61) and compared the findings with previous data (Ramirez-Villegas et al., 2020) from non-human primates (Figure 62, with explicit permission from Prof. Logothetis). The findings show that PGO-SWR and PGO-theta events can indeed be used to characterize states consistently over different species.

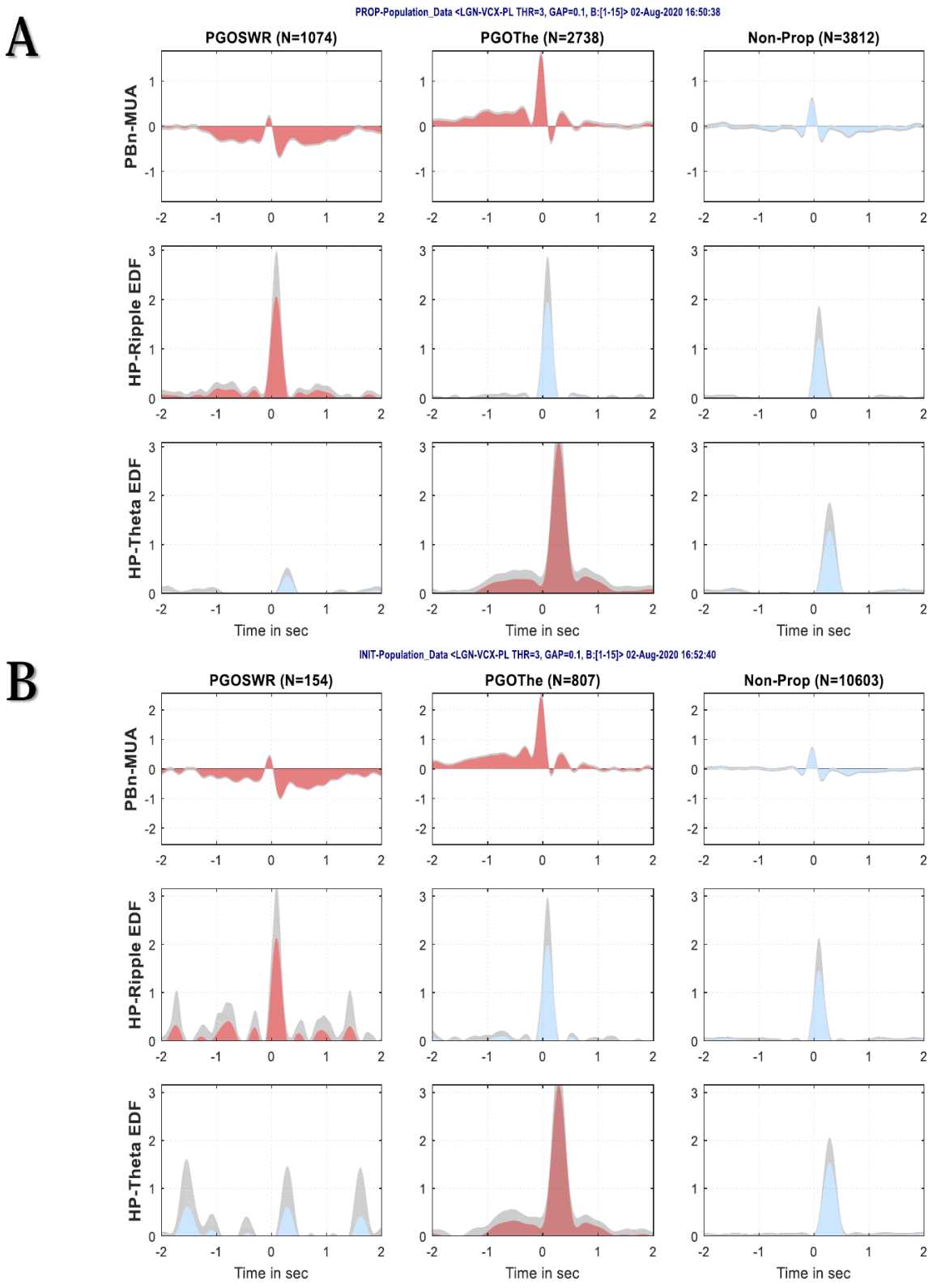

Figure 61. State definition on the basis of PGO-SWR and PGO-Theta events in rats.

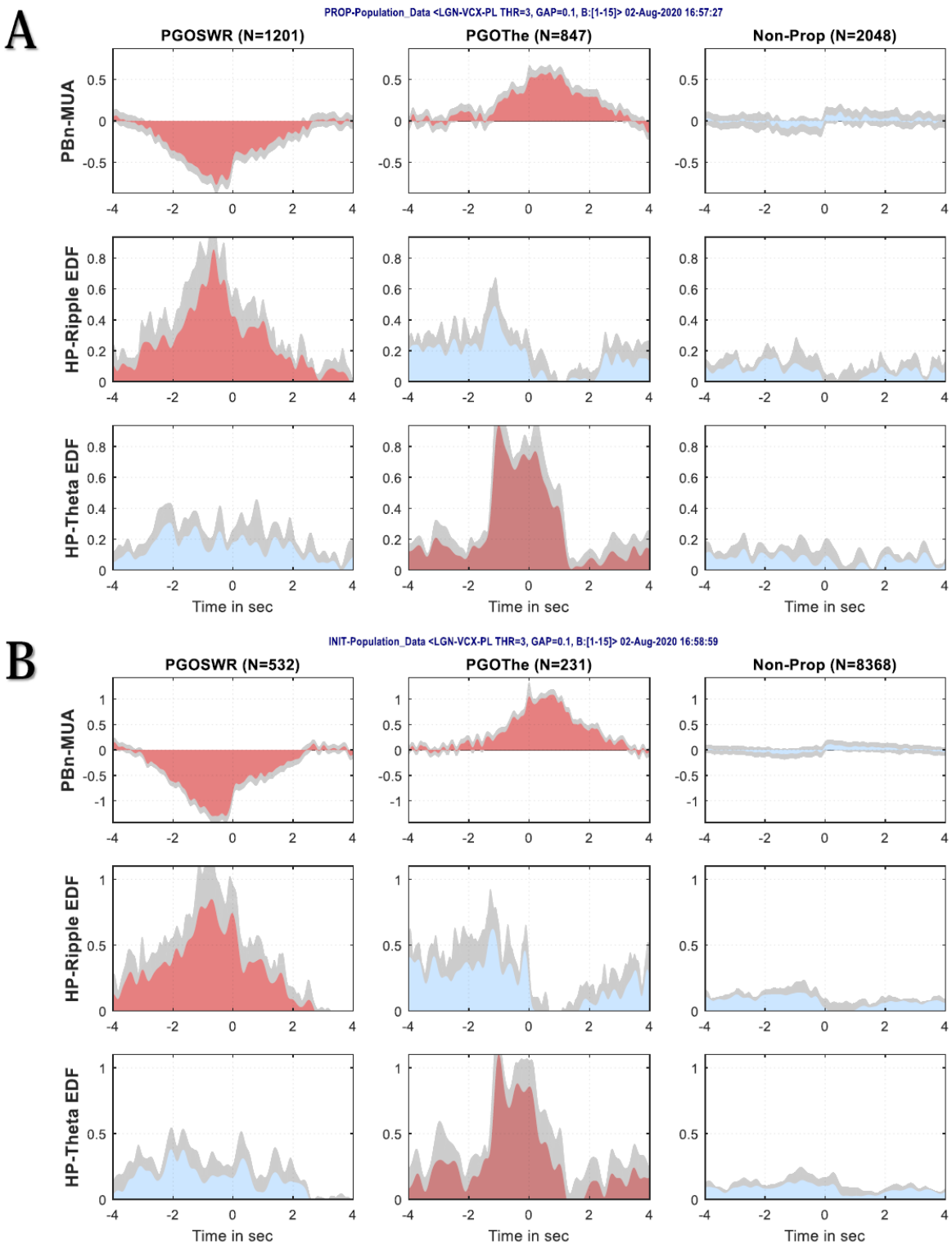

Figure 62. State definition on the basis of PGO-SWR and PGO-Theta events in non-human primates (NHP). Figure and access to data from previous experiments were kindly provided by Prof. Logothetis and permission was explicitly given to use them within the framework of this thesis.

The distribution of ripple, theta and PGO events (Figure 63) as well as spectral analysis (Figure 64) were further used to characterize rapid eye movement (REM) and non-REM like states in the animals.

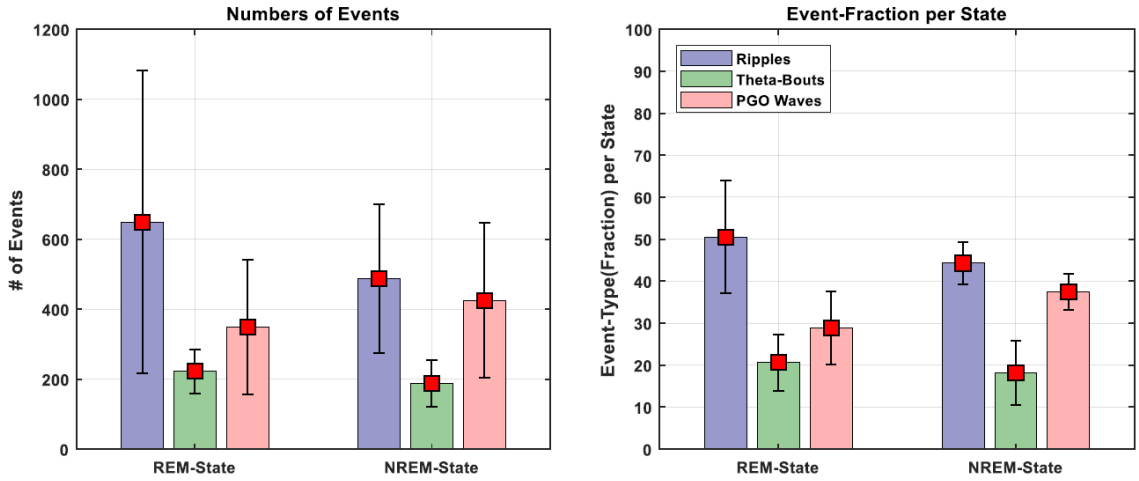

Figure 63. Distribution of different oscillatory events can be used to characterize different states such as REM (rapid eye movement) and non-REM.

Moreover, Logothetis and his team (Ramirez-Villegas et al., 2020) demonstrated that the power-power correlation of wavelets is the most appropriate marker of sleep-like states. Thereby, the authors showed in non-human primates that [paraphrased from Ramirez-Villegas et al., 2020; Methods section and Extended Data] "*REM and non-REM states can be characterized by mean power-power correlations of signals obtained between two electrode contacts placed in the same brain subregion with a distance of ~250 µm between the channels.*" In agreement with these results and a confirmation of an inter-species valid observation, identical results could be seen for rats (Figure 65), showing the general nature of this kind of "state-marking".

Combined with neurochemical decoding of these signals, we can infer the molecular mechanisms that generate different states.

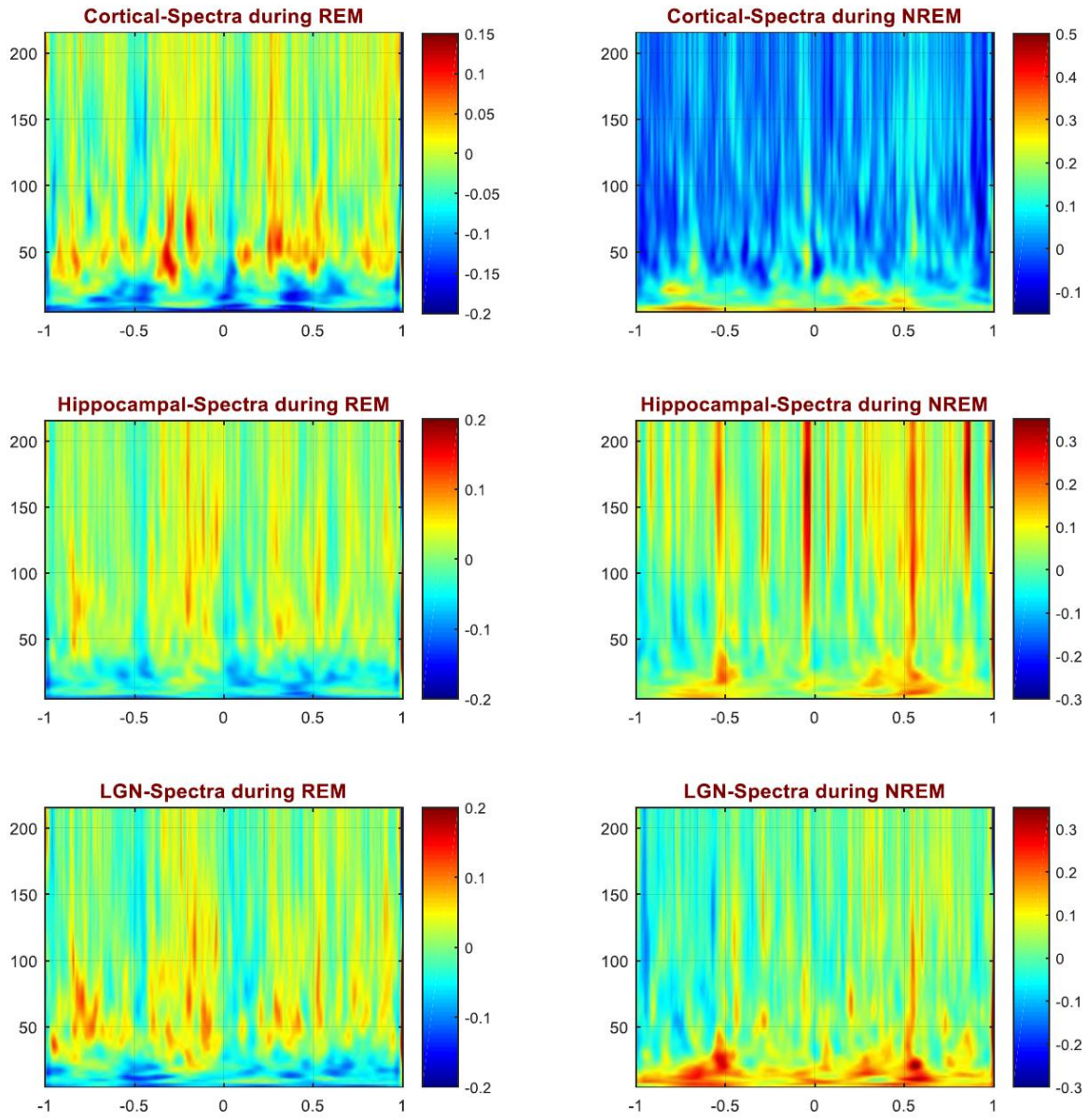

Figure 64. Spectral analysis of the cortico-hippocampo-thalamic pathway recordings further confirms the power of state identification method based on SWR and other oscillatory patterns.

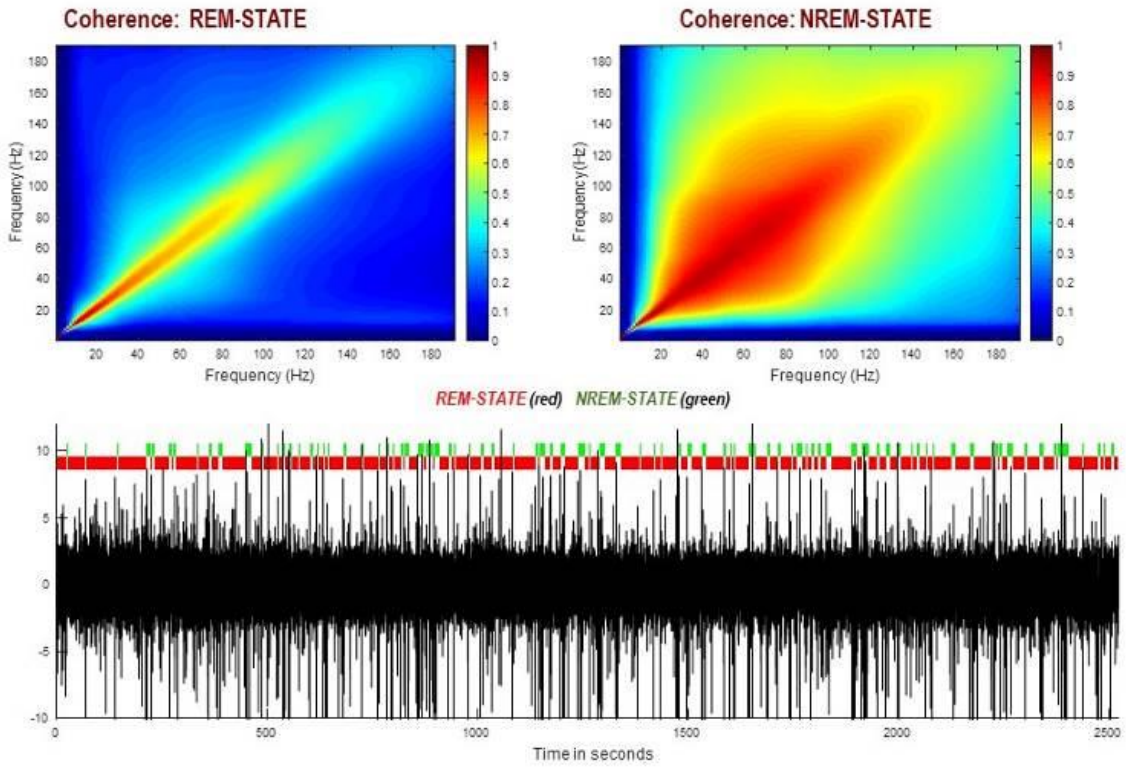

Figure 65. Averaged Power-Power Correlations between two Recording Sites in the Visual Cortex (VCx).

As it be seen here, the REM and NREM have characteristic time-frequency-power-correlation profiles, with substantially higher coupling of high frequency activities in NREM state. These results are in general not very surprising. Sleep-stages have distinctly different hippocampal and cortical events.

In analogy to previous studies (Ramirez-Villegas et al., 2020), we calculated continuous wavelet transforms of local field potentials (<200 Hz) from hippocampus for all experiments (Figure 66). Indeed, the temporal distinction of theta and ripple events as well as their power profiles suggest that time windows are appropriate to characterize states that resemble sleep, particularly the REM and non-REM episodes. Among the electrode channels that were located in the hippocampus, two with maximal ripple-band signal-to-noise ratio (90-190 Hz) were chosen for further analysis. Spectrogram interval was decomposed into 5s-windows. The ‘onsets’ of the state structure are starting with 2.5sec (middle of the range) and continue as 7.5, 12.5, etc. The frequency-pairwise power to power correlation coefficients were calculated within each window leading to 2d-frequency correlation pattern. Using k-

means clustering, these maps (for each 5s window) were then grouped in two classes, representing a non-REM state with highest probability for occurrence of SWR-associated discharges and REM state characterized by theta-like events, and lack of ripple-associated discharges.

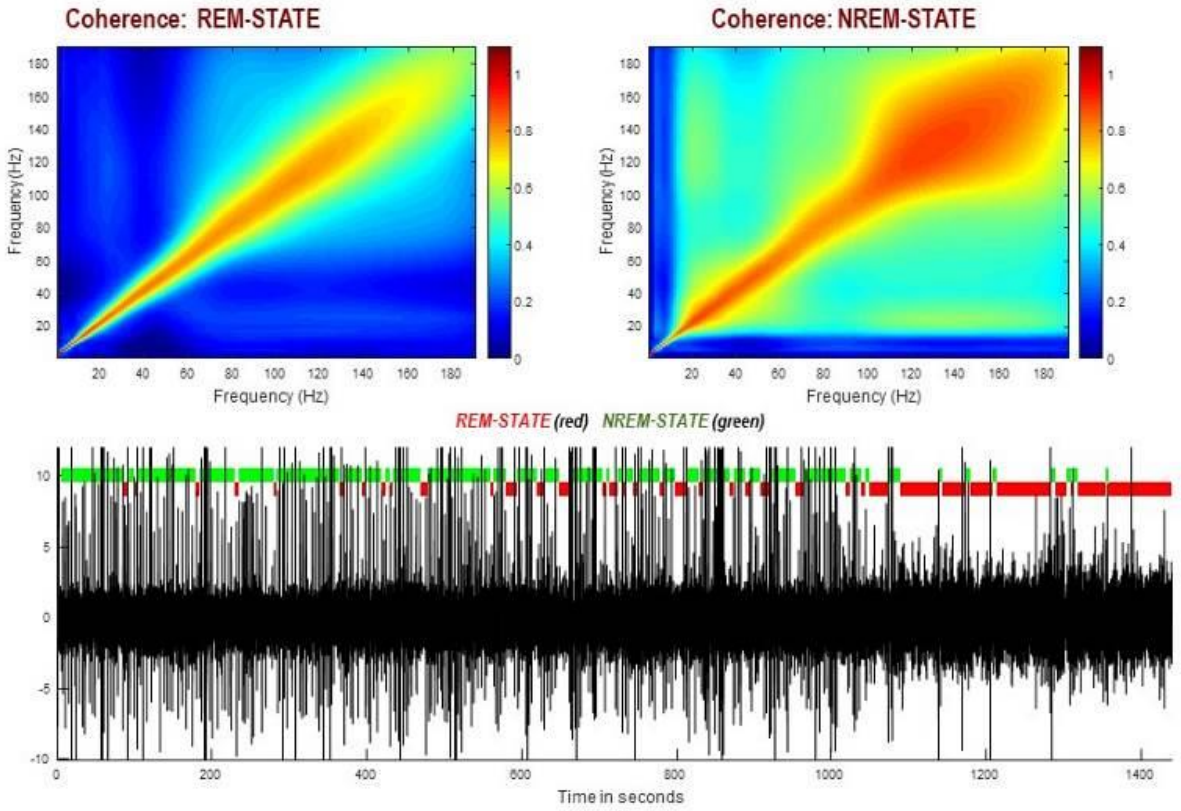

Figure 66. Averaged Power-Power Correlations between two Recording Sites in the Pyramidal Layer (Hippocampus). The bottom plot shows the row signal, and the red/green rectangle show the dynamics states (or meta-states). In some sessions the state-epoch were short, in others mimicking the actual NREM/REM sleep epochs.

More importantly, these states relate directly to specific dynamics of glutamate and GABA (Figure 67). The four images show the time-frequency profile of the neurotransmitter signals during the epochs used for stated definition. Note that the time “0” does not correspond to the occurrence of any event. The epochs were selected starting from 0, and moving one in 5-second steps. The middle of the 5s-period was given in the time-vector (state.t) of the state-structure. No “peaks” in the middle of the plots is therefore expected, as in most of the figures shown in this thesis.

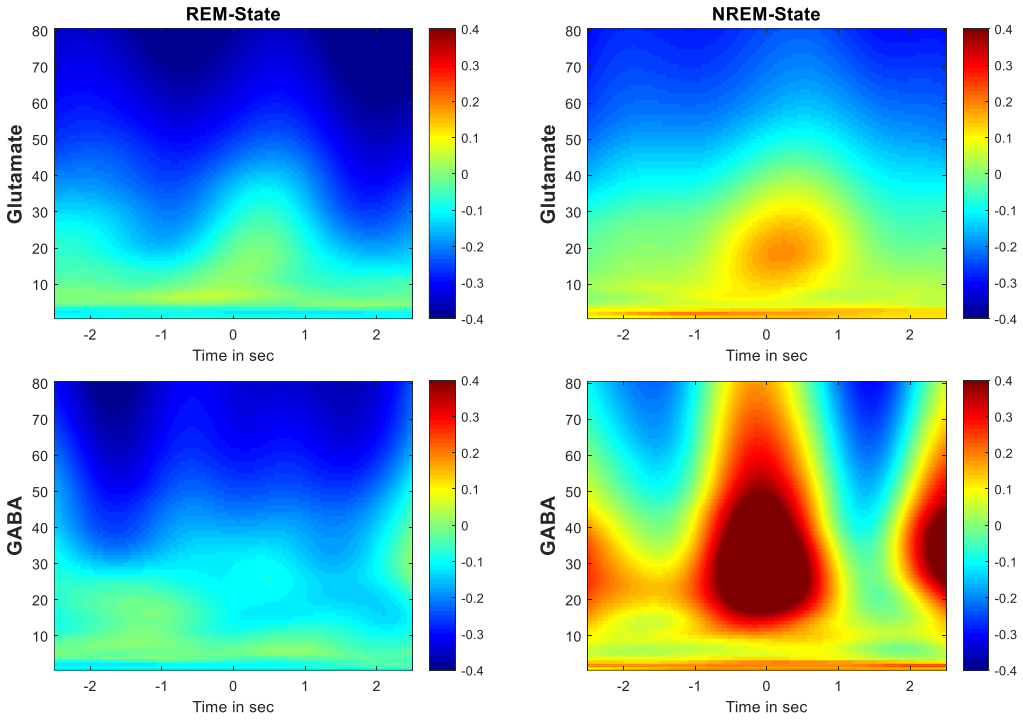

Figure 67. State-dependent behavior of glutamate and GABA in VCX.

The data are the average of all sessions. Interesting for both neurotransmitters is the consistent elevation of gamma-hgamma activities as expected during the REM-period, with drop in the slow-oscillation-range [0.5Hz]. In contrast high-frequencies and slow-oscillations are enhance in the NREM state. The patterns of the two neurochemical signals are different, further supporting the effectiveness of induction-removal through the EMD process. The IMF=4 is here used instead of the raw data.

In addition, coherence analysis can further be applied to characterize the REM and NREM states in terms of glutamate and GABA dynamics (Figure 68).

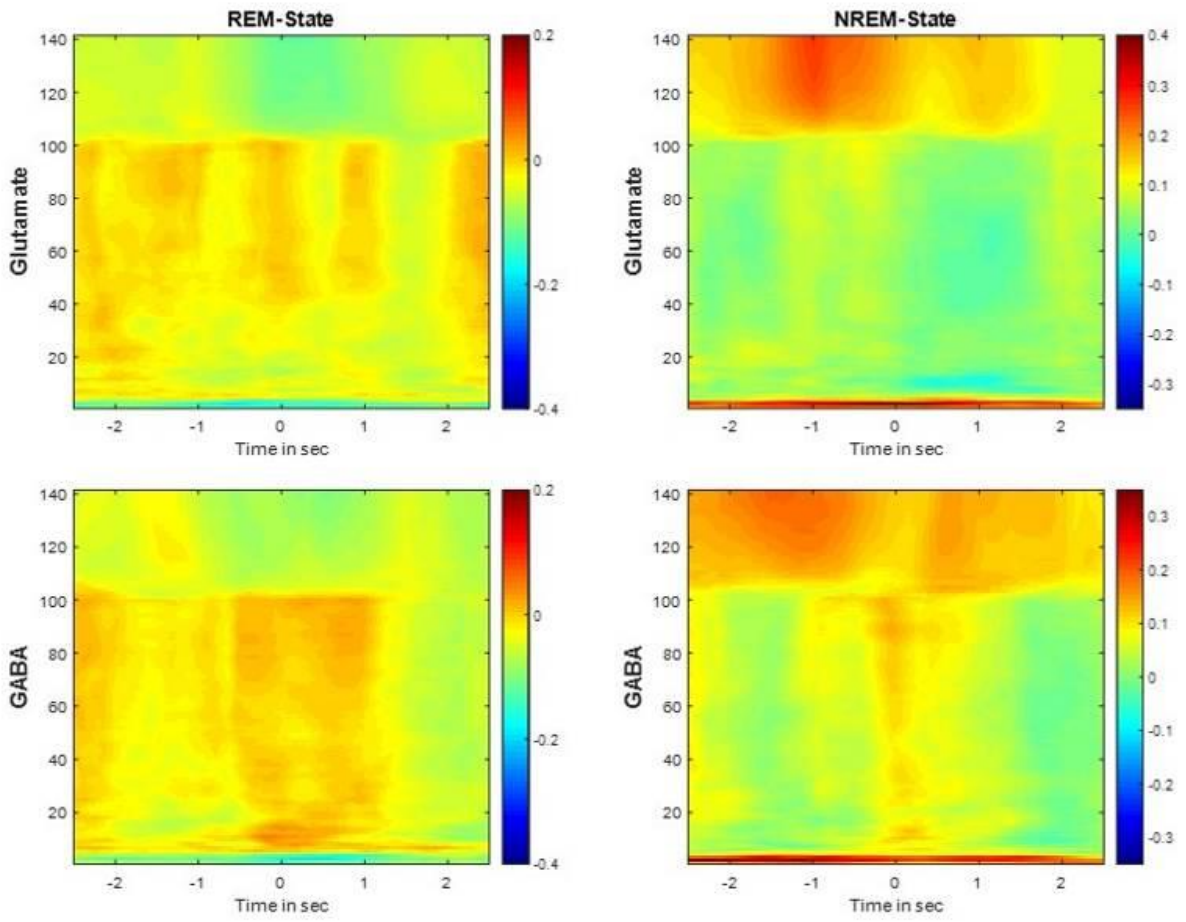

Figure 68. neurochemical characterization of REM and NREM states by glutamate and GABA dynamics.

Interesting for both neurotransmitters is the consistent elevation of gamma-gamma activities as expected during the REM-period, with drop in the slow-oscillation-range (0.5Hz). In contrast high-frequencies and slow-oscillations are enhance in the NREM state. The patterns of the two neurochemical signals are different, further supporting the effectiveness of induction-removal through the EMD process. The neurochemical characterization of the REM and NREM states is not only dynamical and are even reflected by differences in concentration values (Figure 69). The latter is however not consistently observed (Figure 70 & 71), which suggests the presence additional phenomena and state transitions that need further investigations.

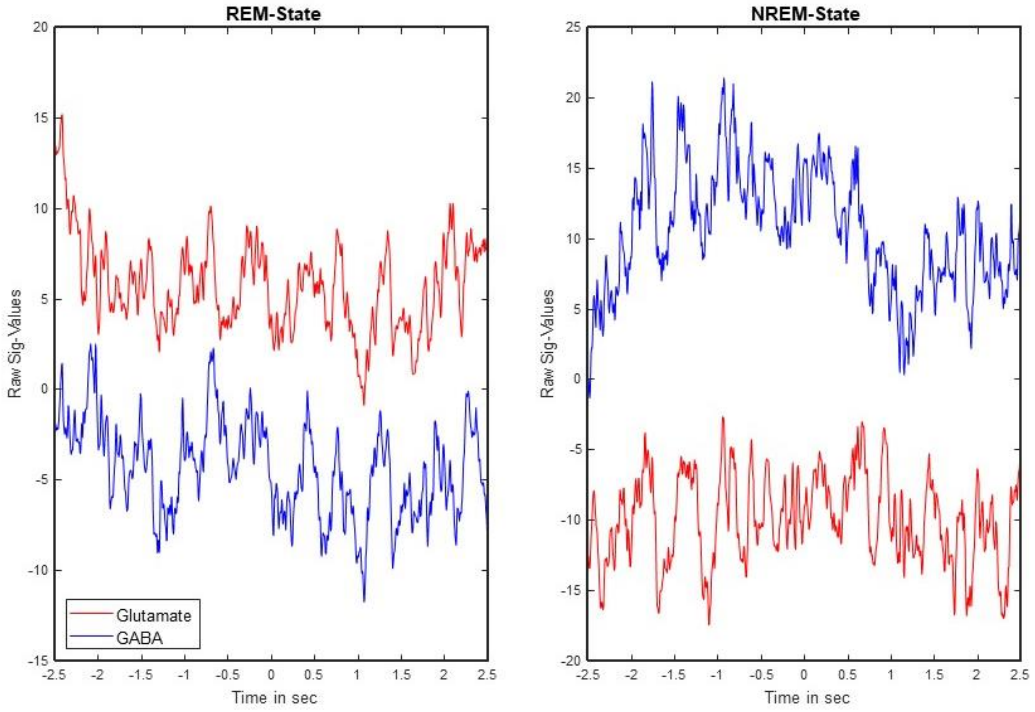

Figure 69. Concentration differences during REM and NREM states. Although the high-frequency epochs (eg, during NREM) are largely glutamatergic, REM sleep is associated with a higher glutamate level, while NREM sleep relates to higher GABA levels.

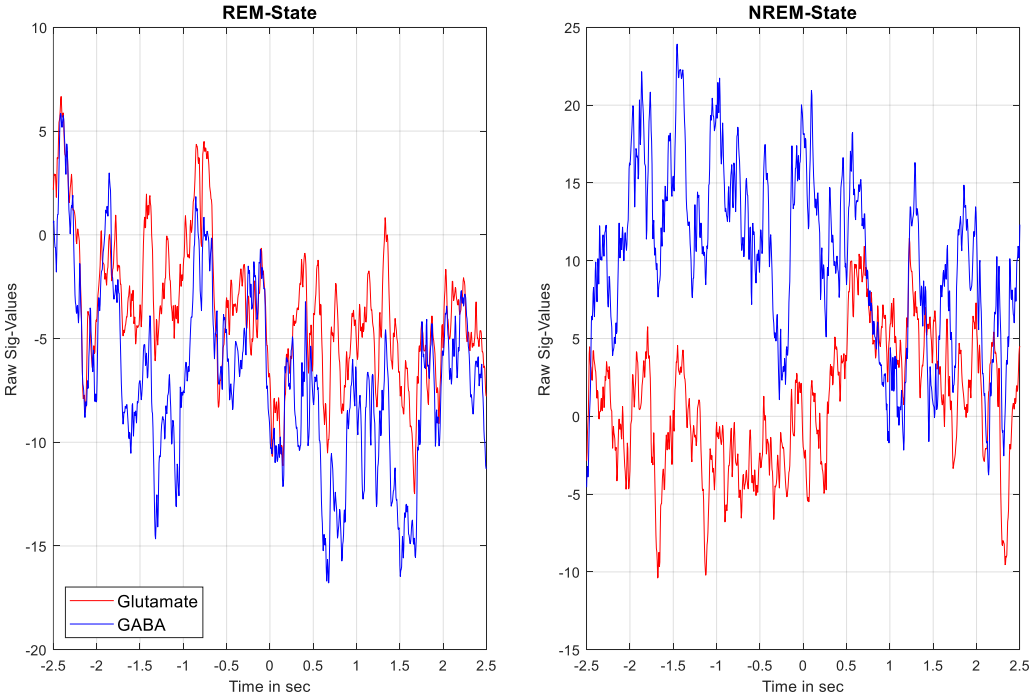

Figure 70. Possible state transitions in concentration levels of glutamate and GABA.

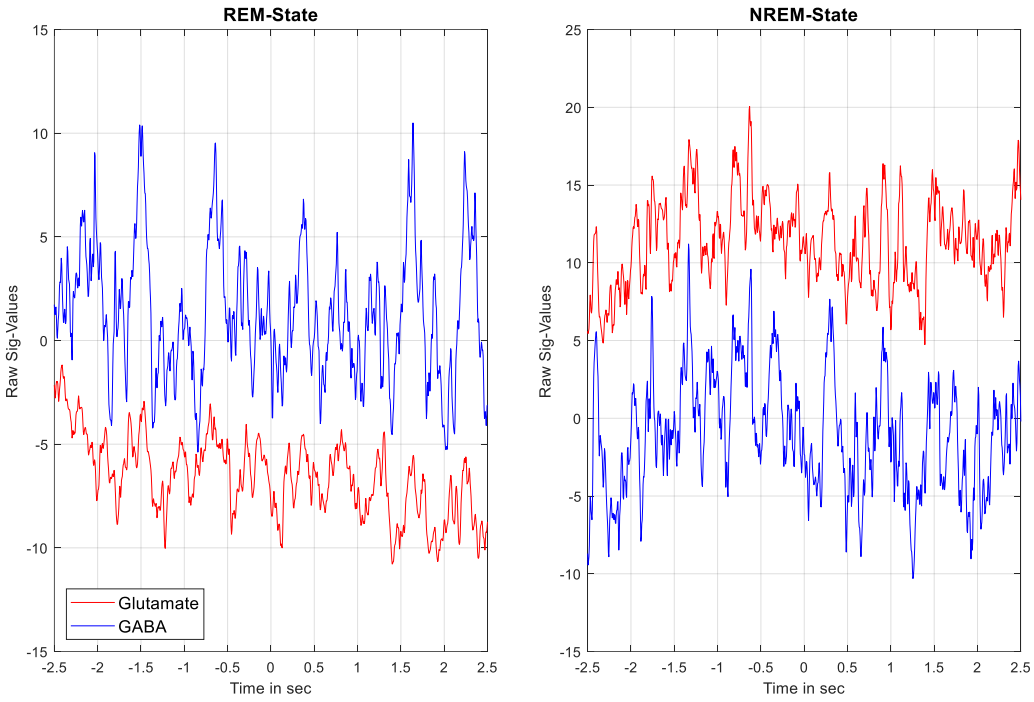

Figure 71. Opposite concentration differences during REM and NREM states observed suggest the existence of underlying, uncharacterized phenomena, that dominate the global behavior of the systems.

3.3.2 Chemical-triggered fMRI

As mentioned above, we used an extensive and time-consuming opioid-based anesthesia regimen to not only achieve a high signal-to-noise ratio for neuroimaging experiments but also to eliminate stress and discomfort of the animals to an absolute minimum. The use of opioids however often affect respiration which requires constant monitoring of vital values and immediate response. This in turn may lead to fluctuations in oxygen levels, which can critically affect chemical measurements inside the MRI. Both glutamate and GABA sensors contain glutamate oxidase which requires oxygen to convert glutamate and changes in oxygen levels will have an influence on the sensitivity of both sensors. Since the respiration effects may be critical we first high-passed filtered the signals and calculated spectral densities to characterize the ranges of meaningful events.

In addition, we analyzed wavelet coherence of glutamate and GABA signals in visual cortex (V1) during visual stimulation (Figure 72). In general, coherence between two signals is used as a measure or statistic to investigate their relationship in terms of estimating the power transfer and under certain conditions even the causality

between the in- and outputs of a system. The findings strongly suggest an anti-correlated relationship between glutamate and GABA signals within a frequency range of 5-10 Hz, while correlated behavior is largely observed in the initial stages of the stimulation and at frequencies above 10 Hz. Interestingly, wavelet analysis of glutamatergic signals further indicates a strong post-stimulation (> 5s after stimulation) echo-response in the frequency range of 5-10 Hz that is largely missing for GABA.

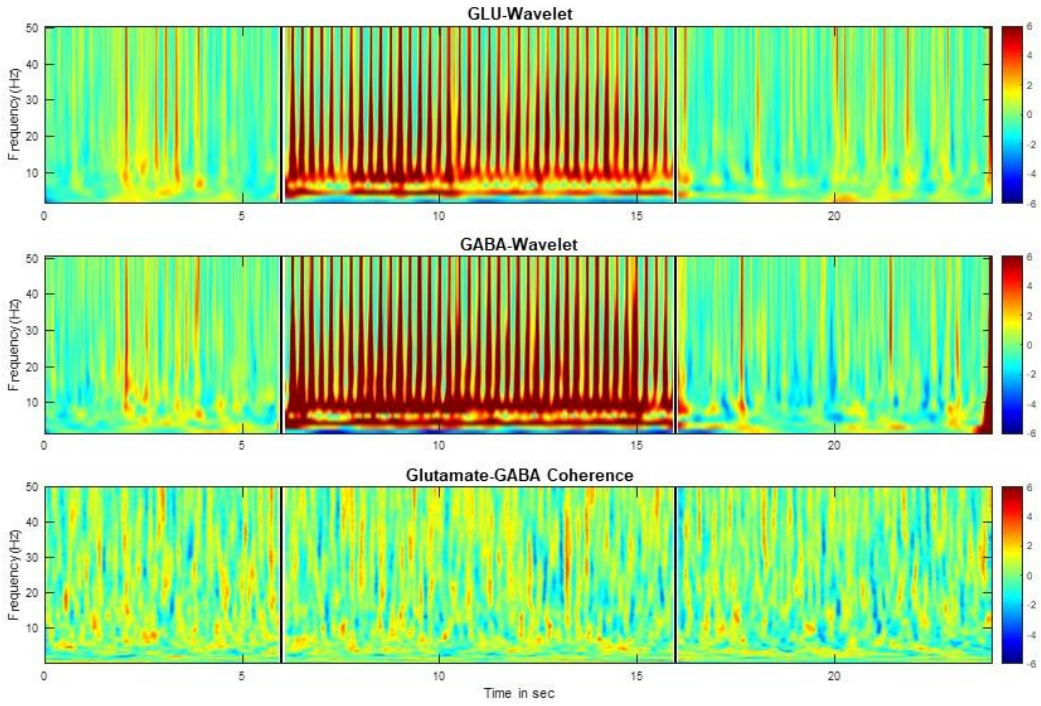

Figure 72. Spectrogram (wavelet coherence analysis) of glutamate and GABA signals over all sessions prior, during and after the visual stimulation.

For a refined analysis of the relationship between the BOLD response and chemical signals, we have also prepared three collective figures (Figures 73-75) showing the Cortical Signal (top), the two NT-signals (middle), and the BOLD response in V1 (lower axes) together with the NT-signals convolved by a data-estimate impulse response function (IRF, top axes).

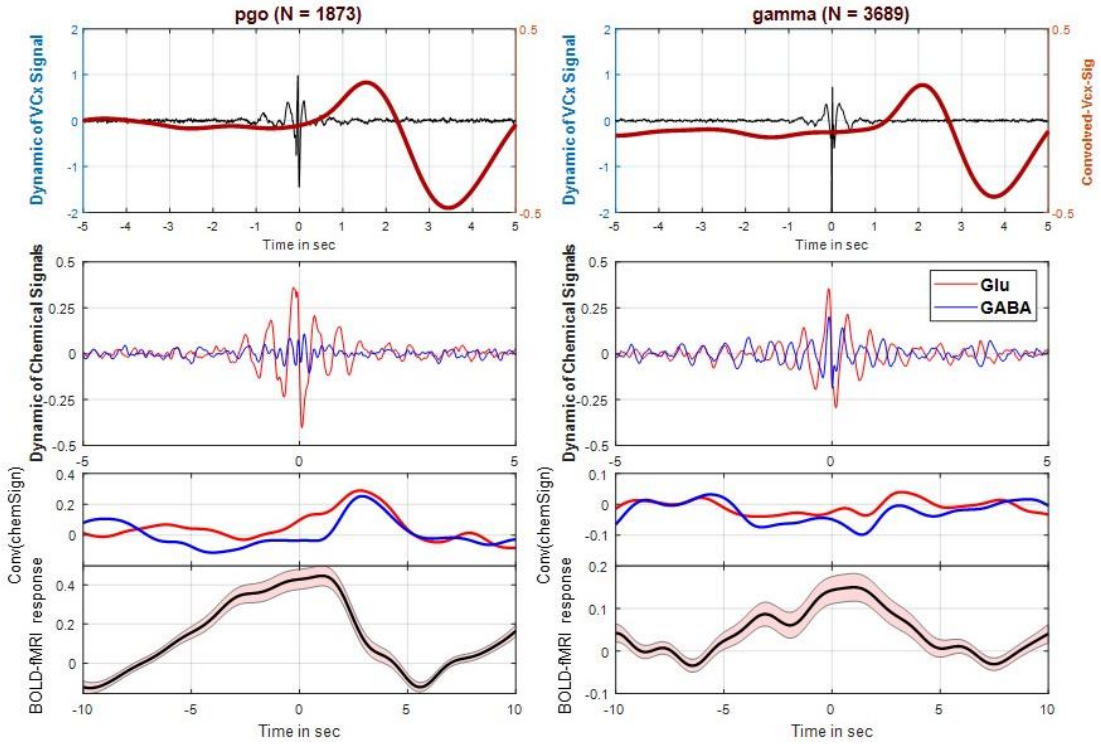

Figure 73. Multi-dimensional relationship of neurophysiological, neurochemical and BOLD signals concurrently measured in VCX.

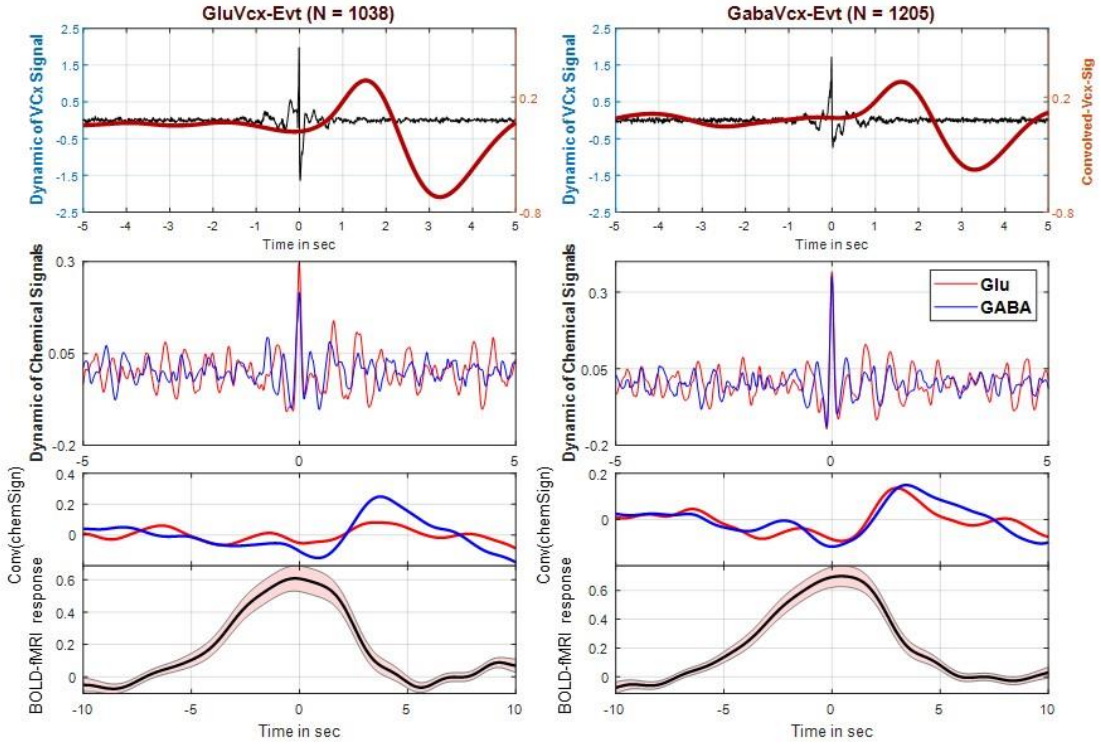

Figure 74. Multi-dimensional relationship of neurophysiological, neurochemical and BOLD signals concurrently measured in VCX.

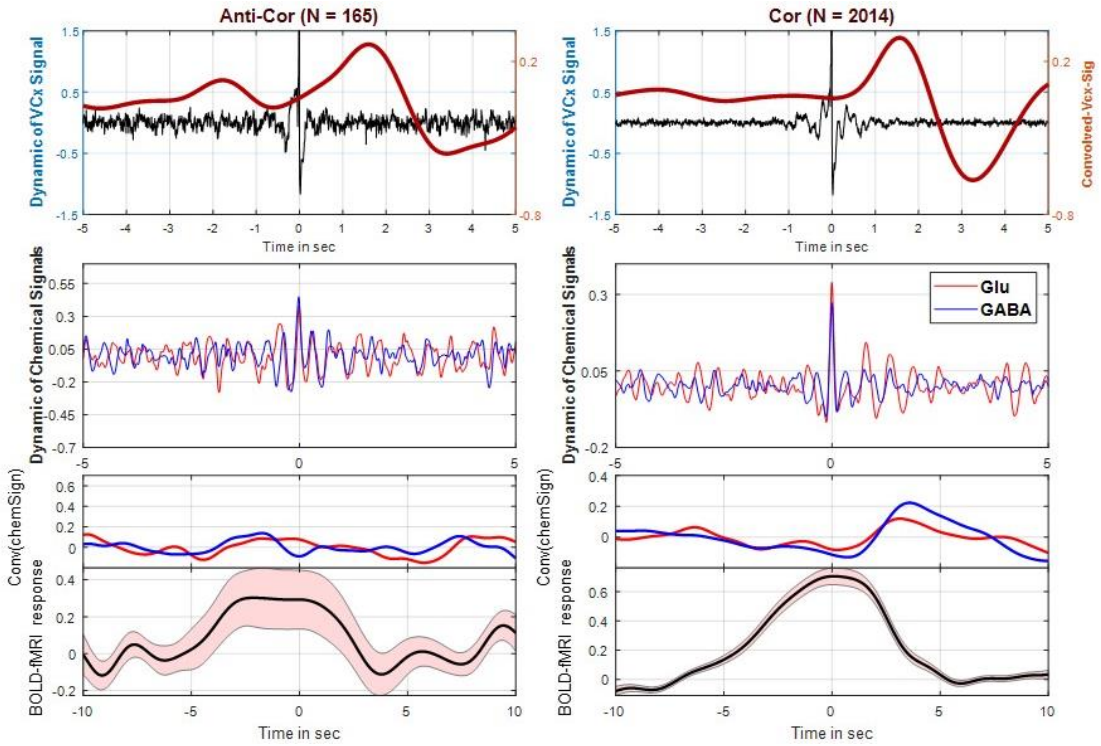

Figure 75. Multi-dimensional relationship of neurophysiological, neurochemical and BOLD signals concurrently measured in VCX.

Based on this analysis and in agreement with previous studies, our experiments suggest that in almost all trials, the negative BOLD response is directly associated with GABAergic signals (Figure 76), while the positive BOLD is a complex superposition of glutamatergic and GABAergic signals. This finding cannot be extrapolated to non-cortical brain areas without further considerations since ultra-structural morphology and microcircuit structure of subcortical brain regions differ significantly from cortical areas. How BOLD signal relates to neurochemistry and neurophysiology, while sharing similar principles, is most likely in governed by patterns and states that differ between cortex and subcortical areas.

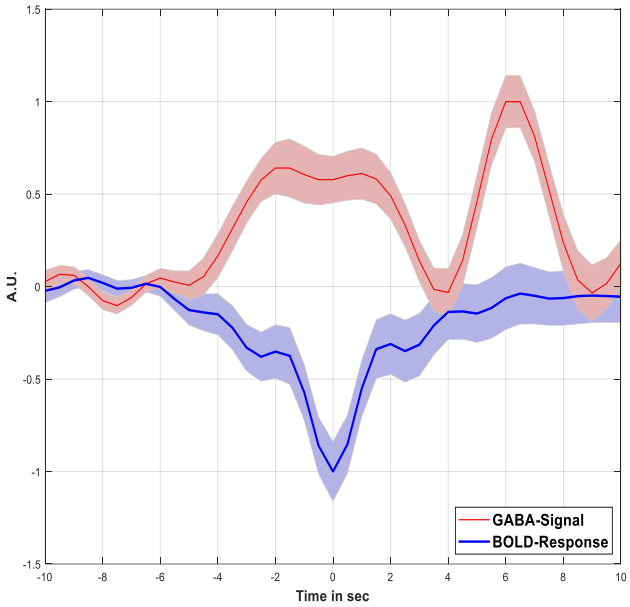

Figure 76. Negative BOLD response is associated with an increase in GABAergic activity.

3.3.3 Excitation-inhibition networks and BOLD signal

Concurrent measurement of neurophysiology, glutamate, GABA signals and BOLD in different brain regions is probably the optimal way to address a question that could not have been answered with each method alone. In this thesis, a novel methodology is presented that enabled us to record all signals simultaneously, at rest and in response to stimulation, in consistent spatiotemporal scale. Indeed, we see the activation maps, the BOLD responses (middle) and the activation/deactivation fractions for Glu-Events (Figure 77), for GABA events (Figure 78) and for anti-correlated events (Figure 79). As it is clearly demonstrated in the figure, the technique sensitively reflects the response to visual stimuli on all dimensions. While negative and positive BOLD responses are consistent with previous literature and spike density function agrees with our assumption that hemodynamic response is directly associated with neural activity, the method further allows to shine a light on how this neural activity is generated. Distinct patterns of glutamate and GABA release indicate on the one hand that the general idea of E-I balance is correct for a large number of trials. Nevertheless, depending on the type of neural events, the balance appears to be more dynamical than just an instantaneous compensation mechanism. In other words, this style of measurement allows us to go beyond a binary assessment of the processes and enable us to temporally decode how BOLD signal is generated in terms of cellular processes.

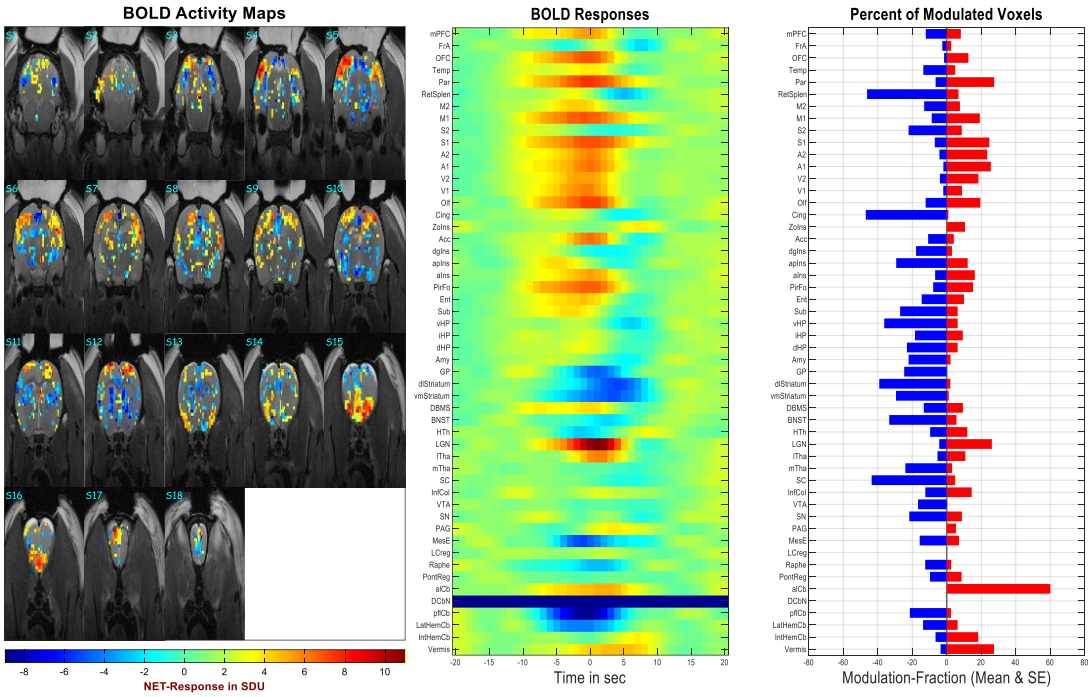

Figure 77. Decomposition of global BOLD signal by activation/inactivation patterns of glutamate.

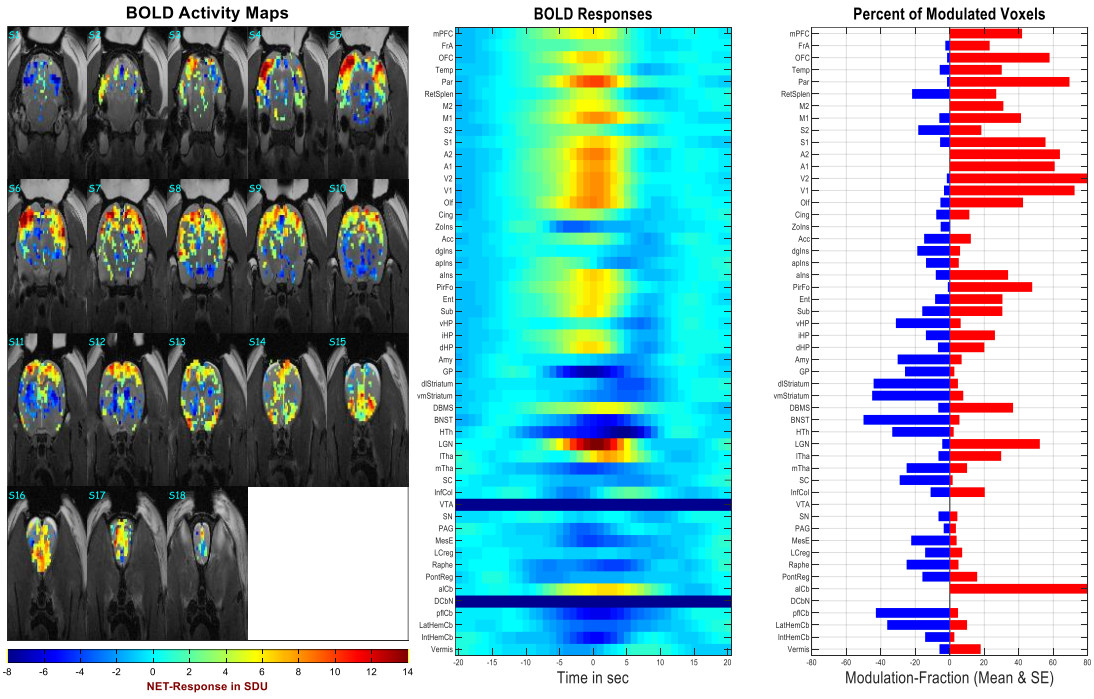

Figure 78. Decomposition of global BOLD signal by activation/inactivation patterns of GABA.

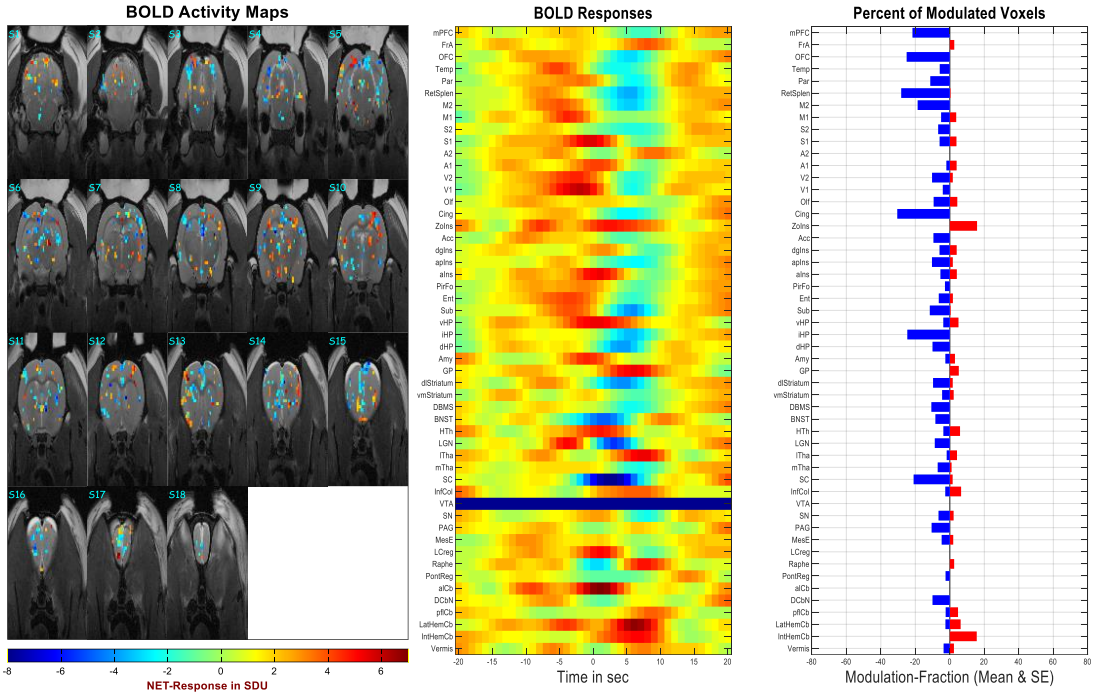

Figure 79. Decomposition of global BOLD signal by anti-correlated neurotransmitter patterns.

It is quite striking that the brain-wide modulation, somewhat similar to what was reported for ripples (Logothetis et al., 2012b), can only observed with GABA events, or when GABA & GLU activity changes proportionally. Glu effects are either mixed or local in terms of activated regions. Anti-correlated activity most likely also refers to local changes, and has no broad maps.

So far, the concept of drivers and modulators in cortex was extended to denote the two different types of operations of the cortical microcircuits. Modeling work, for instance, has suggested the possibility that balanced inputs, which change the excitatory and inhibitory firing rates proportionally, could be considered modulators. Governing inputs in turn are presented when the glutamatergic and GABAergic systems change in opposite directions.

4 Discussion

In order to get a step closer to unraveling the brain function, it is not enough to identify the anatomical structure, it is also necessary to understand how all the structures of the brain interact at the level of macro and microcircuits. Scientists have been able to investigate the cytoarchitectonic of the brain, but how exactly and to what extent brain structures are activated, integrate converging information, and functionally interact with a large number of relevant brain-sites remains unclear. Of paramount importance for the understanding of processes, such as the aforementioned ones, is first of all a fathoming into the nature of signals. Yet, in the past, any knowledge on measurable brain signals was based either on ideas obtained from brain slides in vitro, or based on extrapolations of data at different somewhat isolated scales of consideration.

At microscopic scale, it is well known that neurons are the main anatomical elements of the nervous system. The morphology of the neurons directly relates to how they process information and follows, in general, a certain path, namely from dendrites over to the cell body, and ultimately to the axons. Information travelling along axons by means of so-called action potentials is often transmitted from one neuron to another through synapses that use various neurochemicals as transmitters. These neurotransmitters can induce excitation, inhibition or modulate the activity of the receiving neurons.

The most common excitatory neurotransmitter is the amino acid L-glutamate. In addition to performing the function of a neurotransmitter, glutamate also takes part in protein synthesis. All cortical projection neurons, regardless of their direction in other parts of the cerebral cortex, release glutamate in chemical synapses. Glutamate is synthesized from α-Ketoglutarate, which also serves as a substrate for the GABA synthesis (Meldrum, 2000). GABA is the most common inhibitory mediator involved in about a third of all synapses in the nervous system. GABAergic neurons often present as interneurons but in subcortical brain areas, such as caudate they are also responsible for long-range projections to other brain areas. The actual effect of these neurotransmitters in terms of interneuronal excitation and inhibition is governed by activity of receptors.

In general, neurotransmitter molecules bind to proteins that are located on pre- and postsynaptic membranes. There are two types of receptors: ionotropic and metabotropic. Each group includes receptors whose activation leads to the opening of ion channels, as well as receptors that ensure the closure of these channels.

Ionotropic receptors, in particular the fast AMPA- and relatively slow NMDA receptors, are ligand-gated ion channels. In general, binding of glutamate (and glycine in case of NMDA receptors) changes the conformation of the protein, opens the membrane pore to ions and thus leads to a depolarization of the membrane potential. Stimulation of the AMPA-, or NMDA-receptors leads to the fact that K+ begins to leave the cell, and Ca2+ and Na+ enter the cell. In the course of these processes, neuron excitation occurs, and the latter starts the action potentials. Metabotropic receptors are evenly distributed in all brain structures, and linked to the G-protein system and are involved in neuroplasticity processes. In many inhibitory synapses is the activation of channels for Cl-, which increases its transport into the cell.

The definition of excitatory and inhibitory neurotransmitters at this level cannot be extended to populations of neurons without additional considerations. At systems level, the local excitation induced by glutamate may lead to an overall deactivation of the brain region. In order to investigate how neurotransmitters, relate to activity of populations of neurons (for example within a brain region), in vivo microdialysis emerged in the middle of the last century. However, this method has a significant number of limitations. For example, the sampling time is in minutes, while changes in the concentration of neurotransmitters are actually much faster. Moreover, the size of the microdialysis probes is very large which makes it often inappropriate to investigate smaller brain structures and leads to traumatic brain injury. This aspect makes it also very difficult to combine electrophysiological measurements with neurochemical investigations.

Another approach was to combine electrophysiology with electrochemical measurement via biosensors (amperometry). Undoubtedly, this method would have a significant number of advantages over microdialysis and gives a more realistic idea

of the correlation between neurotransmitter and physiological signal. However, this method was also not optimal as it has often provided us with only partial information, namely on only one brain structure, one neurotransmitter and lacked to show how different systems communicate. Moreover, these studies have not reported the possibility of using this method with anatomical and functional MRI, or of measuring Glutamate and GABA together, thereby expanding the number of neurotransmitters that can be measure with physiology and imaging. All these factors are, obviously among others, of paramount importance also for the understanding the cellular basis of the hemodynamic response, and the correct interpretation of the up and down-modulation patterns observed in functional MR imaging

To investigate functional measurements of the whole-brain the best choice is to use fMRI. In recent years, this method has become very popular and has been combined with other methods to get a broader picture of the brain function. For example, MRI was combined with microdialysis for local measurements of dopamine levels and hemodynamic response induced by cocaine (Schwarz et al., 2004). However, given the time of dialysate sampling (5 minutes), and the lack of data on electrophysiological activity of the brain, it is not possible to investigate properly the cellular basis of the changes in cerebral blood flow with such combination of methods.

While combining fMRI and neurochemistry via microdialysis was unsatisfactory, investigating how neural activity relates to BOLD signals was indeed successful. It was for the first time presented by Nikos Logothetis and allowed us to better understand how the activation of neurons affects the occurrence of the BOLD signal. It was found that changes in the LFP magnitude, rather than simply in MUA or singly neuron activity, all naturally available throughout the entire time of stimulation, is stronger correlated with the BOLD signal. Moreover, it was also found that cytoarchitecture and microcircuits in different anatomical structures (cortical and subcortical structures) are differ from each other. This method provides a deeper understanding of how neural activation leads to the emergence of BOLD response, but how neurotransmitters affect generation of electrophysiological signals or how stimulus-induced BOLD and LFP lead to changes in the concentration in excitatory or/and inhibitory mediators (specifically glutamate and GABA) remains unclear.

A potential way to address this question, could be to combination fMRI (and neural activity measurements) and MRS. Indeed, recent studies have shown that fMRI and MRS can be successfully combined. This method can help to correlate absolute glutamate levels with BOLD dynamics in response to visual stimulus. On the first sight, this technique seems promising for neurochemistry and hemodynamics investigation, but the time resolution is often not good enough to make real conclusions. Moreover, the sensitivity to monitor basal levels of Glu-GABA is not sufficient. In addition to that this technique can't distinguish intra- and extracellular levels of neurotransmitters and don't provide information about electrophysiological signals.

Thus, despite the wide distribution of directions and techniques that are aimed at better understanding the interaction of different brain circuits, there was none that would shed light on all factors and combine local-global levels as well.

To understand how the BOLD signal depends on interaction of the local microcircuits and the changes in neurotransmitters we have developed a method that allows to measure electrophysiological signals, neurochemistry (2 neurotransmitters: Glutamate + GABA) and BOLD signal at consistent time-scales in several brain regions within one voxel (~1 mm^3). Although, our study makes use of information from previous publications for electrochemical detection of neurotransmitters, this step was anything but trivial.
Despite the fact that numerous published papers report on sensitive enzyme preparations, the descriptions of the procedures were not complete or sufficiently accurate, which led to the fact that we were not able to reproduce almost any of the published earlier methods. We prepared and tested several versions of the enzymes in order to find the optimal one.

We further improved the experimental strategy to enhance reproducibility of our own findings. To be able to minimize trauma of the surrounding tissues, as well as to be able investigate small brain structures, the diameter of the electrode was reduced to 35 micrometers. This, in turn, significantly complicated the process of applying the enzyme. Considering that we used a single electrode for simultaneous registration of

the electrophysiological and electrochemical signals, the "dip-coating" technique was inappropriate since the channels should be selectively, without any overlap, covered by an enzyme. To solve this problem, we designed a 3-dimensional manipulator for spot-coating. In addition, we followed a strict standard operating procedure, e.g. all experiments were conducted at exact same times to reduce variability due to circadian oscillations of neurochemical systems. This approach allows us to always trace back potential mistakes and correct them without the need for a major redesign. In summary, these improvements enabled us to measure all signals robustly for up to 7 hours in vivo without a major loss in sensitivity and achieve a very low failure rate which is in full compliance with the 3R principles.

We used our method to investigate two pathways, with the main goal to improve our understanding of how the cortical microcircuits generate neural activity that forms the basis of a BOLD response. The cortical microcircuit, has been investigated for over 100 years, and although there is still some debate regarding its regional functional specificity, a number of structural, immunochemical and theoretical studies suggest that a simple basic circuit, a canonical microcircuit, initially proposed for the cat visual cortex might, in principle, underly the diverse functionality of modules in different areas of higher mammals. We focused on this microcircuit and its interactions from subcortical brain areas.

Overall, we made the following novel observations that can be further studied in extensive details by optimizing this method and also developing data-analysis strategies that now consider intensively the multidimensionality and nature-diversity of various signals.

As mentioned in the results section, we followed to complementary approaches in trying to understand the signals and their interactions. The first one used sensory stimulation. Sensory – in this case visual – stimulation was mainly used for a inducing a causal change in cortical activity, the nature of which has been extensively studied I the past. The data showed that both glutamate and GABA respond to visual stimulation, but most importantly with distinctly correlated, anti-correlated or utterly independent dynamics and in a potentially different manner. The excitatory response of glutamate, for example, has been often characterized by high amplitude

potentiation in release. The inhibitory interneurons, on the other hand, show a characteristically different behavior, by decreasing GABA secretion in response to each light pulse but – at the same time – potentially reducing the reuptake-process, leading to an accumulation of extracellular GABA levels and a long-term depression of neural activity. Understanding the activities of GABA is both a challenge and an extremely interesting undertaken, as GABA may be primarily functioning as an inhibitory neurotransmitter, but also as a neuromodulator of intriguing activity.

Of great interest have also been the study of physiological and chemical changes in cortical signals during “resting state” spontaneous activity. We could successfully demonstrate that different electrical events such as sharp wave ripples, theta band activity or PGOs relate in a specific manner to how glutamate and GABA concentrations change in time. Combining this knowledge with hemodynamic response, allowed us ultimately to decode the BOLD into its excitation-inhibition components. Most importantly however, we could show that the widely accepted excitation-inhibition balance is not an invariant process but shall be characterized by a subtle time-dependent (with variable time-delays) interplay of the activity of pyramidal, interneurons and astrocytes. Indeed, the latter appears to play a key role in glutamatergic signaling and thus, could fundamentally influence how we interpret the neural basis of hemodynamic response.

Instigated by fMRI, fMRS and CBF studies, we also examined the relationship of Glutamate and GABA concentration-changes to the modulation of the cortical signal in the Gamma range. Gamma oscillations in V1 have been reported to correlate with GABAA receptor density (A multi-modal MEG and Flumazenil-PET study (Kujala et al., 2015)). Yet, our detailed analysis of physiological and chemical responses showed that correlations between GABA and Gamma are rather complex, with a subset of trials following this assumption, and another one having inversed activities.

Interesting have also been our first results related to the concentration of chemical signals and their inter-signal relationship in different brain-states, like the rapid eye movement (REM) and non-REM (NREM) states that can be successfully characterized by using power-to-power correlation between signals (Ramirez-Villegas et al., 2020).

All in all, the present thesis was inspired by efforts that over the past two decades attempt to improve our understanding of brain function using MRI technology. Therefore, while it already has the potential to help us investigate the foundations of resting-state fMRI and provide a more in-depth understanding of functional connectivity networks associated with neuropsychiatric disorders, it is only a piece of a larger puzzle to be completed. In particular, studies in the future can use the technology to obtain a more diverse picture of the brain by measuring activity in other brain pathways. The method itself can also be extended such that other neurotransmitter systems including neuromodulators can be assessed. Such spatiotemporally high-resolution neurochemical, neurophysiological and functional maps can pave the way for development of more effective pharmacological treatments for brain disease.

Limitations. This work was conducted to the best of our abilities, yet just as any other scientific study is also not free of limitations. In particular, all reported experiments were conducted in **anesthetized animals**. It is well-known that anesthesia not only affect neural activity but through induction of changes in body physiology, for example changes in breathing patterns, may also influence the sensitivity of amperometric measurements. Moreover, all experiments were conducted in male, adult rats and thus the overall findings cannot be fully extrapolated to every age and sex without care and further considerations. In addition, it is noteworthy that the experiments are incredibly expensive both in terms of money (due to the price of enzymes and electrode) and time as each experiment usually takes approximately 36 hours.

References

Adrian, E.D., and Matthews, B.H.C. (1934). The Berger rhythm: potential changes from the occipital lobes in man. Brain: A Journal of Neurology *57*, 355-385.

Arima, J., Sasaki, C., Sakaguchi, C., Mizuno, H., Tamura, T., Kashima, A., Kusakabe, H., Sugio, S., and Inagaki, K. (2009). Structural characterization of L-glutamate oxidase from Streptomyces sp. X-119-6. FEBS J *276*, 3894-3903.

Axmacher, N., Elger, C.E., and Fell, J. (2008). Ripples in the medial temporal lobe are relevant for human memory consolidation. Brain *131*, 1806-1817.

Besserve, M., Lowe, S.C., Logothetis, N.K., Scholkopf, B., and Panzeri, S. (2015). Shifts of Gamma Phase across Primary Visual Cortical Sites Reflect Dynamic Stimulus-Modulated Information Transfer. PLoS Biol *13*, e1002257.

Bianchi, G., Mazza, F., and T., M. (1962). Catalytic decomposition of acid hydrogen peroxide solutions on platinum, iridium, palladium and gold surfaces. Electrochim Acta *7*, 457–473.

Bigot, J., Longcamp, M., Dal Maso, F., and Amarantini, D. (2011). A new statistical test based on the wavelet cross-spectrum to detect time-frequency dependence between non-stationary signals: application to the analysis of cortico-muscular interactions. Neuroimage *55*, 1504-1518.

Bloch, F., Hansen, W.W., and Packard, M. (1946). The Nuclear Induction Experiment. Phys Rev *70*, 474.

Bohmer, A., Muller, A., Passarge, M., Liebs, P., Honeck, H., and Muller, H.G. (1989). A novel L-glutamate oxidase from Streptomyces endus. Purification and properties. Eur J Biochem *182*, 327-332.

Bosshard, S.C., Baltes, C., Wyss, M.T., Mueggler, T., Weber, B., and Rudin, M. (2010). Assessment of brain responses to innocuous and noxious electrical forepaw stimulation in mice using BOLD fMRI. Pain *151*, 655-663.

Boussida, S., Traore, A.S., and Durif, F. (2017). Mapping of the brain hemodynamic responses to sensorimotor stimulation in a rodent model: A BOLD fMRI study. PLoS One *12*, e0176512.

Briggs, F., and Usrey, W.M. (2008). Emerging views of corticothalamic function. Curr Opin Neurobiol *18*, 403-407.

Britton, J.W., Frey, L.C., Hopp, J.L., Korb, P., Koubeissi, M.Z., Lievens, W.E., Pestana-Knight, E.M., and St. Louis, E.K. (2016). In Electroencephalography

(EEG): An Introductory Text and Atlas of Normal and Abnormal Findings in Adults, Children, and Infants, E.K. St. Louis, and L.C. Frey, eds. (Chicago).

Brown, R.W.e.a. (2014). Classical Response of a Single Nucleus to a Magnetic Field. In Magnetic Resonance Imaging, pp. 19-36.

Bujacz, A. (2012). Structures of bovine, equine and leporine serum albumin. Acta Crystallogr D Biol Crystallogr *68*, 1278-1289.

Burmeister, J.J., Price, D.A., Pomerleau, F., Huettl, P., Quintero, J.E., and Gerhardt, G.A. (2020). Challenges of simultaneous measurements of brain extracellular GABA and glutamate in vivo using enzyme-coated microelectrode arrays. J Neurosci Methods *329*, 108435.

Buzsaki, G., Horvath, Z., Urioste, R., Hetke, J., and Wise, K. (1992). High-frequency network oscillation in the hippocampus. Science *256*, 1025-1027.

Caton, R. (1891). Die Ströme des Centralnervensystems Centralblatt für Physiologie *4*, 785-786.

Costa, M., Goldberger, A.L., and Peng, C.K. (2005). Multiscale entropy analysis of biological signals. Phys Rev E Stat Nonlin Soft Matter Phys *71*, 021906.

Danilevsky, W.Y. (1891). Zur Frage über die elektromotorischen Vorgänge im Gehirn als Ausdruck seines Thätigkeitszustandes Centralblatt für Physiologie *4*, 473-476.

Day, B.K., Pomerleau, F., Burmeister, J.J., Huettl, P., and Gerhardt, G.A. (2006). Microelectrode array studies of basal and potassium-evoked release of L-glutamate in the anesthetized rat brain. Journal of Neurochemistry *96*, 1626-1635.

Domercq, M., Brambilla, L., Pilati, E., Marchaland, J., Volterra, A., and Bezzi, P. (2006). P2Y1 receptor-evoked glutamate exocytosis from astrocytes: control by tumor necrosis factor-alpha and prostaglandins. J Biol Chem *281*, 30684-30696.

Du Bois-Reymond, E. (1848). Untersuchungen über thierische Elektricität. Annalen der Physik *151*, 463.

Duong, T.Q., Ngan, S.C., Ugurbil, K., and Kim, S.G. (2002). Functional magnetic resonance imaging of the retina. Invest Ophthalmol Vis Sci *43*, 1176-1181.

Fathizadeh, F., Mitricheva, E., Kimura, R., Logothetis, N., and Noori, H.R. (2019). Signal detection in extracellular neural ensemble recordings using higher criticism, pp. arXiv:1905.06225.

Fox, P.T., Raichle, M.E., Mintun, M.A., and Dence, C. (1988). Nonoxidative glucose consumption during focal physiologic neural activity. Science *241*, 462-464.

Gerhardt, G.A., Oke, A.F., Nagy, G., Moghaddam, B., and Adams, R.N. (1984). Nafion-coated electrodes with high selectivity for CNS electrochemistry. Brain Res *290*, 390-395.

Goense, J.B., and Logothetis, N.K. (2008a). Neurophysiology of the BOLD fMRI signal in awake monkeys. Curr Biol *18*, 631-640.

Goense, J.B.M., and Logothetis, N.K. (2008b). Neurophysiology of the BOLD fMRI Signal in Awake Monkeys. Current Biology *18*, 631-640.

Hidalgo-Balbuena, A.E., Luma, A.Y., Pimentel-Farfan, A.K., Pena-Rangel, T., and Rueda-Orozco, P.E. (2019). Sensory representations in the striatum provide a temporal reference for learning and executing motor habits. Nat Commun *10*, 4074.

Hinz, R., Peeters, L.M., Shah, D., Missault, S., Belloy, M., Vanreusel, V., Malekzadeh, M., Verhoye, M., Van der Linden, A., and Keliris, G.A. (2019). Bottom-up sensory processing can induce negative BOLD responses and reduce functional connectivity in nodes of the default mode-like network in rats. Neuroimage *197*, 167-176.

Hu, Y., Mitchell, K.M., Albahadily, F.N., Michaelis, E.K., and Wilson, G.S. (1994). Direct measurement of glutamate release in the brain using a dual enzyme-based electrochemical sensor. Brain Res *659*, 117-125.

Huang, N.E., Long, S.R., and Shen, Z. (1996). The Mechanism for Frequency Downshift. Advances in applied mechanics, 59.

Huang, N.E., Shen, Z., and Long, S.R. (1999). A NEW VIEW OF NONLINEAR WATER WAVES: The Hilbert Spectrum. Annual Review of Fluid Mechanics *31*, 417-457.

Huang, N.E., Shen, Z., Long, S.R., Wu, M.C., Shih, H.H., Zheng, Q., Yen, N.-C., Tung, C.C., and Liu, H.H. (1998). The empirical mode decomposition and the Hilbert spectrum for nonlinear and non-stationary time series analysis. Proceedings of the Royal Society of London Series A *454*, 903.

Hurtado, J.M., Rubchinsky, L.L., and Sigvardt, K.A. (2004). Statistical method for detection of phase-locking episodes in neural oscillations. J Neurophysiol *91*, 1883-1898.

Isomura, Y., Sirota, A., Ozen, S., Montgomery, S., Mizuseki, K., Henze, D.A., and Buzsaki, G. (2006). Integration and segregation of activity in entorhinal-hippocampal subregions by neocortical slow oscillations. Neuron *52*, 871-882.

Jang, E.H., Park, S.A., Chi, Y.M., and Lee, K.S. (2014). Kinetic and structural characterization for cofactor preference of succinic semialdehyde dehydrogenase from Streptococcus pyogenes. Mol Cells *37*, 719-726.

Jespersen, B., Knupp, L., and Northcott, C.A. (2012). Femoral arterial and venous catheterization for blood sampling, drug administration and conscious blood pressure and heart rate measurements. J Vis Exp.

Johnson, M.D., Franklin, R.K., Gibson, M.D., Brown, R.B., and Kipke, D.R. (2008). Implantable microelectrode arrays for simultaneous electrophysiological and neurochemical recordings. J Neurosci Methods *174*, 62-70.

Kennedy, R.T. (2013). Emerging trends in in vivo neurochemical monitoring by microdialysis. Curr Opin Chem Biol *17*, 860-867.

Kho, C.M., Enche Ab Rahim, S.K., Ahmad, Z.A., and Abdullah, N.S. (2017). A Review on Microdialysis Calibration Methods: the Theory and Current Related Efforts. Mol Neurobiol *54*, 3506-3527.

Kujala, J., Jung, J., Bouvard, S., Lecaignard, F., Lothe, A., Bouet, R., Ciumas, C., Ryvlin, P., and Jerbi, K. (2015). Gamma oscillations in V1 are correlated with GABA(A) receptor density: A multi-modal MEG and Flumazenil-PET study. Sci Rep *5*, 16347.

Kulagina, N.V., Shankar, L., and Michael, A.C. (1999). Monitoring glutamate and ascorbate in the extracellular space of grain tissue with electrochemical microsensors. Analytical Chemistry *71*, 5093-5100.

Kumar, A., Welti, D., and Ernst, R.R. (1975). NMR Fourier zeugmatography. Journal of Magnetic Resonance (1969) *18*, 69-83.

Kurcyus, K., Annac, E., Hanning, N.M., Harris, A.D., Oeltzschner, G., Edden, R., and Riedl, V. (2018). Opposite Dynamics of GABA and Glutamate Levels in the Occipital Cortex during Visual Processing. J Neurosci *38*, 9967-9976.

Kusakabe, H., Midorikawa, Y., Fujishima, T., Kuninaka, A., and Yoshino, H. (1983). Purification and Properties of a New Enzyme, L-Glutamate Oxidase, from Streptomyces Sp X-119-6 Grown on Wheat Bran. Agricultural and Biological Chemistry *47*, 1323-1328.

Lachaux, J.P., Rodriguez, E., Martinerie, J., and Varela, F.J. (1999). Measuring phase synchrony in brain signals. Hum Brain Mapp *8*, 194-208.

Lauterbur, P.C. (1989). Image formation by induced local interactions. Examples employing nuclear magnetic resonance. 1973. Clin Orthop Relat Res, 3-6.

Lippert, M.T., Steudel, T., Ohl, F., Logothetis, N.K., and Kayser, C. (2010). Coupling of neural activity and fMRI-BOLD in the motion area MT. Magn Reson Imaging *28*, 1087-1094.

Liu, W., Peterson, P.E., Langston, J.A., Jin, X., Zhou, X., Fisher, A.J., and Toney, M.D. (2005). Kinetic and crystallographic analysis of active site mutants of Escherichia coli gamma-aminobutyrate aminotransferase. Biochemistry *44*, 2982-2992.

Logothetis, N.K. (2002). The neural basis of the blood-oxygen-level-dependent functional magnetic resonance imaging signal. Philos Trans R Soc Lond B Biol Sci *357*, 1003-1037.

Logothetis, N.K. (2003). The underpinnings of the BOLD functional magnetic resonance imaging signal. J Neurosci *23*, 3963-3971.

Logothetis, N.K. (2008). What we can do and what we cannot do with fMRI. Nature *453*, 869-878.

Logothetis, N.K., Augath, M.A., Murayama, Y., Rauch, A., Sultan, F.R., Goense, J.B.M., Oeltermann, A., and Merkle, H. (2010). The effects of electrical microstimulation on cortical signal propagation. Nature Neuroscience *13*, 1283-1291.

Logothetis, N.K., Eschenko, O., Murayama, Y., Augath, M., Steudel, T., Evrard, H.C., Besserve, M., and Oeltermann, A. (2012a). Hippocampal-cortical interaction during periods of subcortical silence. Nature *491*, 547-553.

Logothetis, N.K., Eschenko, O., Murayama, Y., Augath, M., Steudel, T., Evrard, H.C., Besserve, M., and Oeltermann, A. (2012b). Hippocampal-cortical interaction during periods of subcortical silence. Nature *491*, 547-553.

Logothetis, N.K., Pauls, J., Augath, M., Trinath, T., and Oeltermann, A. (2001a). Neurophysiological investigation of the basis of the fMRI signal. Nature *412*, 150-157.

Logothetis, N.K., Pauls, J.M., Augath, M.A., Trinath, T., and Oeltermann, A. (2001b). Neurophysiological investigation of the basis of the fMRI signal. Nature *412*, 150-157.

Logothetis, N.K., and Pfeuffer, J. (2004). On the nature of the BOLD fMRI contrast mechanism. Magn Reson Imaging *22*, 1517-1531.

Lopez-Valenzuela, C.L., Morales-Villagran, A., and Medina-Ceja, L. (2015). A novel method for simultaneous glutamate and extracellular activity measurement in brain slices with high temporal resolution. Talanta *144*, 1231-1238.

Magnone, M.C., Bertolucci, C., Piazza, F., and Foa, A. (2003). Daily and circadian rhythms of neurotransmitters and related compounds in the hypothalamic suprachiasmatic nuclei of a diurnal vertebrate. Brain Res *973*, 115-121.

Maier, A., Logothetis, N.K., and Leopold, D.A. (2007). Context-dependent perceptual modulation of single neurons in primate visual cortex. Proc Natl Acad Sci U S A *104*, 5620-5625.

Malarkey, E.B., and Parpura, V. (2008). Mechanisms of glutamate release from astrocytes. Neurochem Int *52*, 142-154.

Mansfield, P. (1977). Multi-planar image formation using NMR spin echoes. Journal of Physics C: Solid State Physics *10*, L55-L58.

Mansfield, P. (2004). Snapshot magnetic resonance imaging (Nobel lecture). Angew Chem Int Ed Engl *43*, 5456-5464.

McCormick, D.A., and Bal, T. (1997). Sleep and arousal - Thalamocortical mechanisms. Annual Review of Neuroscience *20*, 185-215.

Meldrum, B.S. (2000). Glutamate as a neurotransmitter in the brain: review of physiology and pathology. J Nutr *130*, 1007S-1015S.

Mervin, L.H., Mitricheva, E., Logothetis, N.K., Bifone, A., Bender, A., and Noori, H.R. (2020). Neurochemical underpinning of hemodynamic response to neuropsychiatric drugs: A meta- and cluster analysis of preclinical studies. J Cereb Blood Flow Metab, 271678X20916003.

Messerschmidt, A., Ladenstein, R., Huber, R., Bolognesi, M., Avigliano, L., Petruzzelli, R., Rossi, A., and Finazzi-Agro, A. (1992). Refined crystal structure of ascorbate oxidase at 1.9 A resolution. J Mol Biol *224*, 179-205.

Mosso, A. (1880). Sulla circolazione del sangue nel cervello dell'uomo. Atti della R Acad Lincei, Mem Cl Sci Fis Mat Nat *3*, 237-358.

Niwa, O., Kurita, R., Horiuchi, T., and Torimitsu, K. (1998). Small-volume on-line sensor for continuous measurement of gamma-aminobutyric acid. Anal Chem *70*, 89-93.

Noori, H.R., Mervin, L.H., Bokharaie, V., Durmus, O., Egenrieder, L., Fritze, S., Gruhlke, B., Reinhardt, G., Schabel, H.H., Staudenmaier, S*., et al.* (2018). Systemic neurotransmitter responses to clinically approved and experimental neuropsychiatric drugs. Nat Commun *9*, 4699.

Noori, H.R., Schottler, J., Ercsey-Ravasz, M., Cosa-Linan, A., Varga, M., Toroczkai, Z., and Spanagel, R. (2017). A multiscale cerebral neurochemical connectome of the rat brain. PLoS Biol *15*, e2002612.

O'Keefe, J., and Nadel, L. (1978). The Hippocampus as a Cognitive Map (Oxford: Oxford University Press).

Oeltermann, A., Augath, M.A., and Logothetis, N.K. (2007). Simultaneous recording of neuronal signals and functional NMR imaging. Magn Reson Imaging *25*, 760-774.

Ogawa, S., Lee, T.M., Kay, A.R., and Tank, D.W. (1990). Brain magnetic resonance imaging with contrast dependent on blood oxygenation. Proc Natl Acad Sci U S A *87*, 9868-9872.

Oldenziel, W.H., Dijkstra, G., Cremers, T.I.F.H., and Westerink, B.H.C. (2006). In vivo monitoring of extracellular glutamate in the brain with a microsensor. Brain Research *1118*, 34-42.

Pauling, L., and Coryell, C.D. (1936a). The Magnetic Properties and Structure of Hemoglobin, Oxyhemoglobin and Carbonmonoxyhemoglobin. Proc Natl Acad Sci U S A *22*, 210-216.

Pauling, L., and Coryell, C.D. (1936b). The Magnetic Properties and Structure of the Hemochromogens and Related Substances. Proc Natl Acad Sci U S A *22*, 159-163.

Paxinos, G., and Watson, C. (2013). The Rat Brain in Stereotaxic Coordinates, 7th Edition edn (Academic Press).

Paxinos, G., Watson, C., Pennisi, M., and Topple, A. (1985). Bregma, lambda and the interaural midpoint in stereotaxic surgery with rats of different sex, strain and weight. J Neurosci Methods *13*, 139-143.

Perea, G., Navarrete, M., and Araque, A. (2009). Tripartite synapses: astrocytes process and control synaptic information. Trends Neurosci *32*, 421-431.

Pincus, S.M. (1991). Approximate entropy as a measure of system complexity. Proc Natl Acad Sci U S A *88*, 2297-2301.

Pincus, S.M., and Goldberger, A.L. (1994). Physiological time-series analysis: what does regularity quantify? Am J Physiol *266*, H1643-1656.

Poline, J.B., and Brett, M. (2012). The general linear model and fMRI: does love last forever? Neuroimage *62*, 871-880.

Qin, S., Van der Zeyden, M., Oldenziel, W.H., Cremers, T.I., and Westerink, B.H. (2008). Microsensors for in vivo Measurement of Glutamate in Brain Tissue. Sensors (Basel) *8*, 6860-6884.

Rahman, M.A., Kwon, N.H., Won, M.S., Choe, E.S., and Shim, Y.S. (2005). Functionalized conducting polymer as an enzyme-immobilizing substrate: An amperometric glutamate microbiosensor for in vivo measurements. Analytical Chemistry *77*, 4854-4860.

Ramirez-Villegas, J.F., Besserve, M., Murayama, Y., Evrard, H.C., Oeltermann, A., and Logothetis, N.K. (2020). Coupling of hippocampal theta and ripples with pontogeniculooccipital waves. Nature.

Ramirez-Villegas, J.F., Logothetis, N.K., and Besserve, M. (2015). Diversity of sharp-wave-ripple LFP signatures reveals differentiated brain-wide dynamical events. Proc Natl Acad Sci U S A *112*, E6379-6387.

Reimann, H.M., Todiras, M., Hodge, R., Huelnhagen, T., Millward, J.M., Turner, R., Seeliger, E., Bader, M., Pohlmann, A., and Niendorf, T. (2018). Somatosensory BOLD fMRI reveals close link between salient blood pressure changes and the murine neuromatrix. Neuroimage *172*, 562-574.

Renaud-Roy, E., Stöckle, P.A., Maximos, S., Brulotte, V., Sideris, L., Dubé, P., Drolet, P., Tanoubi, I., Issa, R., Verdonck, O.*, et al.* (2019). Correlation between incremental remifentanil doses and the Nociception Level (NOL) index response after intraoperative noxious stimuli. Can J Anaesth *66*, 1049-1061.

Richman, J.S., and Moorman, J.R. (2000). Physiological time-series analysis using approximate entropy and sample entropy. Am J Physiol Heart Circ Physiol *278*, H2039-2049.

Roy, C.S., and Sherrington, C.S. (1890). On the Regulation of the Blood-supply of the Brain. The Journal of Physiology *11*, 85-158.

Schroeter, A., Schlegel, F., Seuwen, A., Grandjean, J., and Rudin, M. (2014). Specificity of stimulus-evoked fMRI responses in the mouse: the influence of

systemic physiological changes associated with innocuous stimulation under four different anesthetics. Neuroimage *94*, 372-384.

Schuvailo, O.M., Soldatkin, O.O., Lefebvre, A., Cespuglio, R., and Soldatkin, A.P. (2006). Highly selective microbiosensors for in vivo measurement of glucose, lactate and glutamate. Analytica Chimica Acta *573*, 110-116.

Schwarz, A.J., Zocchi, A., Reese, T., Gozzi, A., Garzotti, M., Varnier, G., Curcuruto, O., Sartori, I., Girlanda, E., Biscaro, B.*, et al.* (2004). Concurrent pharmacological MRI and in situ microdialysis of cocaine reveal a complex relationship between the central hemodynamic response and local dopamine concentration. Neuroimage *23*, 296-304.

Siapas, A.G., and Wilson, M.A. (1998). Coordinated interactions between hippocampal ripples and cortical spindles during slow-wave sleep. Neuron *21*, 1123-1128.

Sirota, A., Csicsvari, J., Buhl, D., and Buzsaki, G. (2003). Communication between neocortex and hippocampus during sleep in rodents. Proceedings of the National Academy of Sciences of the United States of America *100*, 2065-2069.

Skaggs, W.E., McNaughton, B.L., Permenter, M., Archibeque, M., Vogt, J., Amaral, D.G., and Barnes, C.A. (2007). EEG sharp waves and sparse ensemble unit activity in the macaque hippocampus. Journal of Neurophysiology *98*, 898-910.

Smith, K.S., and Graybiel, A.M. (2013). A dual operator view of habitual behavior reflecting cortical and striatal dynamics. Neuron *79*, 361-374.

Smith, K.S., and Graybiel, A.M. (2014). Investigating habits: strategies, technologies and models. Front Behav Neurosci *8*, 39.

Steriade, M., Nunez, A., and Amzica, F. (1993). A novel slow (< 1 Hz) oscillation of neocortical neurons in vivo: depolarizing and hyperpolarizing components. Journal of Neuroscience *13*, 3252-3265.

Su, C.S., Lai, H.C., Lee, W.L., Ting, C.T., Yang, Y.L., Lee, H.W., Wang, L.C., Peng, C.Y., Wang, K.Y., and Liu, T.J. (2012). A secure and rapid method for orotracheal intubation of laboratory rats utilising handy instruments. Eur J Anaesthesiol *29*, 515-519.

Totah, N.K., Neves, R.M., Panzeri, S., Logothetis, N.K., and Eschenko, O. (2018). The Locus Coeruleus Is a Complex and Differentiated Neuromodulatory System. Neuron *99*, 1055-1068 e1056.

Tseng, T.T., Chang, C.F., and Chan, W.C. (2014). Fabrication of implantable, enzyme-immobilized glutamate sensors for the monitoring of glutamate concentration changes in vitro and in vivo. Molecules *19*, 7341-7355.

Underwood, E.A. (1945). Wilhelm Conrad Rontgen (1845-1923) and the Early Development of Radiology. Proc R Soc Med *38*, 697-706.

Walter, W.G. (1936). THE LOCATION OF CEREBRAL TUMOURS BY ELECTRO-ENCEPHALOGRAPHY. The Lancet *228*, 305-308.

Wei, W., Song, Y., Wang, L., Zhang, S., Luo, J., Xu, S., and Cai, X. (2015). An implantable microelectrode array for simultaneous L-glutamate and electrophysiological recordings in vivo. Microsystems & Nanoengineering *1*, 15002.

Wierzynski, C.M., Lubenov, E.V., Gu, M., and Siapas, A.G. (2009). State-dependent spike-timing relationships between hippocampal and prefrontal circuits during sleep. Neuron *61*, 587-596.

Ylinen, A., Bragin, A., Nadasdy, Z., Jando, G., Szabo, I., Sik, A., and Buzsaki, G. (1995). Sharp wave-associated high-frequency oscillation (200 Hz) in the intact hippocampus: network and intracellular mechanisms. Journal of Neuroscience *15*, 30-46.

Zhang, S., Song, Y., Wang, M., Xiao, G., Gao, F., Li, Z., Tao, G., Zhuang, P., Yue, F., Chan, P.*, et al.* (2018). Real-time simultaneous recording of electrophysiological activities and dopamine overflow in the deep brain nuclei of a non-human primate with Parkinson's disease using nano-based microelectrode arrays. Microsystems & Nanoengineering *4*, 17070.

Zitnik, G.A., Clark, B.D., and Waterhouse, B.D. (2014). Effects of intracerebroventricular corticotropin releasing factor on sensory-evoked responses in the rat visual thalamus. Brain Res *1561*, 35-47.